



**UNIVERSITÀ DEGLI STUDI DI MILANO**

FACOLTÀ DI SCIENZE AGRARIE E ALIMENTARI

Department of Food, Environmental and Nutritional Sciences (DeFENS)

**Graduate School in Molecular Sciences and Plant, Food and  
Environmental Biotechnology**

**PhD programme in Food Science, Technology and Biotechnology**

**XXV cycle**

**DEVELOPMENT OF HIGH PERFORMANCE  
BIOPOLYMER COATINGS  
FOR FOOD PACKAGING APPLICATIONS**

**Scientific field AGR/15**

**LAURA INTROZZI**

Tutor: Prof. Alberto Schiraldi

Co-tutor: Prof. Luciano Piergiovanni

PhD Coordinator: Prof. Maria Grazia Fortina

2011/2012

*“The boundary is the best place for acquiring knowledge”*

*Paul Tillich, 1929*

# INDEX

Abstract (English and Italian)	1
0. Preface	3
1. State of the art	4
1.1 References	8
2. Aim of the study	9
3. Part 1 – ONE COMPONENT COATINGS	10
3.1 OXYGEN BARRIER PROPERTIES OF BIO-COATED FILMS	12
3.1.1 Materials and methods	11
3.1.1.1 Materials	11
3.1.1.1.a Biopolymers	11
3.1.1.1.b Films (PLA and PET)	15
3.1.1.1.c Oil-based polymers	16
3.1.1.2 Methods	17
3.1.1.2.a Coating dispersions preparation	17
3.1.1.2.b Coated films preparation	17
3.1.1.2.c Thickness determination	18
3.1.1.2.d Haze	18
3.1.1.2.e Oxygen barrier properties	18
3.1.1.2.f Statistical analysis	18
3.1.2 Results and discussion	19
3.1.2.1 Coating thickness	19
3.1.2.2 Haze	19
3.1.2.3 Oxygen barrier properties	20
3.1.3 Conclusions	24
3.1.4 References	25
3.2 SURFACE PROPERTIES OF BIO-COATED FILMS	26
3.2.1 Materials and methods	27
3.2.1.1 Materials	27
3.2.1.2 Methods	27
3.2.1.2.a Coating dispersions preparation	27
3.2.1.2.b Coated films preparation	27
3.2.1.2.c Thickness determination	27
3.2.1.2.d Contact angle measurements	27
3.2.1.2.e Atomic Force Microscopy	29
3.2.1.2.f Modeling and statistical analysis	29
3.2.2 Results and discussion	30
3.2.2.1 Coating thickness	31
3.2.2.2 Contact angle measurements	31

3.2.2.3 Modeling	35
3.2.2.4 Contact angle/image analysis combined approach	37
3.2.3 Conclusions	43
3.2.4 References	44
<b>3.3 APPLICATION OF PULLULAN AS ANTIFOG COATING</b>	<b>46</b>
3.3.1 Materials and methods	48
3.3.1.1 Materials	48
3.3.1.2 Methods	48
3.3.1.2.a Coating dispersions preparation	48
3.3.1.2.b Coated films preparation	48
3.3.1.2.c Contact angle measurements	48
3.3.1.2.d Atomic Force Microscopy	49
3.3.1.2.e Optical microscopy	49
3.3.1.2.f Antifog test	49
3.3.1.2.g Optical properties	49
3.3.1.2.h Statistical analysis	50
3.3.2 Results and discussion	51
3.3.2.1 Contact angle measurements and Atomic Force Microscopy	51
3.3.2.2 Antifog tests and optical properties	54
3.3.2.3 Optical microscopy	55
3.3.3 Conclusions	57
3.3.4 References	58
<b>4. Part 2 – TWO COMPONENT COATINGS</b>	<b>59</b>
<b>4.1 BIO-NANOSTRUCTURED COATINGS</b>	<b>60</b>
4.1.1 Materials and methods	61
4.1.1.1 Materials	61
4.1.1.2 Methods	61
4.1.1.2.a Coating dispersions preparation	61
4.1.1.2.b Coated films preparation	63
4.1.1.2.c Thickness determination	63
4.1.1.2.d Fourier Transform Infrared - Attenuated Total Reflectance (FTIR-ATR)	63
4.1.1.2.e Microscopy analyses	63
4.1.1.2.f Oxygen barrier properties	63
4.1.1.2.g Statistical analysis	63
4.1.2 Results and discussion	64
4.1.2.1 Coating thickness	64
4.1.2.2 FTIR/ATR analyses	64
4.1.2.3 Transmission electron microscopy analyses	65
4.1.2.4 Oxygen barrier properties and optical microscopy analyses	66
4.1.3 Conclusions	68
4.1.4 References	69

<b>4.2 BIO-NANOCOMPOSITE COATINGS</b>	<b>70</b>
<b>4.2.1 Materials and methods</b>	<b>72</b>
<b>4.2.1.1 Materials</b>	<b>72</b>
<b>4.2.1.2 Methods</b>	<b>72</b>
<b>4.1.1.2.a Coating dispersions preparation</b>	<b>72</b>
<b>4.1.1.2.b Coated films preparation</b>	<b>73</b>
<b>4.2.1.2.c Oxygen permeability (<math>P'O_2</math>) measurements</b>	<b>73</b>
<b>4.2.1.2.d Haze</b>	<b>74</b>
<b>4.2.1.2.e Experimental design</b>	<b>74</b>
<b>4.2.1.2.f Particle size analysis</b>	<b>74</b>
<b>4.2.1.2.g Electron microscopy analysis</b>	<b>75</b>
<b>4.2.1.2.h Atomic force microscopy</b>	<b>75</b>
<b>4.2.2 Results and discussion</b>	<b>76</b>
<b>4.2.2.1 Effect of clay concentration and ultrasound treatment time on oxygen barrier and haze properties</b>	<b>76</b>
<b>4.2.2.2 Modeling the <math>P'O_2</math> data</b>	<b>79</b>
<b>4.2.2.3 Characterization of the best pullulan/clay nanocomposite coating</b>	<b>82</b>
<b>4.2.3 Conclusions</b>	<b>86</b>
<b>4.2.4 References</b>	<b>87</b>
<b>5. Part 3 - THREE COMPONENT COATINGS –PERSPECTIVES</b>	<b>89</b>
<b>5.1 References</b>	<b>91</b>
<b>6. Glossary</b>	<b>92</b>
<b>Acknowledgements</b>	<b>93</b>
<b>Appendix 1 <i>Conference's abstract</i></b>	<b>94</b>
<b>Appendix 2 <i>Honors and Awards</i></b>	<b>105</b>
<b>Appendix 3 <i>Patents and Publications</i></b>	<b>108</b>

# ABSTRACT

---

## **Development of high performance biopolymer coatings for food packaging applications**

This PhD project aims to the optimization of the food packaging materials currently available on the market. The purpose is to develop high performance coatings able to improve the original characteristics of the plastic substrate beneath, as a consequence of the coating deposition. In particular, to fulfil the increasing request for replacing synthetic polymers already used in the nowadays packaging applications as well as to reduce the overall amount of plastics, biomacromolecules, possibly combined with inorganic compounds, will be used to generate a new class of “bio-nanocomposite-hybrid-coatings”. This will lead to a “greener” packaging structure with the same overall performances of the conventional ones.

Some films properties will be considered, in particular the oxygen barrier performances at high relative humidity values, the surface properties and the optical properties.

The overall project has been divided in three parts. In the first part, selected biomacromolecules have been used as individual coatings onto polyethylene terephthalate (PET) and polylactid acid (PLA) films and the changes induced by the coating application were investigated by different techniques. Rising from the contact angle investigation, a new potential antifog coating has been disclosed, while the barrier analysis allowed highlighting the great potential of pullulan as oxygen barrier coating even at high relative humidity values. A comparison with some commercial synthetic coatings has also been performed.

Ensuing from the obtained results, the second part of the project focused on the coating barrier performance, with special focus on the nanotechnology approach adopted. Specifically, both a bottom-up and a top-down approach were used. With regards to the former, a metal alkoxides was properly treated and combined with a biopolymer (pullulan) to design a final bio-nanostructure to be applied on PET, and the barrier performance was analyzed; concerning the latter, an inorganic clay was exfoliated through an ultrasonication process and mixed with pullulan; the Design of Experiment technique was then used to optimize the formulation in terms of permeability coefficient ( $P'O_2$ ) at the following condition: 23°C and 70% of relative humidity. The best coating formulation allowed decreasing  $P'O_2$  of ~84% with respect to the bare substrate (PET), and of ~77% with respect to the film composed by PET coated with pure pullulan (i.e without clays). In addition, microscopy analyses revealed some features of these bionanocomposites and supported the indication about a good exfoliation process.

The third and last part of the PhD project, that is still an ongoing project, concerns the simultaneous combination of the aforementioned approaches (i.e. bottom-up and top-down). In principle, this would allow exploiting benefits arising from each individual approach, as well as exploiting any potential synergism.

## **Sviluppo di coatings biopolimerici altamente performanti per applicazioni nel settore dell'imballaggio alimentare**

Il presente lavoro di dottorato ha come scopo l'ottimizzazione dei materiali di confezionamento alimentare attualmente presenti sul mercato. L'obiettivo è sviluppare sottili strati polimerici di copertura (coatings) in grado di migliorare le caratteristiche originali del substrato plastico sul quale vengono depositati. In particolare, per soddisfare la crescente richiesta di sostituzione dei polimeri sintetici e di riduzione del materiale plastico da immettere sul mercato, si è scelto di lavorare con biomacromolecole, eventualmente in combinazione con composti inorganici, per generare una nuova classe di coatings bio-nanocompositi/ibridi. Ciò può portare all'ottenimento di strutture di imballaggio più "eco-compatibili", mantenendo allo stesso tempo le prestazioni dei film tradizionali.

Verranno considerate alcune proprietà dei film finali (coating con substrato plastico), in particolare: la barriera all'ossigeno a condizioni di alta umidità relativa, le proprietà di superficie e le proprietà ottiche.

L'intero progetto può essere suddiviso in tre parti. Nella prima, alcune biomacromolecole sono state selezionate e applicate su polietilene tereftalato (PET), oltre che su film di acido polilattico (PLA): i cambiamenti apportati dall'aggiunta dello strato di coating sono stati confrontati con i films tal quali attraverso l'utilizzo di diverse tecniche sperimentali. In particolare, le analisi di angolo di contatto hanno condotto allo sviluppo di un materiale per applicazioni antifog, mentre le analisi di permeabilità hanno evidenziato come il pullulano, polisaccaride di origine microbica, sia un biopolimero promettente per lo sviluppo di un film barriera alle alte umidità relative. È stato inoltre effettuato un confronto delle performances rispetto a films con coatings commerciali di origine fossile.

Partendo dai risultati fin qui ottenuti, la seconda parte del lavoro si è focalizzata sulle prestazioni dei films in termini di proprietà barriera, ed il settore delle nanotecnologie è stato indagato. In particolare, sono stati considerati due approcci, quello "bottom-up" e quello "top-down". Per quanto riguarda il primo approccio, un alcossido di metallo è stato opportunamente sottoposto a processo sol-gel ed è stato combinato con un biopolimero (pullulano) per ottenere, dopo fase di stesura su film ed evaporazione del solvente, un coating bio-nano-strutturato. Per il secondo approccio, invece, un'argilla (montmorillonite) è stata opportunamente dispersa in soluzione acquosa attraverso un metodo di ultrasonificazione ed è poi stata miscelata con pullulano, per ottenere infine un coating bio-nano-composito. In entrambi i casi le soluzioni bi-componenti di partenza sono state depositate su PET, ottenendo coating dello spessore di  $\sim 1.6 \mu\text{m}$  e  $\sim 0.6 \mu\text{m}$ , rispettivamente. Mentre per il primo approccio sono state considerate sei diverse formulazioni in cui variava il rapporto tra componente inorganica e organica ed è stata poi valutata l'Oxygen Transmission Rate (OTR), nel secondo caso è stata applicata la tecnica del disegno sperimentale (Design of Experiment, DoE), per trovare la formulazione ottimale in grado di dare il più basso valore di coefficiente di permeabilità (permeability coefficient,  $P'O_2$ ) e contemporaneamente un valore di opacità (haze) accettabile ( $\leq 3\%$ ). La migliore formulazione di coating ha permesso di ottenere una diminuzione del valore di  $P'O_2$  (condizioni:  $23^\circ\text{C}$  e  $70\%$  di umidità relativa) di  $\sim 84\%$  rispetto al solo substrato di PET, e di  $\sim 77\%$  rispetto ad uno stesso PET con coating di solo pullulano (senza clays). Inoltre, sono state effettuate delle analisi di microscopia che hanno evidenziato caratteristiche molto interessanti delle strutture nano composite ed hanno confermato l'avvenuta esfoliazione dei clays utilizzati.

La terza e ultima parte del progetto di dottorato, ancora in corso, riguarda la simultanea combinazione dei due approcci sopra citati, con l'obiettivo di sfruttare al meglio i benefici derivanti da ciascun singolo approccio, nonché eventuali sinergie.

# 0. PREFACE

---

This PhD project focused on the optimization of the food packaging plastic materials currently available on the market, pursuing a “green” approach. The increasing worldwide interest in biopolymers as polymer materials led to the idea that their applications as coatings on plastics can be an interesting way to optimize the current packaging solutions. The application of a biopolymer coating has the potential to replace synthetic coatings of oil origin, maintaining or even improving the overall performance of the final structures; moreover, the existing coating deposition technology can be exploited and, finally, a “greener” packaging structure can be obtained.

To achieve these goals, the development of new bio-based coating materials has been undertaken with the overall goal of improving the performance of the final packaging, in particular the barrier against oxygen at high relative humidity values, which is an appealing property for a natural, water-based material. At the same time, a suitable optical appearance was constantly monitored, together with some other important packaging properties, among which surface properties deserve to be mentioned.

The development of new coating architectures has been done following three main steps, which also represent an increasing level of system complexity:

## 1. Phase 1: One-component coatings development

Different biopolymers were tested on the basis of their attitude to form coatings. Physical and chemical characteristics were specifically considered after coating deposition on different plastic and bio-plastic films.

In addition to some analyses made to characterize the final packaging films, a relevant part of the work was devoted to the coatings’ surface properties, by means of the contact angle technique.

In turn, this part brought to a special application, namely an antifog layer.

## 2. Phase 2: Two-component coatings development

The aim of the second part was to overcome some of the drawbacks of the single-component coating, in particular the poor oxygen barrier performance at high relative humidity values.

To address this issue, inorganic components were added to the formulation, following two approaches drawn from nanotechnology:

- the bottom-up approach, to design a nanostructured coating;
- the top-down approach, to design a bionanocomposite coating.

## 3. Phase 3: Three-component coatings development

In the third part the research was focused on the combination of the two aforementioned nanotechnology approaches to create a bionanocomposite hybrid coating. The aim was to gain the best performance in terms of oxygen barrier at high relative humidity value (still ongoing research).

# 1. STATE OF THE ART

For more than 50 years plastics have been used as the most practical, cheaper and useful solutions for food packaging applications. However, over the last decade the interest in using natural resources in order to replace, totally or partially, synthetic packaging has increased, as shown by the number of research papers, reviews and book chapters reported in the scientific literature. The market itself is demanding for sustainable solutions too, as reported by some prediction (Figure 1, web source: European Bioplastic).

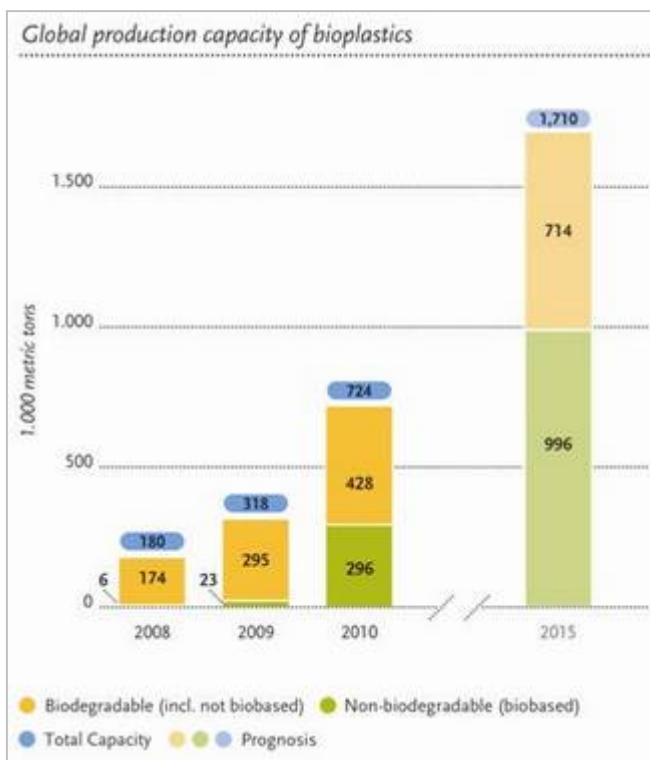


**Figure 1** Source: European Bioplastics, University of Applied Sciences and Arts Hanover (Status May 2011).

In most circumstances, this was due to potential showed by biomacromolecules directly extracted from biomass (proteins, polysaccharides, lipids) or from microorganisms (polyhydroxyalkanoates), or obtained from chemical synthesis (polylactic acid). They have shown properties similar to those of plastic films and they can be used to generate new structures with the additional feature of being biodegradable (Tharanathan 2003). Moreover, they can act as releasing system of active compounds under the effect of specific triggers like temperature, relative humidity, or pH. A wide range of biomacromolecules has already been used in the biomedical field to create capsules, contact lenses, membranes, while in the food packaging area it is only starting to come. Figure 2 reports an overview of bio-based polymers.

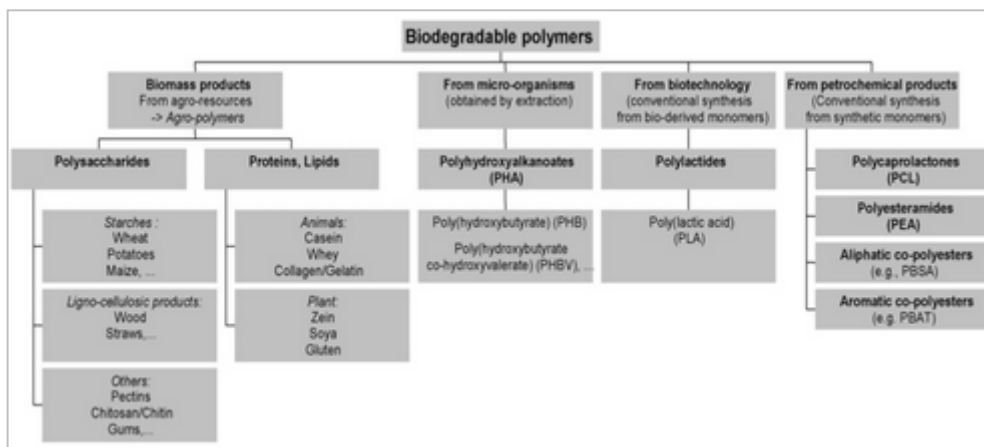


**Figure 2** Classification of biodegradable polymers (Bordes *et al.* 2009).

It is currently acknowledged that replacing food packaging using a stand-alone edible film represents a difficult task to achieve, because of some drawbacks, like poor mechanical properties and the great sensitivity to humidity. A promising way to see biopolymers promptly used as packaging materials is represented by their deposition as thin layers on plastics or bio-derived materials. To date, common plastic films are coated or laminated with synthetic polymers in the form of thin layers in order to increase specific properties of the substrate, such as barrier (to gases, vapors, UV radiations), mechanical (friction of coefficient), optical (transparency), and thermal properties (sealability). Till now these results have been obtained through different approaches:

- ✓ coupling different materials through a “lamination” process, in which different polymers are joined together with a tie, in order to exploit the performance of each individual layer. The main disadvantage of this approach, especially from an environmental impact perspective, is the obtainment of a heavy packaging (often made by more than 5 layers);
- ✓ coating of synthetic polymers of different origin (vinylic, acrylic, inorganic) that bring to an expensive final packaging due to the price of the materials. Some examples are: the use of polyvinyl alcohol (PVOH) or ethylene vinyl alcohol (EVOH), for their oxygen barrier properties up to a relative humidity of about 60%; polyvinylidene chloride (PVDC), for water vapor barrier too and acrylic resins, as cold-sealable layers.
- ✓ plasma deposition or metallization, other surface treatments that involve negative aspects like technical efforts and environmental impact (Farris *et al.* 2009b). In particular, the use of plasma for coating deposition is known as PECVD, plasma enhanced chemical vapor deposition.

The last approach represents the most recent trend, where transparent films able to give the barrier performance of aluminized polymers are required. They are called silicon oxides (SiOx) or aluminum oxide (AlOx) coatings, depending on the metal used during vapor evaporation. Nevertheless, the commercialization of transparent gas barrier coatings is not a simple matter of

depositing this layer, but instead involves the complex interaction between the thin coating, the substrate (polymer film) and the transformations that lead into the final package (Felts 1993). For the aforementioned types of coating, one of the obstacles for a successful commercialization is the flex durability or, in other word, the maintenance of the brittle oxide structures during packaging operations.

It is clear that the replacement of multi-layered structures with lighter, cheaper and bio-based solutions appears a compelling and an attainable opportunity.

Also at a European level there are numerous EU-Initiatives supporting the development of bio-based materials.

The Directive 2008/98/EC on waste (known as the Waste Framework Directive, WFD) gives the guidelines to all Member States about the proper implementation, application and enforcement of EU waste legislation, that is one of the key priorities of EU environmental policy.

Waste legislation and policy of the EU Member States shall apply as a priority order the following waste management hierarchy (web source: ec.europe.eu):

1. Prevention (non-waste)
2. Preparing for re-use
3. Recycling
4. Recovery
5. Disposal

The first point of the hierarchy (prevention) is defined by Article 3(12) WFD as follows:

‘Measures taken before a substance, material or product has become waste that reduce:

- the quantity of waste, including through the re-use of products or the extension of the life span of products;
- the adverse impacts of the generated waste on the environment and human health; or
- the content of harmful substances in materials and products’.

Whereas reducing the amounts of waste can be called quantitative waste prevention, reducing the content of harmful substances in materials and products can be termed qualitative waste prevention (web source: ec.europe.eu).

At a higher level, the Europe 2020, that is the EU's growth strategy for the coming decade, together with its flagship initiative on “A Resource Efficient Europe” (COM (2011)21) underlines the importance of renewable resources in our future economy. (web source: Plastic Europe). As the European President José Manuel Barroso said: “In a changing world, we want the EU to become a smart, sustainable and inclusive economy. These three mutually reinforcing priorities should help the EU and the Member States deliver high levels of employment, productivity and social cohesion” (web source: ec.europe.eu).

If the European Directive underlines the trends for the growth of the future, including the priority to reduce the potential waste material, there is an economical reason too that pushes the researcher to find alternative packaging solutions.

In fact, the use of fossil materials, whose price is increasing, is becoming an important driver in this sense, as visible in Figure 3 (web source: European Bioplastic). Therefore, our reliance on oil should be somehow faced in advance, to avoid being in late when it will come.



**Figure 3** Web source: *European Bioplastics*.

The use of coatings based on biomacromolecules, deposited on plastic webs, is probably one of the most convenient and efficient techniques to see innovative and sustainable new solutions on the market, with the advantage to be a promising way to face the packaging waste disposal issue (Farris et al, 2009c), a key point at a European level too.

Lot of examples of applications can be found in literature, for instance coatings made of whey protein isolate have been credited of excellent both transparency (Hong et al, 2003) and barrier properties against oxygen (Hong et al. 2006), chitosan has been proved to be effective as coating material on paper and paperboard (Gällstedt et al, 2005), gelatin has been applied as a component of thin sealing layers (Farris et al, 2009a).

The use of matrices with different characteristics in the coating formulation could improve some performances of the final films. The coating solutions can be deposited onto different substrates (e.g., flexible plastic films) through different techniques (Farris, 2009d), among which the gravure coating technique seems to afford a number of advantages over other techniques (e.g., reverse roll coaters, calendar coaters, knife-over-roll coaters, blade coating, wire wound rod coater). One important advantage is that removal of the solvent, generally achieved by hot air and infrared lamps, is facilitated by the thin coating thickness achieved by gravure coating (usually from 0.2 to 2  $\mu\text{m}$ ) (Farris et al, 2009c).

Having said that, this PhD project will be specifically addressed to the development of bio-coatings able to provide a high barrier against oxygen at high relative humidity value, which is one of the most appealing properties for a water-based coating. To this scope, biomacromolecules will be tested as coatings, while some of the new, emerging technologies pertaining to the nanotechnology field will be adopted to create engineered structures.

## 1.1 References

- <http://en.european-bioplastics.org/market/> (accessed 13/04/12).
- <http://en.european-bioplastics.org/market/market-development/market-drivers/> (accessed 25/09/12).
- [http://www.plasticseurope.org/documents/document/20120522112447-plastics\\_industry\\_view\\_on\\_bioplastics\\_v16052012.pdf](http://www.plasticseurope.org/documents/document/20120522112447-plastics_industry_view_on_bioplastics_v16052012.pdf) (accessed 12/11/12).
- <http://ec.europa.eu/environment/waste/framework/index.htm> (accessed 12/11/12).
- [http://ec.europa.eu/environment/waste/framework/pdf/guidance\\_doc.pdf](http://ec.europa.eu/environment/waste/framework/pdf/guidance_doc.pdf) (accessed 12/11/12).
- [http://ec.europa.eu/europe2020/index\\_en.htm](http://ec.europa.eu/europe2020/index_en.htm) (accessed 12/11/12).
- Bordes P, Pollet E, Avérous L. 2009, Nano-biocomposites: biodegradable polyester/nanoclay systems. *Prog Polym Sci* 34:125-155.
- Farris S, Cozzolino CA, Introzzi L, Piergiovanni L. 2009a, Effects of different sealing conditions on the seal strength of polypropylene films coated with a bio-based thin layer. *Packag Technol Sci*. 22:359-369.
- Farris S, Introzzi L, Piergiovanni L. 2009b, Evaluation of a bio-coating as a solution to improve barrier, fiction and optical properties of plastic films. *Packag Technol Sci* 22:69-83.
- Farris S, Schaich KM, Liu LS, Piergiovanni L, Yam K. 2009c, Development of polyion-complex hydrogels as an alternative approach for the production of bio-based polymers for food packaging applications: a review. *Trends Food Sci Tech* 20:316-332.
- Farris S. Coating equipment. In *The Wiley Encyclopedia of Packaging Technology*, 3rd Edition, edited by Kit L. Yam, Wiley, 2009d pp. 285-294.
- Felts JT, 1993, Transparent barrier coatings update: flexible substrates. *Society of Vacuum Coaters, 36th Annual Technical Conference Proceedings*.
- Gällstedt M, Brottman A, Hedenqvist MS. 2005, Packaging-related properties of protein- and chitosan-coated paper. *Packag Technol Sci* 18:161-170.
- Hong S, Krochta CM. 2003, Oxygen barrier properties of whey protein isolate coatings on polypropylene films. *J Food Sci* 68:224-228.
- Hong S, Krochta CM. 2006, Oxygen barrier performance of whey-protein-coated plastic films as affected by temperature, relative humidity, base film and protein type. *J Food Eng* 77:739-745.
- Tharanathan RN. 2003, Biodegradable films and composite coatings: past, present and future. *Trends Food Sci Tech* 14:71-78.

## 2. AIM OF THE STUDY

---

### GENERAL AIM

The general aim of this PhD project was the development of new high-performance biopolymer coatings for food packaging applications. It arises from the worldwide need to decrease the amount of food packaging materials that can be found in the market, maintaining at the same time the expected efficiency, namely the same, or even better, shelf-life protection. In other words, the aim was to develop feasible “green” alternatives to the synthetic polymer solutions for food preservation.

In particular, some specific properties of food packaging have been considered, on the basis of the potential market applications of the final films.

These properties are:

- the surface properties
- the oxygen barrier properties
- the optical properties (haze and transparency).

To accomplish this, the engineering of the polymers structure represent the key point to obtain a coating with the final desired characteristics.

Different techniques were exploited to gain the broadest information about the developed coatings, especially:

- the contact angle technique
- the ultrasound treatment based on cavitation phenomena
- the Design of Experiment technique (DoE)
- microscopy analyses
- particle size analysis.

They were used in addition to some of the routine instruments typically used within the food packaging industry (such as the permeabilimeter and the spectrophotometer).

### SPECIFIC AIMS

The main specific aim was the engineering of a high oxygen barrier biocoating at high relative humidity conditions, which represents a challenge for the water based polymers used in this study. Keeping suitable optical appearance of the final films was included in this goal.

On the other hand, the inherent biopolymer water sensitivity has been exploited to develop an antifog layer, which is deemed very important for specific food packaging applications.

Both the mentioned type of coatings represents a big appeal for the industry that want to gain shares of the market with competitive alternative solutions.

# 3. PHASE 1

## ONE-COMPONENT COATING

---

In this first part of the PhD project biopolymers in the form of natural biomacromolecules were considered. They were used as a single component in the coating formulation, and different properties were analyzed after their application on flexible film substrates. The choice of using biomacromolecules directly extracted from biomass (see Fig. 2, par. 1) arises from an economical reason: they do not need chemical modifications or extraction/purification phases. One of the obstacles that prevent a larger use of bio-based plastics is, in fact, the high price due to processes they have to be subjected before commercialization.

The final different films were analyzed mainly to check the oxygen barrier properties and the surface properties, and the different results were explained according to the chemo-physical features of each biopolymer.

## **3.1 Oxygen barrier properties of bio-coated films**

In this part five different biomacromolecules were considered, belonging to two different classes of biomacromolecules: polysaccharides (pectins, chitosan and pullulan) and proteins (gelatin). They were applied both on a plastic film, polyethylene terephthalate (PET) and on a bio-based polymer, i.e. polylactic acid (PLA). This last choice has been made to develop a totally bio-based film, composed by a bio-derived flexible film coated with a bio-polymer.

An important food packaging property was considered for analyses: the oxygen transmission rate at 23°C and at different relative humidity values. Moreover, a comparison with some commercially available coatings has been made.

## 3.1.1 Materials and methods

### 3.1.1.1 Materials

#### 3.1.1.1.a Biopolymers

The following polymers were considered:

- pullulan
- chitosan
- two different pectins
- gelatin

Pullulan (PF-20 grade,  $M_n \approx 200$  kDa, Hayashibara Biochemical Laboratories Inc., Okayama, Japan) is an exopolysaccharides of microbial origin, produced aerobically by the fungus *A. Pullulans*. Its structure can be seen as a series of three glucose units connected by an  $\alpha$ -1,4 glycosidic bond, linked together by an  $\alpha$ -1,6 glycosidic bond (Figure 4).

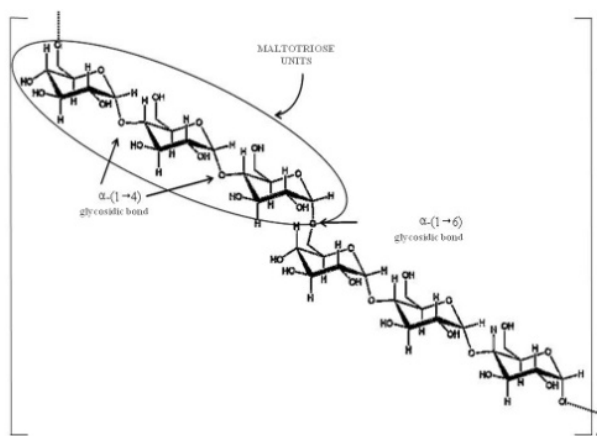


**Figure 4** Pullulan chemical structure.

Chitosan is a polycation polymer (Figure 5) obtained commercially from shrimps and crabshell chitin (a *N*-acetylglucosamine polymer) by alkaline deacetylation (Rabea et al, 2003). In this research shellfish chitosan was used (GiustoFaravelli SpA, Milan, Italy) with a degree of deacetylation of 85% and a molecular weight ranging from 50000 to 60000 (data provided by the supplier).

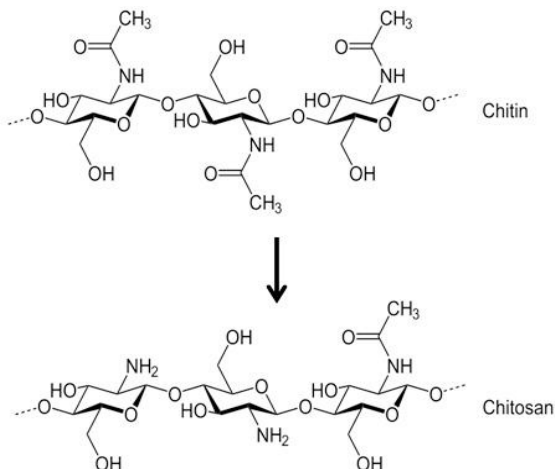


**Figure 5** Chemical structures of chitin and deacetylated chitosan.

Two different pectin were considered:

- high methoxyl pectin with a 72% degree of esterification (DE)
- amidated pectin with a 20% degree of amidation (DA) with a lower DE, 27%.

Both pectins (Genu pectin B-rapid set the former, Genu pectin LM-104-AS the latter) were supplied by CP Kelco, San Diego, CA (Figure 6).

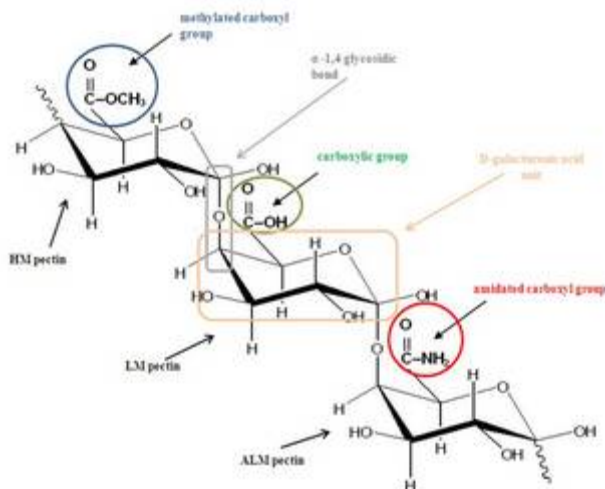


**Figure 6** Representative part of a pectin molecule with the different functional groups.

As a protein (Figure 7), pig skin gelatin powder type A, 133 Bloom (Weishardt International, Grauliet Cedex, France) was used.

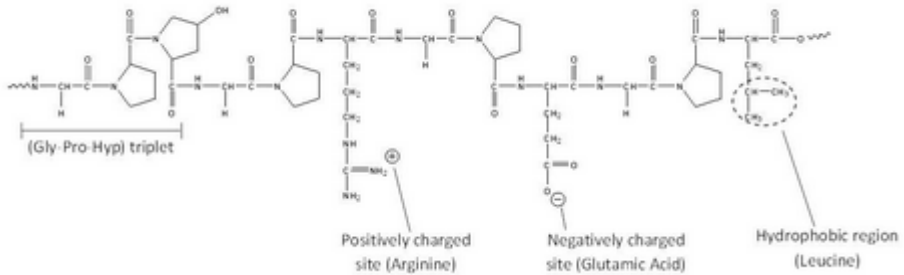


**Figure 7** Representative part of a gelatin molecule.

### 3.1.1.1.b Films (polylactic acid and polyethylene terephthalate)

Two flexible films were considered as coating substrates:

- polyethylene terephthalate (PET)
- polylactic acid (PLA)

The former is a thermoplastic polymer of the polyester family, commonly used in the food packaging field for different purposes, such as liquids container, thermoforming applications, as a layer for flexible packaging solutions. Figure 8 shows the molecular structure of this polymer.

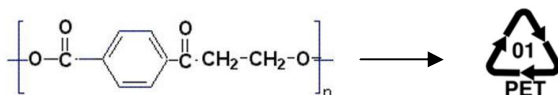


**Figure 8** Molecular structure and plastic identification code of PET.

In this PhD work, PET  $12.0 \pm 0.5 \mu\text{m}$  thick (Radici Film, San Giorgio di Nogaro, Italy) was used as the plastic substrate for coating deposition.

The latter is an aliphatic polyester and is a sustainable alternative to petrochemical-derived products, since its production is a multistep process which starts from the production of lactic acid. Lactic acid is the basic monomer obtained from renewable resources (carbohydrates, such as corn or starch) by fermentation (Avérous et al, 2012).

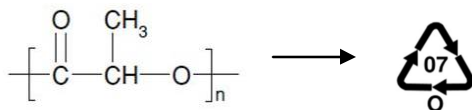


**Figure 9** Chemical structure of PLA (from Avérous et al, 2012) and plastic identification code (“other”).

In this work, PLA  $40.0 \pm 0.5 \mu\text{m}$  thick (Polyfilms SAS, Mantes-la-Ville, France) was used as the bio-based substrate for coating deposition.

### 3.1.1.1.c Oil-based polymers

Two petrol-based polymers were considered as coating materials, to make a comparison with the performance of the final biocoated films:

- Polyvinyl alcohol (PVOH)
- Oxaqua<sup>®</sup>

PVOH (Figure 10) (Mowiol<sup>®</sup> 10-98, Sigma-Aldrich, Milan, Italy), with the following characteristics:

- molecular weight: Mw ~ 61.000
- hydrolysis: 98.0 - 98.8 mol%
- viscosity: 9-11 mPa\*s; 4 % in H<sub>2</sub>O (20 °C)

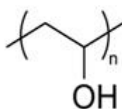


*Figure 10* Chemical structure of PVOH.

As for the second polymer is concerned, it is a product specialty developed by the Metalvuoto Spa (Roncello, MB, Italy) under the brand name “Oxaqua<sup>®</sup>”, a high barrier water based coating for transparent flexible packaging applications. They confidentially provide it as coating solution to carry out the comparison analyses between coated films.

#### Adhesion promoter

Another polymer was considered with the aim to provide an improved adhesion of coating on the substrates, in particular on PLA. It is the water-based primer “P” provided by Flint Group Italia SpA (Cinisello Balsamo, MI, Italy) as a polymer dispersion 50 wt %.

## 3.1.1.2 Methods

### 3.1.1.2.a Coating dispersions preparation

#### Biopolymer coating dispersion preparations

Chitosan water dispersion (3 wt %) was prepared dissolving the polysaccharide powder in acidic water (5 wt % hydrochloric acid, 1M HCl, Sigma-Aldrich) at 25°C for 1h under vigorous stirring (1000 rpm). After 1 hour, the hydrogel was used for coating deposition.

Gelatin (15 wt %) water dispersion was obtained dissolving the protein in distilled water at 60°C for 1 hour under gentle stirring (500 rpm). The temperature was then decreased to 45°C and maintained to prevent gelification. After an additional hour, gelatin hydrogel was coated onto the substrate.

The two types of pectins (DE 72 is the non amidated one; the amidated one is DE 27 DA 20) were separately prepared dissolving the powder in distilled water (3 wt %) at 80°C for 1 hour under vigorous stirring (1000 rpm). The temperature was then decreased to 25°C and after 1 hour the dispersions were ready to coat the substrate.

Pullulan water dispersion (12 wt %) was prepared mixing the polysaccharide in distilled water at 25°C for 1 hour under gentle stirring (500 rpm). An additional hour passed before coating deposition.

#### Oil-based coating dispersion preparations

PVOH powder was dissolved in distilled water (3 wt %) at 90°C for 1 hour, under vigorous stirring (1000 rpm). Then the temperature was decreased to 25°C and after 1 hour the polymer solution was ready for coating deposition.

Oxaqua<sup>®</sup> was provided by the supplier ready to be applied on the film substrates.

The primer P was diluted to 0.5 wt % with a mixture of water/ethanol (95:5) at environmental temperature. It was maintained under gentle stirring for half an hour and then used as promoting agent, applied as a coating solution before the bio-coating/oil-based coating deposition.

### 3.1.1.2.b Coated films preparation

An aliquot of each coating dispersion was placed on the corona treated side of rectangular (24 X 18 cm<sup>2</sup>) PET or PLA film. Specifically, to enhance the adhesion between PLA and biopolymers, PLA surface was previously modified with the deposition of a thin layer (~ 0.02 µm) of primer. The biocoating deposition was performed using an automatic film applicator (ref. 1137, Sheen Instrument, Kingston, U.K.) at a constant speed of 2.5 mm s<sup>-1</sup>, according to ASTM D823-07, practice C. Differences in solid contents among the formulations were reset using horizontal steel rods with different engraved patterns, yielding final coatings with comparable thickness. Water evaporation was performed under a constant and perpendicular flux of mild air (25.0 ± 0.3 °C for 2 min) at a distance of about 40 cm from the applicator. Coated films were then stored under controlled conditions (23 ± 2°C, 40 ± 2.0% RH) for 24

hours. Finally, coated films were stored in a sealed anhydrous desiccator for 24 hours before analyses.

### 3.1.1.2.c Thickness determination

For coating thickness determination, a 10 × 10 cm sample (plastic substrate + coating) was cut and weighed ( $M_1$ ). The coating was then mechanically removed by immersion in hot water (80°C) and the resulting substrate film weighed ( $M_2$ ). The apparent thickness of the coating was obtained according to the following equation:

$$l = \frac{M_1 - M_2}{\rho} \times 100 \quad (1)$$

where  $\rho$  ( $\text{g cm}^{-3}$ ) is the density of the aqueous dispersion. Three replicates were analyzed for each biopolymer.

### 3.1.1.2.d Haze

Haze is defined as the percentage of transmitted light deviating by more than an angle of 2.5° from the direction of the incident beam and it is important especially from a commercial point of view, as it is responsible for the reduction in the contrast between objects viewed through the specimen (e.g., the coated plastic film). For haze determination, a UV-Vis high-performance spectrophotometer (Lambda 650, PerkinElmer, Waltham, MA, USA) was used, coupled with a 150 mm integrating sphere (which allows the trapping of the diffuse transmitted light), in accordance with ASTM D 1003–00. At least three replicates were considered for each film.

### 3.1.1.2.e Oxygen barrier properties

The oxygen barrier properties of both uncoated and coated PET and PLA films were assessed on a 50 cm<sup>2</sup> surface sample using a MultiPerm permeability analyzer (ExtraSolution® Srl, Navacchio, Italy), according to the standard method ASTM F2622-08, with a carrier flow ( $\text{N}_2$ ) of 10 mL min<sup>-1</sup>. With the goal of quantifying the influence of the external relative humidity conditions on the barrier properties of coated films, measurements were performed at 23°C and at five different relative humidity conditions for PET (i.e., 0%, 20%, 40%, 60%, and 80% RH), and at four different relative humidity conditions for PLA (i.e., 0%, 30%, 60%, and 80% RH). The results were expressed as the Oxygen Transmission Rate (OTR, mL m<sup>-2</sup> 24 h<sup>-1</sup> at one atmosphere pressure difference), which has been indicated as the most suitable unit for heterogeneous packaging materials (e.g., multilayer and coated films), that is, whenever a linear relationship between permeability and thickness is not maintained (Lee et al, 2008). The final OTR values were from three replicates for each film.

### 3.1.1.2.f Statistical analysis

The results were analyzed using Statgraphics Plus 4.0 software (STSC, Rockville, MD, USA), and one-way analysis of variance was performed to check the differences between and within groups. The significance level ( $p$ ) was fixed at 0.05.

## 3.1.2 Results and discussion

### 3.1.2.1 Thickness determination

The average coating thickness, determined with equation (1), is here reported:

- $1.11 \pm 0.11 \mu\text{m}$  for biocoatings (Figure 11)
- $1.02 \pm 0.38 \mu\text{m}$  for the oil-based coatings

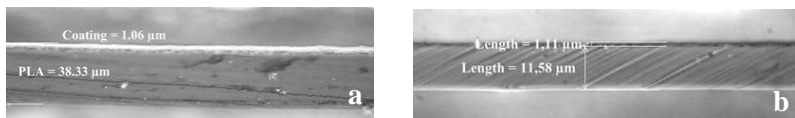


**Figure 11** Optical microscope section images of: PLA film with coating on the left (a); PET film with coating on the right (b).

No statistically significant differences between samples has been revealed ( $p < 0.05$ ). The thicknesses are lower if compared to the coating solutions available on the market: oxygen barrier coatings of EVOH or PVOH, used in multilayer structures, can reach thickness between 3 and 25  $\mu\text{m}$ .

### 3.1.2.2. Haze

The measured haze for PLA film (Table 1), was  $0.99 \% \pm 0.05$ , less than the 3% stated generally by the producers, and considered as the maximum acceptable value for packaging applications where the food product has to be seen clearly by the consumers through the package.

Regarding the coated PLA, only gelatin and the two pectins gave statistically different results compared with the substrate. However, being below 3%, these values agree with the requirements of the PLA's technical sheet.

The obtained results probably reflect the morphology of the bio-coatings and their irregularities at the surface level, rather than the chemical structure, as highlighted by Hernandez et al, 1997.

**Table 1** Haze values (%) for uncoated and coated PLA and PET films

Film	PLA	PET
Substrate	$0.99 \pm 0.05^a$	$1.50 \pm 0.05$
+ pectin DE 72	$1.72 \pm 0.21^{bc}$	$2.08 \pm 0.23$
+ pectin DE 27 DA 20	$1.98 \pm 0.11^c$	$2.35 \pm 0.13$
+ chitosan	$1.74 \pm 0.73^{bc}$	$1.84 \pm 0.19$
+ gelatin	$1.05 \pm 0.15^{ad}$	$1.33 \pm 0.09$
+ pullulan	$1.20 \pm 0.13^{bd}$	$1.44 \pm 0.16$
+ PVOH 10-98	$1.27 \pm 0.11^d$	n.d.
+ Oxaqua®	$1.23 \pm 0.07^d$	n.d.

*Different letters denote statistically significant differences ( $p < 0.05$ )*

### 3.1.2.3 Oxygen barrier properties

Table 2 and Figure 12 show the results obtained from the OTR analysis of the different PLA films at different relative humidity values.

Starting from the bare substrate, the observed results are typical for a medium-barrier film, thus confirming what stated in the technical data-sheet provided by the supplier. It can be noticed that the decrease of permeability from 0% to 80% RH it is due to an occupancy of the free volume by water molecules that start to compete with the oxygen ones, bringing to a reduction of the gas solubility (Auras et al, 2004) and, therefore, of OTR values.

The application of biopolymer coatings brought to an almost totally reduction of permeability at least in anhydrous conditions, except for gelatin which has a slight higher value if compared with the other ones. A good barrier is maintained till 60% of relative humidity, then the permeability increases exponentially. Pectins revealed the higher barrier at 0% RH, followed by chitosan, pullulan and finally gelatin. At 80% RH, the scenario changes oppositely (except for pullulan): films with pectins lost their barrier capacity, while PLA + gelatin even shows a barrier capacity. As for pullulan is concerned, it revealed the lowest OTR values at 80% RH, similarly to PVOH at the same thermo-hygrometric conditions.

It is reasonable to explain the trends observed on the basis of the physio-chemical characteristics of the biopolymers used. It is well known that the chemical groups in polymers are one of the main factors affecting permeability. In this respect, it is well known that all biopolymers, especially polysaccharides, have a high hydrophilic character, basically due to the high number of -OH groups. It is well known that these groups, (together with other groups such as amino groups), are responsible for the barrier performance (Lange et al, 2002) of materials, due to the formation of hydrogen bonds. However, not only the chemical groups are responsible for the barrier performances of a film. Other factors are related for example to the crystallinity, chain stiffness, orientation, free volume (Zhang et al, 2001). Pectins, for example, have a more crystalline structure than other biopolymers, together with a rigid and compact organization owing to the linear structure given by D-galacturonic acid (GalA) units (from a few hundred to about 1000 saccharide) joined together by  $\alpha$ -1,4 glycosidic linkages in a chain-like configuration. In turn, chains arrange relative to each other through extensive hydrogen bonding (Sriamornsak, 2003). Eventually, such physicochemical organization could be the reason for the good barrier performances they maintain up 60% relative humidity condition.

However, as the relative humidity increases, the physical structure of biopolymers starts changing due to the interaction of water molecules with the polar hydroxyl groups along the biopolymer backbone (Zhang et al, 2001). Ultimately, this leads to an increase in the mobility of oxygen molecules in the polymer bulk phase (Mujica-Paz et al, 1997). Therefore, whereas at 40% RH biopolymers generally retain their structure, at approximately 60% RH the vapor tension is significantly high insomuch as water molecules hinder the establishment of inter- and intra-molecular hydrogen bonds. This phenomenon is even marked for biopolymers that can establish less intra-molecular hydrogen bonds, such as chitosan and, to a minor extent, gelatin. Gelatin in particular, due to its hydrophobic aminoacids (leucine, valine, phenylalanine, isoleucine and methionine), does not totally lose its barrier capacity at 80% RH, as it happens, conversely, for pectins. The gelatin performance can be useful in food packaging application where a total barrier is not required, but where improving the barrier properties of some highly permeable substrates (e.g., PLA) is a sought-after requirement to prolong the shelf-life of vegetables products.

As for chitosan, it is important to note that at 60% RH the OTR value has a higher increase than the other biopolymers, and this can be ascribed to the non-polar impurities present in even the highest-quality commercial samples, as pointed out by Cunha et al, 2008. It is the presence of

apolar components that reduce the film's oxygen barrier, because they hinder the formation of intramolecular hydrogen bonds.

Among all the matrices analyzed, pullulan appears as the most intriguing polymer, because despite its high hydrophilicity, it resembles the synthetic coating performances, revealing itself as a potential substitute of petroleum-derived polymers. This behavior has been attributed (Leathers, 2003) to its unique pattern, in which the presence of  $\alpha$ -(1-6) linkages interrupt what would be a linear amylose chain. This feature confers flexibility and other characteristics lacking in many other polysaccharides.

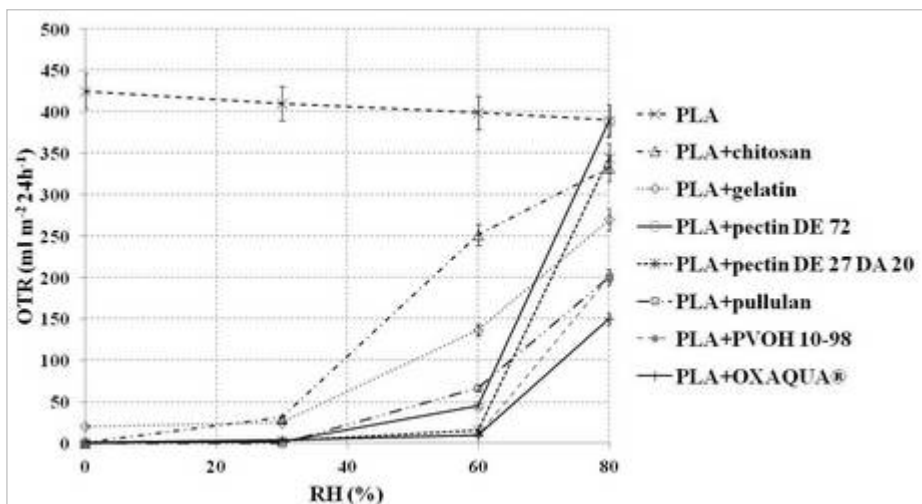


Figure 12 OTR trends of uncoated and coated PLA films at 23°C and at four different relative humidity values.

Table 2 OTR values of uncoated and coated PLA films at 23°C and at four different relative humidity values.

OTR 23°C (mL m <sup>-2</sup> 24h <sup>-1</sup> )	Relative Humidity (%)			
	0	30	60	80
PLA	428.00 ± 4.24 <sup>aE</sup>	411.50 ± 2.12 <sup>aH</sup>	400.00 ± 1.41 <sup>aO</sup>	391.00 ± 1.41 <sup>aP</sup>
PLA + pectin DE72	0.70 ± 0.28 <sup>jBC</sup>	1.88 ± 0.40 <sup>iF</sup>	42.95 ± 2.66 <sup>kL</sup>	337.05 ± 74.26 <sup>iPQ</sup>
PLA + pectin DE27 DA20	0.48 ± 0.25 <sup>mC</sup>	2.60 ± 0.24 <sup>nFG</sup>	14.59 ± 0.99 <sup>oJ</sup>	341.57 ± 3.92 <sup>pPQ</sup>
PLA + chitosan	1.38 ± 0.67 <sup>bB</sup>	23.99 ± 2.67 <sup>cI</sup>	271.73 ± 28.11 <sup>dN</sup>	353.07 ± 28.95 <sup>eP</sup>
PLA + gelatin	18.74 ± 2.45 <sup>dD</sup>	23.58 ± 1.45 <sup>qI</sup>	134.96 ± 2.96 <sup>rK</sup>	270.92 ± 1.03 <sup>sQR</sup>
PLA + pullulan	0.91 ± 0.06 <sup>iBC</sup>	3.79 ± 0.87 <sup>eF</sup>	80.84 ± 19.31 <sup>hM</sup>	228.80 ± 39.99 <sup>iRS</sup>
PLA + PVOH 10-98	0.81 ± 0.06 <sup>xBC</sup>	3.05 ± 0.56 <sup>yFG</sup>	7.98 ± 2.01 <sup>zJ</sup>	165.49 ± 49.21 <sup>aS</sup>
PLA + Oxaqua®	1.09 ± 0.15 <sup>iBC</sup>	3.29 ± 0.49 <sup>uFG</sup>	9.90 ± 0.35 <sup>vJ</sup>	151.65 ± 2.21 <sup>wS</sup>

Different letters denote statistically significant differences ( $p < 0.05$ )

The trends observed for PLA bio-coated films is the same as for the bio-coated PET (Figure 13).

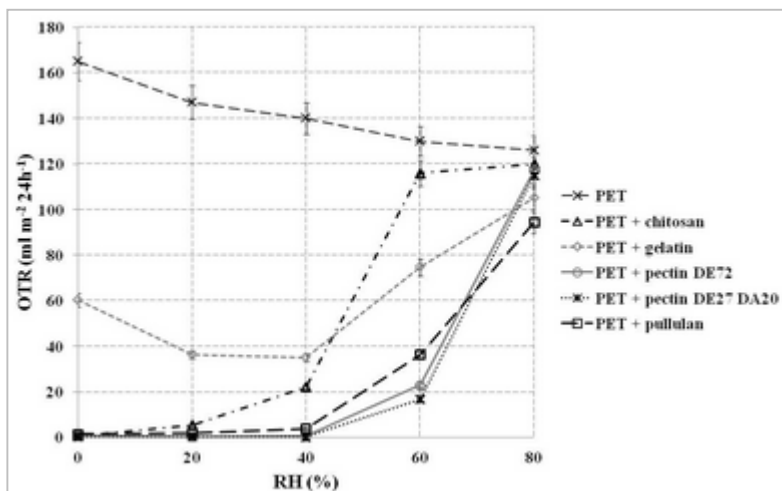


Figure 13 OTR trends of uncoated and coated PET films at 23°C and at five different relative humidity values.

To understand the contribution of each individual coating to the overall barrier performance of the final films, the following equation (2), usually used for multi-layers film, can be used (Labuschagne et al, 2008):

$$OTR_{coating} = \frac{1}{\frac{1}{OTR_{total}} - \frac{1}{OTR_{PLA}}} \tag{2}$$

The results for PLA films are reported in Table 3.

Table 3 OTR values of the different single layers on PLA, calculated from equation (2).

OTR 23°C (mL m <sup>-2</sup> 24h <sup>-1</sup> )	Relative Humidity (%)			
	0	30	60	80
PLA	428.00	411.50	400.00	391.00
Pectin DE 72	0.70	1.89	48.13	2482.52
Pectin DE 27 DA 20	0.48	2.62	15.14	2750.62
Chitosan	1.38	25.48	851.89	3728.60
Gelatin	19.60	25.02	203.94	887.29
Pullulan	0.91	3.83	101.38	553.55
PVOH 10-98	0.81	3.07	8.14	287.48
Oxaqua®	1.09	3.32	10.15	248.14

These results confirm the general exponential trend ensuing from the effect arising from a constant increase of the relative humidity, as also seen before. In addition, it is worth noting that the barrier effect due to the coating on the final OTR values is increasingly less significant as the RH increases. Moreover, it can be noticed that at 80% RH, only the commercial coating

Oxaqua<sup>®</sup> still retains an oxygen barrier capacity that is below the PLA film; the biopolymers, and the PVOH coating as well, reveal values that reflect their higher hydrophilic nature, due to the extensive distribution of –OH groups.

### 3.1.3 Conclusions

The obtained results indicated that the deposition of biopolymers can successfully modify the performance of food packaging flexible films. In particular, the final oxygen barrier properties of the films improved without worsening their optical appearance and these improvements can be attributed to the chemo-physical characteristics of the biopolymers used. It is worth mentioning that the thickness of the coatings was  $1.11 \pm 0.11 \mu\text{m}$ , which is lower than the commercially available barrier coatings (such as PVOH or EVOH, generally 3 to 25  $\mu\text{m}$  thick).

In addition, the combination of such kind of biopolymer coatings with a bio-based substrate such as PLA can be a promising way to see a fully bio-based packaging with enhanced features, reducing the amount of plastics on the market.

In details, films with biocoatings determine an increase in the oxygen barrier property especially at low relative humidity values, then the OTR increases almost exponentially: this would suggest to use pure biopolymers only to package food with low water activity and to be stored at low temperatures (e.g. refrigerator) and dry conditions.

In conclusion, the results obtained until now represent the basis to improve the final performance of the films, performances which can be accomplished by working both on the formulation and on the process, in such a way to widen the biocoating barrier capacity to higher relative humidity values.

### 3.1.4 References

- Auras R, Harte B, Selke S. 2004, Effect of water on the oxygen barrier properties of poly(ethylene terephthalate) and polylactide films. *J Appl Polym Sci* 92:1790–1803.
- Avérous L, Pollet E. Biodegradable polymers. In *Environmental silicate Nano-Biocomposites*, Springer 2012, pp 13-39.
- Cunha AG, Fernandes SCM, Freire CSR, Silvestre AJD, Neto CP, Gandini A. 2008, What is the real value of chitosan's surface energy? *Biomacromolecules* 9:610–614.
- Hernandez R (1997) Polymer properties. In *The Wiley Encyclopedia of Packaging Technology*, 2nd edn, Brody AL, Marsh KS (eds). John Wiley and Sons Inc.: New York, 1997, pp 758–765.
- Labuschagne PW, Germishuizen WA, Verryn SMC, Moolman FS. 2008, Improved oxygen barrier performance of poly(vinyl alcohol) films through hydrogen bond complex with poly(methyl vinyl ether-co-maleic acid). *Eur Polym J* 44:2146-2152.
- Lange J, Nicolas B, Galy J, Gerars JF. 2002, Influence of structure and chemical composition on oxygen permeability of crosslinked epoxy-amine coatings. *Polymer* 43:5985-5994.
- Leathers TD. 2003, Biotechnological production and applications of pullulan. *Appl Microbiol Biotechnol* 62:468-473.
- Lee DS, Yam KL, Piergiovanni L. Permeation of gas and vapor. In *Food Packaging Science and Technology*. CRC Press: Boca Raton, FL, 2008 pp. 79-108.
- Mujica-Paz H, Gontard N. 1997, Oxygen and carbon dioxide permeability of wheat gluten film: effect of relative humidity and temperature. *J Agric Food Chem* 45:4101-4105.
- Rabea EI, Badawy ME-T, Stevens CV, Smaghe G, Steurbaut W. 2003, Chitosan as antimicrobial agent: applications and mode of action. *Biomacromolecules* 4:1457-1465.
- Sriamornsak P. 2003, Chemistry of pectin and its pharmaceutical uses: a review. *Silpakorn University International Journal*, 3:206–228.
- Zhang Z, Britt IJ, Tung MA. 2001, Permeation of oxygen and water vapor through EVOH films as influenced by relative humidity. *J Appl Polym Sci* 82:1866-1872.

## 3.2 Surface properties of bio-coated films

In this part of the PhD research the biomacromolecules as described in the section 3.1 were considered and applied on a PET film, to investigate the modifications occurred on the surface of the final film after the deposition of the biomacromolecules in the form of coatings. The possibility of modifying the surface properties of packaging materials by the deposition of biocoatings has not so far been fully investigated. There are very few detailed works in the literature dealing with the behavior of different biopolymer-coated surfaces in respect to water, especially concerning the physicochemical phenomena involved at the solid/liquid interface. Most papers mainly focus on the wettability of polymer systems after some chemically induced modifications (e.g. crosslinking, grafting, etc.) and the addition of a minor polymer phase. Indeed, new theoretical findings on the surface properties of biopolymers can provide a supplementary understanding of film behavior, leading to an enhanced design of new materials (Han et al, 2005). In this direction, a strict comparison of the surface features of different biopolymers through a systematic approach might be very useful as a screening tool, especially for designing new bio-based structures carrying new surface attributes that can profitably be exploited in many fields like packaging (Tang et al, 2007; Bangyekan et al, 2006; Jin et al, 2004; Kampeerappun et al, 2007; Karbowski et al, 2006a). Accordingly, Karbowski and co-workers have emphasized the necessity for more insightful studies on the surface properties of solids, especially for the packaging industry (Karbowski et al, 2006b). From this perspective, the possibility of tuning, in a controlled manner, the wettability properties of packaging materials can pave the way to new specific applications.

To investigate the surface properties of polymers, the contact angle technique is one of the most established methods. It allows the geometric measurement of the angle  $\theta$  formed at the intersection of the liquid, gas and solid phases, thus providing a direct evaluation of surface wettability. According to Białopiotrowicz and Jańczuk, 2002, the contact angle technique is also very helpful for obtaining information about the structure of the matrix, especially when dealing with biopolymer substrates. In addition, the development of sophisticated, easy-to-use software has greatly improved the overall performance of contact angle instruments. Surface wettability can be quantified not only on the basis of the relevant energy ( $\text{J m}^{-2}$ ), but also according to the results of any specific mechanisms (i.e. absorption, spreading and swelling) which are reflected by changes in  $\theta$  at the liquid/solid interface. The phenomenological kinetics of these changes enables a description of the trend of the experimental data (Karbowski et al, 2006a; Muszynski et al, 2003).

Based on these assumptions, the aim of this part of the work was to investigate the wettability of biopolymers with potential applications as coating materials by monitoring the changes in  $\theta$ . For this purpose, a simple decay function was firstly fitted to the experimental  $\theta$  data, while a combined contact angle (CA)/image analysis (IA) approach was used in a second step in order to elucidate the different physicochemical phenomena involved at the solid/liquid interface and their correlation with the surface topography.

The work presented in this part is here reported:

Farris S, Introzzi L, Biagioni P, Holz T, Schiraldi A, Piergiovanni L. 2011, Wetting of biopolymer coatings: contact angle kinetics and image analysis investigation. *Langmuir*. 27:7563-7574.

## 3.2.1 Materials and methods

### 3.2.1.1 Materials

Five biopolymers were considered: gelatin, chitosan, 2 types of pectins and pullulan. See paragraph 3.1.1.1.a for details.

The substrate for coating deposition was PET film: see paragraph 3.1.1.1.b for details.

### 3.2.1.2 Methods

#### 3.2.1.2.a Coating dispersions preparation

See paragraph 3.1.1.2.a (biopolymer coating dispersion preparations).

#### 3.2.1.2.b Coated films preparation

See paragraph 3.1.1.2.b.

#### 3.2.1.2.c Thickness determination

See paragraph 3.1.1.2.c.

#### 3.2.1.2.d Contact angle measurements

Contact angle analyses were performed using an optical contact angle apparatus (OCA 15 Plus – Data Physics Instruments GmbH, Filderstadt, Germany) equipped with a video measuring system with a high resolution CCD camera and a high performance digitizing adapter. The software SCA 20 (Data Physics Instruments GmbH, Filderstadt, Germany) was used for data acquisition. Rectangular ( $5 \times 2$  cm) coated plastic films were fixed and kept flat throughout the analysis by means of a special sample holder with parallel clamping jaws. The contact angle of water in air was measured by the sessile drop method, by gently dropping a droplet of  $4 \pm 0.5$   $\mu\text{L}$  of Milli-Q water ( $18.3 \text{ M}\Omega$ ) onto the coated surface of the plastic substrate. The whole analysis was conducted at  $20$   $^{\circ}\text{C}$ . The evolution of the contact angle ( $\theta$ , the angle between the baseline of the drop and the tangent at the drop boundary), the droplet volume ( $V$ ,  $\mu\text{L}$ ), the droplet surface area ( $A$ ,  $\text{mm}^2$ ), the droplet height ( $h$ , mm), and the droplet basal diameter ( $2r$ , mm) were monitored using a software-assisted image processing procedure. The values of these parameters were collected 12.5 times per second with a video-capturing system, starting from the deposition of the drop ( $t_0 = 0$  s) up to 8 min after ( $t_{480} = 480$  s). A minimum of 10 droplets were examined for each polymer sample on both the left and right sides and the resulting mean  $\theta$  values were then used for the following calculations. With the goal of gathering further information about the influence of the surface chemistry of biopolymers on the interaction between the water droplet and the coatings, advancing contact angle measurements were also conducted by continuously dispensing  $0.15$   $\mu\text{L}$  of liquid onto a  $2$   $\mu\text{L}$  droplet previously deposited on the coating surface, according to the sessile drop ‘needle-in’ method. The advancing contact angle was then considered as the angle measured at the plateau of  $\theta$  versus the time plot. The surface energy of the different films was calculated by means of the van Oss’

adaptation of Young's theory (van Oss, 2003), with the aid of the software SCA 21 (Data Physics Instruments GmbH, Filderstadt, Germany). In particular, the quantitative determination of all of the surface thermodynamic properties of the five biopolymers coatings was performed using the Young-Dupré equation (van Oss, 1994):

$$(1 + \cos \theta_a) \gamma_L = 2 \left( \sqrt{\gamma_S^{LW} \gamma_L^{LW}} + \sqrt{\gamma_S^+ \gamma_L^-} + \sqrt{\gamma_S^- \gamma_L^+} \right) \quad (3)$$

where:

- $\theta_a$  = advancing contact angle ( $^\circ$ )
- $\gamma_L$  = surface tension of the liquid in contact with the solid surface ( $\text{mJ/m}^2$ )
- $\gamma_L^{LW}$  = apolar component (LW) of the surface tension of the liquid ( $\text{mJ/m}^2$ )
- $\gamma_L^+$  = electron-acceptor parameter of the polar component (AB) of the liquid ( $\text{mJ/m}^2$ )
- $\gamma_L^-$  = electron-donor parameter of the polar component (AB) of the liquid ( $\text{mJ/m}^2$ )
- $\gamma_S^{LW}$  = apolar component (LW) of the surface energy of the solid ( $\text{mJ/m}^2$ )
- $\gamma_S^+$  = electron-acceptor parameter of the polar component (AB) of the solid ( $\text{mJ/m}^2$ )
- $\gamma_S^-$  = electron-donor parameter of the polar component (AB) of the solid ( $\text{mJ/m}^2$ )

Moreover, the following relationships applied (van Oss et al, 1988):

$$\gamma_S^{LW} = \frac{A_i}{24\pi l_0^2} \quad (4)$$

where  $A_i$  is the Hamaker constant (J) and  $l_0$  the minimum equilibrium distance to which two condensed-phase surfaces can approach one another ( $= 0.157 \pm 0.01 \text{ nm}$  at  $20^\circ\text{C}$ );

$$\gamma_S^{AB} = 2\sqrt{\gamma_S^+ \gamma_S^-} \quad (5)$$

$$\gamma_S = \gamma_S^{LW} + \gamma_S^{AB} \quad (6)$$

where  $\gamma_S^{AB}$  is the polar (AB) surface energy component of the solid surface ( $\text{mJ/m}^2$ ) and  $\gamma_S$  the surface energy of the solid in contact with the liquid ( $\text{mJ/m}^2$ ). Since  $\gamma_L$ ,  $\gamma_L^{LW}$ ,  $\gamma_L^+$  and  $\gamma_L^-$  were known, the three thermodynamic parameters (i.e.  $\gamma_S^{LW}$ ,  $\gamma_S^+$ , and  $\gamma_S^-$ ) related to the solid surfaces were determined by measuring the  $\theta_a$  of three different liquids, two polar (i.e. water and formamide) and one apolar (i.e. diiodomethane) (Tables 4a and 4b).

**Table 4a** Surface tension components ( $\gamma_L^{LW}$  and  $\gamma_L^{AB}$ ) and parameters of  $\gamma_L^{AB}$  ( $\gamma_L^+$  and  $\gamma_L^-$ ) for water, formamide and diiodomethane, in  $\text{mJ/m}^2$  at  $20^\circ\text{C}$ .<sup>a</sup>

Liquid	Thermodynamic parameter				
	$\gamma_L$	$\gamma_L^{LW}$	$\gamma_L^{AB}$	$\gamma_L^+$	$\gamma_L^-$
Water	72.8	21.8	51.0	25.5	25.5
Formamide	58.0	39.0	19.0	2.28	39.6
Diiodomethane	50.8	50.8	0	$\approx 0.01$	0

<sup>a</sup>Adapted from van Oss (van Oss, 2003)

**Table 4b** Advancing contact angles ( $\theta_a$ ), surface energy components ( $\gamma_s^{LW}$  and  $\gamma_s^{AB}$ ) and parameters of  $\gamma_s^{AB}$  ( $\gamma_s^+$  and  $\gamma_s^-$ ) for the five biopolymers coatings tested in this work.

Solid	Thermodynamic parameter							
	$\theta_{a(w)}$ <sup>a</sup>	$\theta_{a(f)}$ <sup>b</sup>	$\theta_{a(d)}$ <sup>c</sup>	$\gamma_s$	$\gamma_s^{LW}$	$\gamma_s^{AB}$	$\gamma_s^+$	$\gamma_s^-$
Chitosan	97.55 ±1.79	58.31 ± 3.60	25.09 ± 1.25	46.21	46.21	0	0.03	0
Gelatin	81.68 ± 2.56	59.89 ± 0.88	48.40 ± 2.41	37.39	35.16	2.23	0.24	5.2
Pectin DE 72	89.99 ±1.94	86.81 ± 3.45	41.19 ± 2.86	38.82	38.82	0	0	13.5
Pectin DE 27 DA 20	92.47 ± 2.24	39.98 ± 1.47	41.84 ± 1.58	38.54	38.54	0	4.97	0
Pullulan	68.99 ± 2.03	76.36 ± 6.29	28.23 ± 2.76	44.72	44.72	0	0	35.59

<sup>a</sup>Advancing water contact angle; <sup>b</sup>advancing formamide contact angle; <sup>c</sup>advancing diiodomethane contact angle

### 3.2.1.2.d Atomic force microscopy

Atomic force microscopy images were collected in soft contact mode, and stabilized by means of the standard optical lever method with a very small force offset, using a commercial setup (AlphaSNOM, WITec GmbH, Germany). The height variation in the resulting topography maps is represented by a color scale, in which bright and dark colors denote higher and lower areas for all images, respectively. Although most of the relevant information can be directly and reliably inferred by simple visual inspection of the acquired maps, the root mean square roughness  $S$  was also evaluated for each sample as the standard deviation of the topography over the  $25 \times 25 \mu\text{m}^2$  scanning area ( $M \times N$  pixels):

$$S = \sqrt{\frac{1}{MN} \sum_{i=1}^M \sum_{j=1}^N |z(x_i, y_j) - \bar{z}|^2} \quad (7)$$

where  $\bar{z}$  is the mean value of the topography  $z(x,y)$ .

### 3.2.1.2.f Modeling and statistical analysis

In order to describe the phenomenology of the water droplet kinetics, a semi-empirical approach was used where a decay function was fitted to the experimental contact angle data with no intended physical meaning (physical models of the process were beyond the scope of the present work). Nonlinear curve-fitting software (Tablecurve 4.0, Jandel Scientific, San Rafael, CA) was used. The time derivative of the fitting function was then plotted in order to evaluate the rate of contact angle evolution ( $^\circ \text{s}^{-1}$ ). The results were analyzed using Statgraphics Plus 4.0 software (STSC, Rockville, MD, USA), and one-way analysis of variance was used to check for differences between and within groups. The significance level ( $p$ ) was fixed at 0.05.

## 3.2.2 Results and discussion

### 3.2.2.1 Coating thickness

The average coating thickness, determined according to equation (1), was  $1.18 \pm 0.13 \mu\text{m}$ , with no statistically significant difference between samples ( $p < 0.05$ ).

### 3.2.2.2 Contact angle measurements

At the beginning, the overall trend of the water droplet profile was monitored during a long (8 min) temporal window. As can be seen from Figure 14, although appreciable differences were detected between the biopolymers, variations in  $\theta$  mostly occurred within the first 60 s of analysis. Thus, mathematical treatment of the experimental  $\theta$  data was limited to this narrower time period (60 s), which contained most of the information on the main physical phenomena occurring at the biopolymer/water interface.

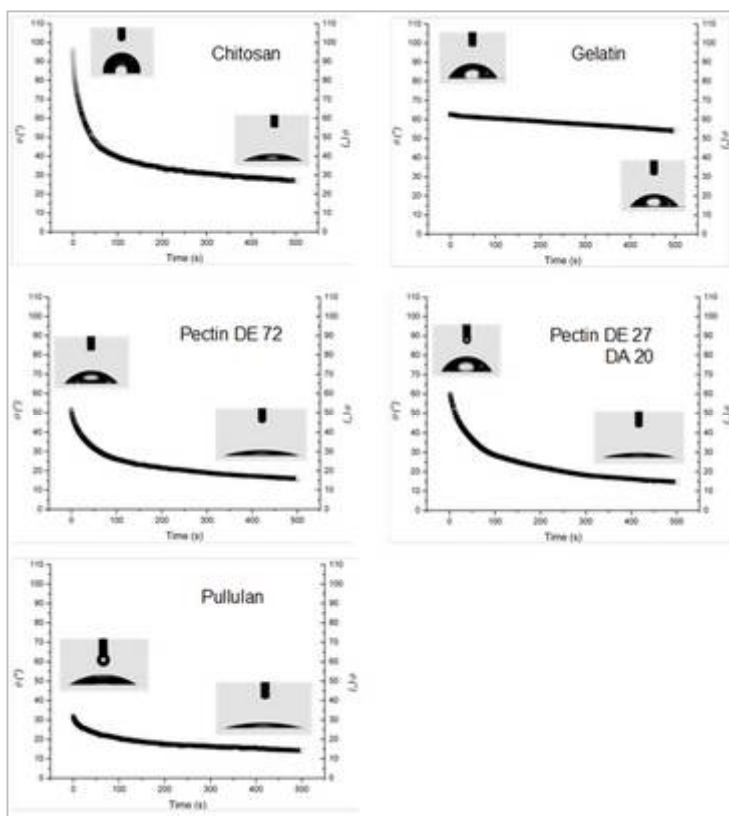


**Figure 14** Mean observed water contact angle evolution over 8 min of monitoring.

It is well established that the main driving forces governing drop evolution on biopolymer surfaces are absorption (Karbowiak et al, 2006a) spreading (Modarelli et al, 2002), swelling (Kokoszka et al, 2010) and evaporation (Solaro et al, 2010). In the present work, the

contribution of evaporation to the total water droplet kinetics was first examined by directly measuring the contact angle on the neat plastic substrate (PET), according to the method proposed by Karbowskiak and co-workers (Karbowskiak et al, 2006b). As shown in Table 5 (first row), the effect of evaporation can be considered negligible, because no statistically significant differences were detected between the contact angle values recorded throughout the 60 s time span of the analysis.

**Table 5** Main parameters derived from CA measurements of the uncoated PET substrate and the five biopolymer coatings. The presumed phenomena involved are reported in the last column on the right.

Substrate	$\theta$ ( $^{\circ}$ ) <sup>A</sup> $t_0$	$\theta$ ( $^{\circ}$ ) <sup>B</sup> $t_{60}$	$\Delta\theta$ ( $^{\circ}$ ) <sup>C</sup> $t_{60} - t_0$	$\Delta V$ ( $\mu\text{l}$ ) <sup>D</sup> $t_{60} - t_0$	$\Delta A$ ( $\text{mm}^2$ ) <sup>E</sup> $t_{60} - t_0$	Phenomenon
PET	52.40 <sup>a</sup> $\pm 1.42$	51.88 <sup>a</sup> $\pm 1.45$	-0.53 $\pm$ 0.03	-0.05 <sup>f</sup> $\pm$ 0.008	-0.04 <sup>c</sup> $\pm$ 0.02	Evaporation (negligible)
Chitosan	91.53 <sup>l</sup> $\pm 6.97$	52.26 <sup>a</sup> $\pm 5.05$	-39.27 $\pm 4.63$	-0.36 <sup>i</sup> $\pm$ 0.11	0.98 <sup>s</sup> $\pm$ 0.38	Absorption + spreading
Gelatin	65.93 <sup>m</sup> $\pm 1.67$	63.62 <sup>q</sup> $\pm 1.82$	-2.31 $\pm$ 0.44	-0.13 <sup>gh</sup> $\pm$ 0.05	-0.7 <sup>c</sup> $\pm$ 0.11	Absorption + spreading
Pectin DE72	54.12 <sup>n</sup> $\pm 4.50$	35.49 <sup>b</sup> $\pm 1.50$	-18.63 $\pm 3.09$	-0.12 <sup>gl</sup> $\pm$ 0.05	2.52 <sup>d</sup> $\pm$ 0.27	Spreading
Pectin DE27 DA20	58.34 <sup>o</sup> $\pm 2.92$	33.98 <sup>b</sup> $\pm 1.06$	-25.04 $\pm 3.14$	-0.19 <sup>i</sup> $\pm$ 0.10	3.07 <sup>e</sup> $\pm$ 0.79	Spreading
Pullulan	30.58 <sup>p</sup> $\pm 1.22$	23.83 <sup>r</sup> $\pm 1.26$	-6.75 $\pm$ 0.72	-0.19 <sup>hl</sup> $\pm$ 0.07	2.35 <sup>de</sup> $\pm$ 0.24	Spreading

<sup>A</sup>Initial contact angle; <sup>B</sup>final contact angle; <sup>C</sup>contact angle variation during the time of analysis (60s); <sup>D</sup>water droplet volume variation; <sup>E</sup>drop surface area variation. Different small letters denote statistically significant differences ( $p < 0.05$ ).

Given the negligible evaporation effects, the contact angle evolution was considered as being related to changes in the droplet volume and the solid/liquid surface contact area for all biocoatings tested in this work. This would reflect, at least in the early stages, two different physicochemical phenomena occurring at the solid/liquid interface: absorption and spreading. At first glance, rather large differences in  $\theta$  were observed within the first 60 s for the five biocoatings analyzed in this work. This evidence was confirmed by the data reported in Table 5 and by Figure 15, which displays water droplet images recorded:

- immediately after droplet deposition ( $t_0$ );
- after 30 s ( $t_{30}$ );
- after 60 s ( $t_{60}$ ) of analysis.

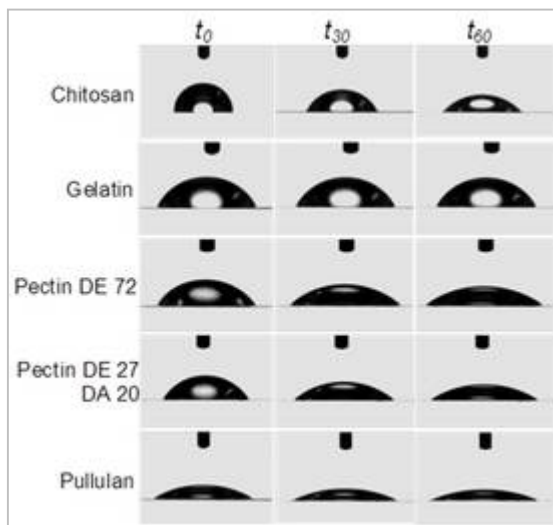


**Figure 15** Water droplet images captured immediately after droplet deposition ( $t_0$ ), after 30 s ( $t_{30}$ ), and after 60 s ( $t_{60}$ ) of analysis.

According to the widely accepted relationship between contact angle and hydrophobicity (Vogler, 1998) the initial contact angles values,  $\theta_0$ , suggested that only chitosan behaved as a fully hydrophobic polymer ( $\theta \sim 90^\circ$ ), whereas the gelatin-coated surface exhibited a less pronounced hydrophobicity ( $\sim 66^\circ$ ). Clearly, the biocoatings obtained from the pectins and pullulan displayed hydrophilic features ( $\theta \sim 55^\circ$  and  $\sim 30^\circ$ , respectively). However, with the exception of gelatin, this trend was not observed throughout the 60 s of analysis. Indeed, the contact angles changed as the analysis progressed, revealing a peculiar pattern for each biocoating. A first attempt to clarify the relationship between water drop evolution and the driving forces that presumably underlie the relevant kinetics may be based on some intuitive considerations concerning the physicochemical attributes of the biopolymer coatings.

For the chitosan coated substrate, the highest initial contact angle was in agreement with values reported in the literature (Péroval et al, 2002) and can be tentatively understood based on its chemical properties. Indeed, the large initial  $\theta$  value observed might indicate reorganization of the molecule, presumably associated with the methyl moieties of the residual acetyl groups along the polysaccharide backbone, which may have become exposed at the solid/air interface for thermodynamic reasons (Bangyekan et al, 2006). However, Cunha and co-workers (Cunha et al, 2008) pointed out that the presence of relatively low polar acetylamide moieties cannot significantly affect contact angle values but only the presence of non-polar impurities, which are contained in even the highest-quality commercial samples. Data on the surface energy obtained through the advancing contact angle measurements were in line with the general trend reported by other authors and with the results obtained by Cunha and co-workers on unpurified chitosan. From Table 4b it can be seen that the polar component ( $\gamma^{AB}$ ) of the surface energy of chitosan-coated surfaces was equal to zero, with only very low electron acceptor ( $\gamma^+$ ) interactions. Once again, this abnormal behavior is most likely due to the nonpolar impurities on the chitosan surface, rather than to the possible orientation of the acetyl moieties at the solid/air interface. In contrast, the relatively high value of the dispersive component ( $\gamma^{LW}$ ) looks consistent with the typical values found for polysaccharides.

The water droplet profile began to change immediately upon deposition onto the chitosan-coated surface. Figure 16a shows that, in an early step (at approximately 14 s), the perceptible

reduction in the solid/liquid contact area is accompanied by a steep decrease in volume, possibly because of two distinct but concurrent phenomena:

- I. the apolar acetylamide moieties of chitosan at the solid/vapor interface might have induced a reduction in the solid/liquid contact area, consistent with the observed reduction in the surface area of the drop;
- II. the spontaneous penetration of the liquid inside the texture of the material via percolation (absorption).

The drop surface area data suggest that, after this early phase, spreading began to take place and contribute to the overall kinetics of the evolution of the droplet profile (presumably because of interactions with the polar and positively charged moieties of the biopolymer, such as  $-OH$  and  $-NH_3^+$ ). Both the absorption and spreading phenomena then continued to contribute until the end of the 60 s period of analysis, when  $\theta$  approached  $52^\circ$ .

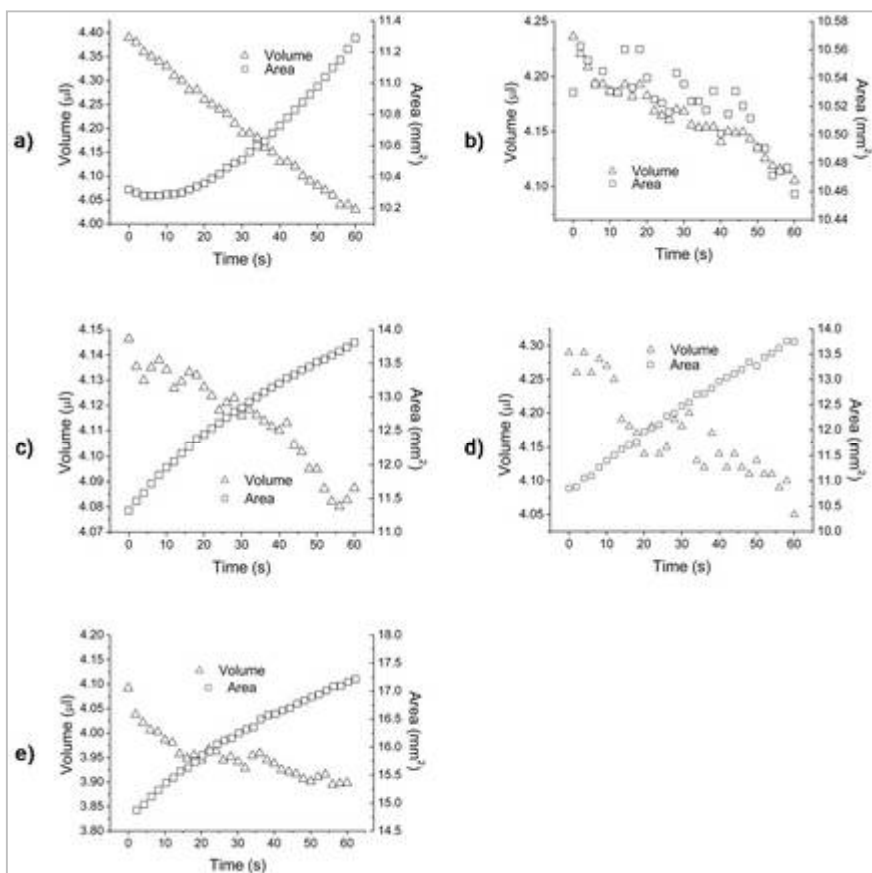


**Figure 16** Water droplet volume and solid/liquid contact area evolution over time (60 s) for: a) chitosan; b) gelatin; c) pectin DE 72; d) pectin DE 27 DA 20; and e) pullulan bio-coatings.

The surface properties of gelatin have already been thoroughly investigated by many authors, who confirm our observation of fairly high  $\theta$  values for gelatin surfaces, despite its inherent hydrophilicity (Białopiotrowicz et al, 2002; Holly et al, 1975; Yasuda et al, 1994). The free surface energy investigation showed that gelatin behaved as the only bipolar surface among the five tested in this work (Table 4b). In particular, the dispersive component value ( $\gamma^L^D$ ) was in

agreement with values found in the literature (Białopiotrowicz et al, 2002) while the electron-donor ( $\gamma$ ) interactions represented the major contribution to the polar component. The water droplet profile did not change substantially during the entire 60 s analysis (Figure 15), although the difference between  $\theta_0$  ( $\sim 66^\circ$ ) and  $\theta_{60}$  ( $\sim 63^\circ$ ) was statistically significant (Table 5). According to the literature, these observations may be due to:

- I. the tendency of the water droplet to minimize its surface area when interacting with the gelatin surface, which is capable of changing its free energy through reorientation of the hydrophobic amino acid side chains (leucine, valine, phenylalanine, isoleucine and methionine) exposed at the solid/air interface (Holly et al, 1975). This preferred orientation of functional hydrophobic groups could justify the  $\theta$  values observed, as well as the slight decrease in drop surface area ( $\sim 0.7 \text{ mm}^2$ , see Table 5) measured at the end of the analysis (Figure 16b);
- II. molecular conformation changes could also play a major role. The aqueous dispersion of gelatin proteins is composed of a mixture of random coiled chains that, upon deposition on the plastic substrate, randomly rearrange themselves through a disorder-to-order transition, partially recovering the original triple-helix structure of collagen, yielding so-called 'renatured' or 'structural' gelatin (Dai et al, 2006). Structural gelatin is characterized by a 3D network containing amorphous regions of random coiled gelatin chains interconnected by domains of spatially ordered molecules (called 'micro-crystallites') that are stabilized by hydrogen bonds between glycine NH groups and proline C=O groups (Brodsky et al, 1997) The presence of ordered domains would hinder the absorption of water.

The two pectin-based coatings analyzed in this work behaved differently to the other biocoatings. In particular, both pectin coatings exhibited lower  $\theta_0$  values, consistent with the higher hydrophilic character of these molecules. The statistically significant difference between amidated ( $\sim 58^\circ$ ) and high-methoxyl pectin ( $\sim 54^\circ$ ) coatings was not in line with what one might expect based on their chemical structures (i.e. methyl group contents) (Sriamornsak et al, 2008). Such a mismatch might be justified by the peculiar intermolecular alignment of pectin, which consists of right-handed helices (Rees et al, 1971) packed in parallel arrangements with very limited internal flexibility (based on X-ray fiber diffraction patterns (Walkinshaw et al. 1981)), leaving no chance for methyl moieties to remain exposed at the solid/liquid interface. Nonetheless, this must be confirmed experimentally. The advancing contact angle experiments did not provide any significant difference between the dispersive components of the two pectins (Table 4b), thus confirming the probability that factors other than the displacement of methyl groups on the solid/air interface govern the surface wettability of pectins. Interestingly, both high-methoxyl and amidated pectins behaved as monopolar surfaces. However, the former showed typical electron-donor features, the latter electron-acceptor interactions, which presumably reflect the different chemical compositions (i.e., the presence of amino groups on the amidated pectin backbone) of the two biopolymers. In the case of pectin DE 72, the decrease in droplet volume after 60 s was quite small ( $\sim 2.8\%$ , see Table 5), suggesting that absorption of the solvent across the biopolymer layer was limited. The increased drop surface area (Figure 16c) is consistent with an early interaction of water with the hydrophilic groups of pectin, and with the hypothesis that spreading governs the evolution of  $\theta$ . Conversely, the fairly larger  $\theta$  observed for the amidated pectins (DE 27 DA 20), as well as its evolution during the time span of the analysis, could be explained by considering the number of intra- and intermolecular hydrogen bonds between the hydroxyl and amide groups, which would hinder any early interaction with the solvent (that wets the biopolymer surface). However, the evolution of  $\theta$  during the time span of the analysis was in parallel to that of the high-methoxyl pectin, indicating that in this case spreading also appeared to be the prevailing phenomenon (see Table 5 and Figure 16d).

The unique regular linkage pattern of pullulan (alternations of  $\alpha$ -(1 $\rightarrow$ 4) and  $\alpha$ -(1 $\rightarrow$ 6) bonds) is responsible for its structural flexibility (centered on the  $\alpha$ -(1 $\rightarrow$ 6)-linkages) and enhanced solubility (Leathers, 1993; Buliga et al, 1987; Dais et al, 2001). These characteristics were clearly reflected by the results of our water contact angle analysis. Indeed, pullulan-coated surfaces exhibited the lowest  $\theta_0$  and  $\theta_{60}$  values among the biopolymers tested in this work ( $\sim 30^\circ$  and  $\sim 23^\circ$ , respectively, see Table 5). In addition, the surface energy analysis unequivocally demonstrated that pullulan had the most hydrophilic surface among the tested polymers. Like most solid, polar, non-ionic hydrophilic surfaces, pullulan behaved as a strong monopolar electron-donor, with a  $\gamma^-$  value similar to those encountered for synthetic polymers such as polyethylene oxide (PEO) and polyvinyl alcohol (PVOH) (van Oss, 1994). This explains the high affinity between the surface of pullulan and water molecules via hydrogen bonds at the solid/liquid interface. The evolution of the droplet volume and droplet surface area (Figure 16e) supports the possibility that the observed variation in  $\theta$  values was predominantly due to spreading, which can be linked to the highest hydroxyl group content of pullulan compared to the other biopolymers. Moreover, unlike gelatin, chitosan and high-methoxyl pectin, pullulan lacks hydrophobic functional groups, while its physical arrangement and molecular mobility promote interactions with the solvent. Pullulan's inherent structural flexibility results in a predominantly amorphous polysaccharide organization, allowing the solvent to promptly interact with polar functional groups along the backbone of pullulan.

### 3.2.2.3 Modeling

A semi-empirical approach was adopted in order to describe the evolution of the water contact angle. A mathematical function was first fitted to the experimental  $\theta$  values collected during the 60 s period of analysis with the goal of obtaining an adequate and simple analytical expression and its first derivative. To accomplish this, a three-parameter decay function was selected:

$$\theta(t) = \theta(0) \exp(-kt^n) \quad (8)$$

with its first derivative:

$$\frac{\partial \theta}{\partial t} = (kn)\theta(t)t^{n-1} \quad (9)$$

As shown in Figure 17, the experimental data satisfactorily fitted the selected function, as further demonstrated by the regression coefficient values (Table 6). The first derivatives of the fitted curves are shown in Figure 18, from which it is possible to notice that, with the only exception of gelatin, none of the curves attained a 'zero-speed rate' state at the end of the 60 s of analysis (see the inset in Figure 18), although all of the curves tended to reach a steady state asymptotically. This evidence suggests that both absorption and spreading were still occurring at the end of the analysis period at the solid/liquid interface, albeit to a greater extent for chitosan and the pectins.

In order to determine whether or not any mechanistic meaning could be derived from the mathematical function above, we compared equation (8) to the well-known Avrami model, expressed below in its general form to describe the kinetics of crystallization (e.g. fat crystallization) (Marangoni, 2005):

$$1 - X = \exp(-kt^n) \quad (10)$$

By analogy with the Avrami model, coefficients  $k$  and  $n$  of equation (8) apparently provide an indication of the physicochemical phenomena involved. In particular, the higher negative  $k$  values for the pectin (-0.043 and -0.040 for amidated and high-methoxyl pectin, respectively) and chitosan (-0.016) coatings are reflected by their starting ( $\partial\theta/\partial t$ ) values (Figure 18), since the highest initial rates were those of amidated and high-methoxyl pectins ( $-4.12^\circ \text{ s}^{-1}$  and  $-3.63^\circ \text{ s}^{-1}$ , respectively), followed by chitosan ( $-1.74^\circ \text{ s}^{-1}$ ). In addition, it is worth noting that the  $k$  and ( $\partial\theta/\partial t$ ) values for the same biocoatings had the same relative magnitudes: the  $k$  values for pectins (which were similar to each other) were approximately 2.8-fold larger than the  $k$  value for chitosan (this trend holds true for the  $\partial\theta/\partial t$  values as well). Therefore, the coefficient  $k$  might be a measure of the reaction rate (i.e. contact angle evolution), since the  $k$  coefficient in the Avrami equation represents the crystallization rate constant. Concerning the exponent  $n$ , we hypothesized that it is linked to the physicochemical phenomena underlying the overall process. As with the corresponding exponent in the Avrami model,  $n$  assumes fractional values, which are normally attributed to the occurrence of two (or more) simultaneous phenomena, which in this case would be represented by absorption and spreading. Theoretically,  $n = 0$  and  $n = 1$  should be thus encountered in the case of pure absorption and pure spreading, respectively. However, this hypothesis necessitates experimental confirmation.

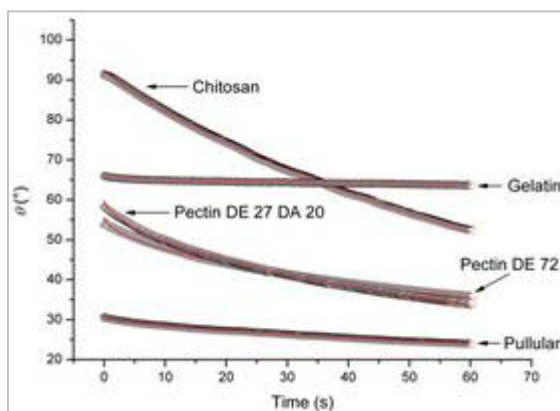


**Figure 17** Water contact angle evolution during the 60 s period of analysis. The red solid lines were obtained by fitting equation 8 to the experimental data.

**Table 6** Summary of the main parameters arising from fitting equation (8) to the experimental data

Biocoating	Adj. $r^2$ <sup>a</sup>	Fit. Std. Err. <sup>b</sup>	Parameters		
			$\theta$	$k$	$n$
Chitosan	0.999	0.190	92.56	-0.016	0.88
Gelatin	0.991	0.046	66.06	-0.007	0.39
Pectin DE72	0.998	0.175	55.69	-0.040	0.59
Pectin DE27 DA20	0.999	0.156	59.82	-0.043	0.63
Pullulan	0.999	0.055	30.55	-0.015	0.69

<sup>a</sup> Adjusted regression coefficient. <sup>b</sup> Standard error of the fitting.

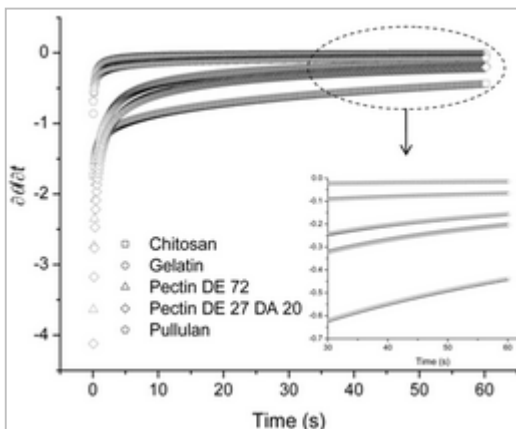


**Figure 18** First derivative of the fitted curves for the five biocoatings tested. A magnification of the final 30 s is displayed in the inset.

### 3.2.2.4 Contact angle/image analysis combined approach

The phenomena involved at the water droplet-biopolymer interface can also be profitably investigated also by using a suitable Image Analysis (IA) procedure (Von Bahr et al, 1999; Daniel et al, 2006; Starov et al, 2002a, Starov et al, 2002b; Von Bahr et al, 2001). A combined trigonometric (detection of  $\theta$ ) and geometric (changes in the droplet shape) approach can add useful information, allowing a reliable description of droplet evolution, which depends on two major effects, namely absorption and spreading. The assumption is that the coating polymer has been randomly (and therefore isotropically) deposited onto the support surface, so the droplet shape is a dome with a circular base (Figure 19). The dome may be perfectly spherical or a little skewed, depending on the topography of the coated surface.

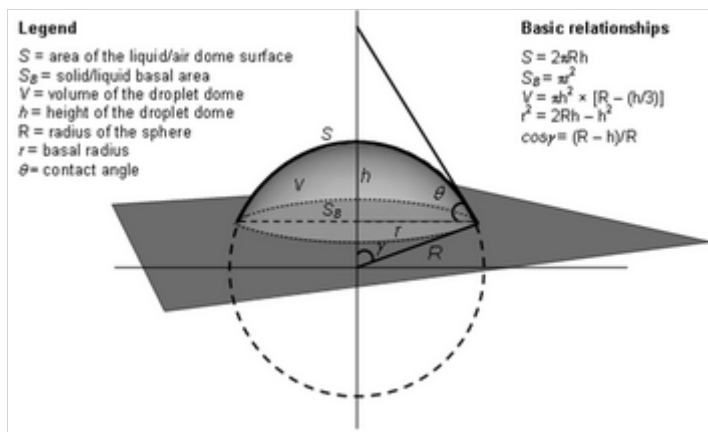


**Figure 19** Schematic representation of a droplet on a solid surface, with the relevant shape parameters underlying the relationships to be obeyed for a perfect spherical shape of the dome.

The water adsorption looks like the sinking of the water droplet beneath the contact surface, with a decrease of its volume ( $V$ ) and basal area ( $S_B$ ), while the water spreading does not affect  $V$ , although it widens  $S_B$ . Spreading is usually faster than absorption since the diffusion of the

absorbed water beneath the substrate surface is slow, unless percolation can take place through large pores or capillary tubing. It can thus be said that spreading is the main phenomenon affecting the starting shape of the droplet. In this work, the simultaneous detection of  $\theta$  and the shape parameters (height  $h$ , basal radius  $r$ , dome surface area  $S$ , basal area  $S_B$ , and droplet volume  $V$ , see Figure 19) determined by IA allowed to check for deviations from a perfect spherical geometry, which imposes well-defined relationships between  $\theta$  and what can be indicated as 1D, 2D and 3D shape parameters (Table 7). This combined approach made it possible to quantitatively describe both absorption and spreading as well as their correlation with the surface topography of biopolymer coatings.

**Table 7** Relationships to be obeyed for a perfect spherical shape of the dome formed by a water droplet laid on a flat surface. They concern 1D, 2D and 3D geometrical parameters (see text).

1D	2D	3D
$\frac{h}{r} = \frac{1 - \cos \theta}{\sin \theta}$	$\frac{S}{2\pi h^2} = \frac{1}{1 - \cos \theta}$	$\frac{3V}{\pi h^3} = \left( \frac{2 + \cos \theta}{1 - \cos \theta} \right)$
	$\frac{S_B}{\pi h^2} = \frac{1 + \cos \theta}{1 - \cos \theta}$	$\frac{3V}{S_B h} = \left( \frac{2 + \cos \theta}{1 + \cos \theta} \right)$
		$\frac{6V}{S h} = (2 + \cos \theta)$

To this purpose, the six different relationships pertaining to three different geometrical parameters (see Table 7) were used in this work. An additional check was possible through the following expression (coming from the 2D and 3D relationships reported in Table 7), which only applies to geometrical parameters determined with IA:

$$\frac{3V}{h} - \frac{S}{2} = S_B \quad (11)$$

Figures 20 a,b show that, as a rule, the water droplet kept a spherical shape throughout the 60 s time span, with the largest (although still modest) deviation concerning pullulan. An early explanation for such a deviation could be related to two physicochemical features of pullulan, namely:

- the absence of charged groups along its backbone (the only one among the five biopolymers tested in this work);
- the already mentioned inherent structural flexibility;

both of which are recognized as crucial factors in dictating the extent of folding and aggregation at the molecular level (Podestà et al, 2005).

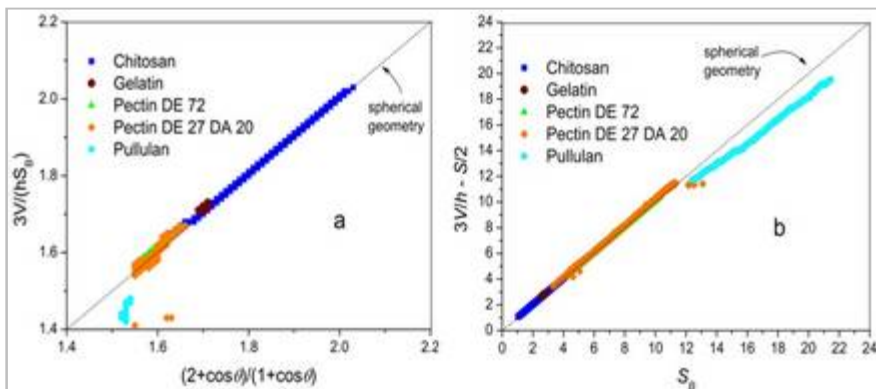


**Figure 20 (a,b)** Graphical representation of the deviation from the spherical geometry of 3D shape parameters and the relationship expressed by equation 11 and on the basis of shape parameters detected with the image analysis investigations.

At first glance, this would explain the lowest degree of roughness that was measured for the pullulan coatings (Table 8), which showed the highest smooth surface compared to the other biopolymer coatings (Figure 21 a–e) with no evidence of either discontinuities or molecular aggregations. Secondly, but no less important, it is plausible that pullulan molecular chains experienced orientation after coating deposition (which was performed via a wire-wound rod running onto the coating dispersion longitudinally to the plastic substrate). Such an orientation, although limited, could be the reason for the slight deviation observed. However, this hypothesis still needs to be confirmed by experimental data.

**Table 8** Roughness values calculated for each biocoating

Bio-coating	Roughness (nm)
Chitosan	30
Gelatin	7
Pectin DE 72	30
Pectin DE 27 DA 20	36
Pullulan	3

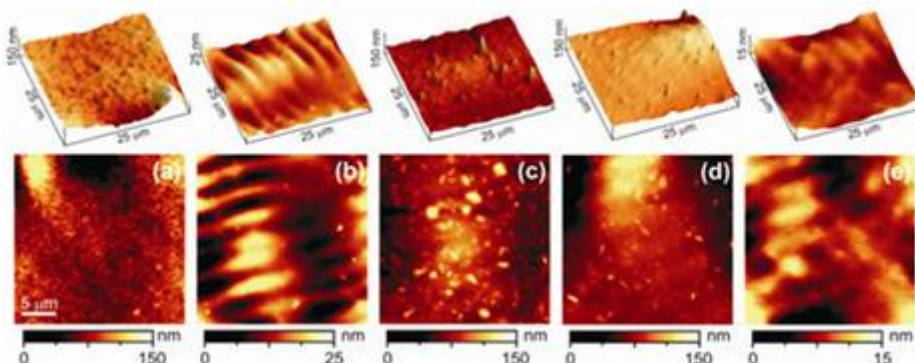


**Figure 21a-e** AFM three-dimensional (up) and height (down) images ( $25 \times 25 \mu\text{m}^2$ ) of: a) chitosan; b) gelatin; c) pectin DE 72; d) pectin DE 27 DA 20; and e) pullulan coated surfaces.

The relevant relationships between  $S_B$  and the trigonometric functions of the contact angle,  $\theta$ , may therefore be reliably used to evaluate the overall variation of the basal area,  $\Delta S_B$ :

$$\Delta S_B = 3 \left[ \frac{V}{h} \left( \frac{1 + \cos \theta}{2 + \cos \theta} \right) - \frac{V_0}{h_0} \left( \frac{1 + \cos \theta_0}{2 + \cos \theta_0} \right) \right] \quad (12)$$

where the subscript ‘0’ stands for the initial conditions. The change that would occur in the case of a constant droplet volume (i.e., pure spreading) is:

$$(\Delta S_B)_{sp} = 3V_0 \left[ \frac{1}{h} \left( \frac{1 + \cos \theta}{2 + \cos \theta} \right) - \frac{1}{h_0} \left( \frac{1 + \cos \theta_0}{2 + \cos \theta_0} \right) \right] \quad (13)$$

Since:

$$\Delta S_B = (\Delta S_B)_{absorption} + (\Delta S_B)_{spreading} \quad (14)$$

one can easily evaluate the effect of droplet absorption on the variation of SB:

$$(\Delta S_B)_{absorption} = 3 \left[ \frac{(V - V_0)}{h} \times \left( \frac{1 + \cos \theta}{2 + \cos \theta} \right) \right] \quad (15)$$

In order to compare the two effects for each biopolymer coating, it is expedient to scale  $\Delta(S_B)_{spreading}$  and  $\Delta(S_B)_{absorption}$  with respect to the relevant starting value of the basal area,  $S_{B,0}$  (Figure 22a and 22b).

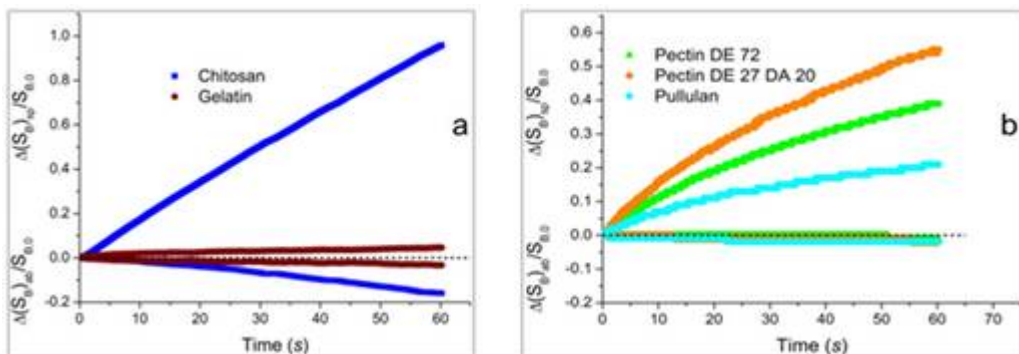


**Figure 22 a, b** Changes in basal area of the water droplet: spreading and absorption effects for chitosan and gelatin (a) and for pectin DE 72, pectin DE 27 DA 20 and pullulan (b).

Chitosan showed the largest variations for both spreading and absorption, the former (~95% of  $S_{B,0}$ ) being largely superior to the latter (~16% of  $S_{B,0}$ ). Gelatin showed two quasi-equivalent and counterbalancing effects (both less than 5% of  $S_{B,0}$ ), with the consequence that the  $S_B$  did not change substantially during the 60 s time span. Smaller effects were observed for the other three coatings, where spreading (20, 40 and 55% of  $S_{B,0}$  for pectin DE72, pectin DE27DA20 and pullulan, respectively, after 60 s) was always superior to absorption, which, in fact, was almost negligible (less than 3% of  $S_{B,0}$  for all of them). The poor extent of absorption was the reason why practically no swelling of the coating was observed for all of the biopolymers considered.

An indication of this is also provided in Figure 23, where both the experimental and the theoretical heights of the droplet under the hypothesis of pure spreading (i.e.  $V = \text{constant}$ ) are displayed for the chitosan, amidated pectin and pullulan.

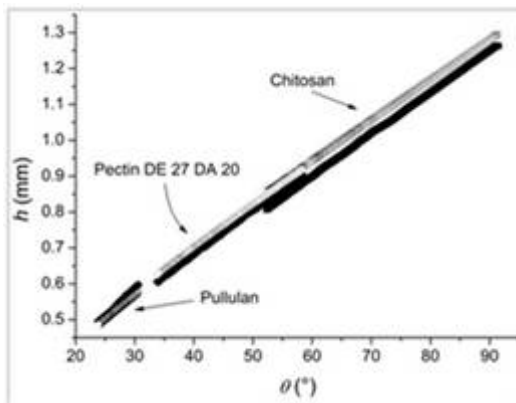


**Figure 23** Experimental (filled symbols) versus theoretical (empty symbols) heights of the droplet for the chitosan, amidated pectin and pullulan coatings.

As can be observed, the difference between the experimental and calculated values is narrow, demonstrating that limited absorption occurred across the thickness of the coatings. A slightly more pronounced difference was detected for chitosan, which allowed a larger and faster rate of absorption, possibly because of its wider and deeper pores, than the other biopolymer coatings. This conclusion is in line with the AFM surface images (Figure 21a), where chitosan’s discrete molecular assembly was found to form spiky surface clusters, probably caused by both the charged groups and intense hydrogen bonding (Figure 24) (Söntjens et al, 2008).

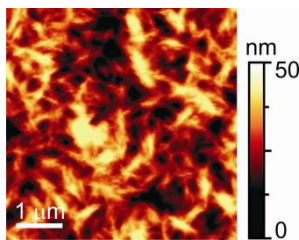


**Figure 24** AFM height image ( $5 \times 5 \mu\text{m}^2$ ) of the chitosan surface illustrating the web-like formation of molecular clusters.

The above data enabled the spreading rate ( $S_R$ ) to be evaluated, namely the time derivative of the trends reported in Figure 22a and 22b, which could all be fitted using the following function:

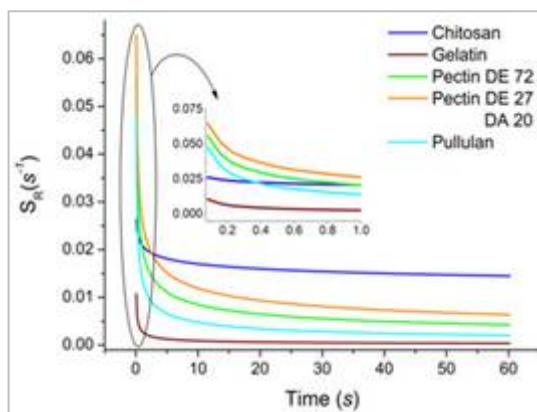
$$S_R = (a + b) \times t^c \tag{16}$$

Table 9 shows coefficients  $a$  and  $b$  and the exponent  $c$ , to which no physical meaning should be given since they are simply best fit parameters.

**Table 9** Fitting parameters for the spreading trends (Figure 22a and 22b) according to equation (16).

Biopolymer	<i>a</i>	<i>b</i>	<i>c</i>
Chitosan	-0.017	0.023	0.910
Gelatin	+0.001	0.006	0.495
Pec DE 72	-0.025	0.034	0.611
Pec DE27 DA20	-0.024	0.041	0.650
Pullulan	-0.018	0.027	0.525

As displayed in Figure 25, the largest initial spreading rates pertained to the pectins and pullulan coatings. This reflects the more hydrophilic nature of these polysaccharides compared to chitosan and gelatin, which conversely exhibited the lowest values. At the same time, chitosan and gelatin showed the quickest approach toward a quasi-steady trend, as clearly revealed by the steepest initial descending tract in the first hundred seconds. The trends evaluated for the remaining three biopolymers are included between these two boundaries. The quasi-steady values observed for chitosan and gelatin were quite far apart from each other, indicating that while spreading seemed to be virtually negligible on the gelatin surface after approximately 5 s, it still represented the main driving force for the  $\theta$  variation for chitosan. The trend approaching the ‘zero value’ of the gelatin coating can be explained through the fact that this biopolymer showed equivalent and opposite effects related to absorption and spreading, namely that spreading was almost fully counterbalanced by absorption. Therefore, the fact that the low spreading rate did not necessarily imply an exceedingly rough surface can be highlighted: the AFM images indisputably show that the roughness of the gelatin coated surface was rather low and similar to the value calculated for the surface coated with pullulan (see Table 8 and Figure 21).



**Figure 25** Spreading rate of the water droplet on the biopolymer coatings.

Finally, it should be noted that chemical peculiarities at both the intra- and supra-molecular level, although important, might have been somehow hindered due to the fact that the biopolymer coatings were randomly cast. Conversely, the control of wettability through the surface chemistry of biopolymers in a deliberate manner may be expected for an iso-oriented biopolymer coating, where the next-neighbor molecular arrangement should substantially affect the interactions with liquid water. As a consequence, the shape of the droplet should not be spherical and spreading should have a different rate whether parallel or orthogonal to the alignment of the biopolymer molecules.

### 3.2.3 Conclusions

Coatings prepared with five biopolymers behaved in a distinct way with respect to their surface interactions with water. They exhibited different wetting properties, as indicated by the combined investigations of contact angle and image analysis. The experimental evidence herein suggests that the trends observed were governed by two main phenomena at the solid/liquid interface, namely absorption and spreading, which affect the overall wetting dynamics.

The interpretation of the data was based on the assessment of the spherical geometry of a water droplet laid onto a coated surface. This allows a separation of the expanding and retracting trends of the contact base area governed by spreading and absorption, respectively. The coating absorption for each biopolymer was very poor; the greatest absorption was detected for the chitosan-coated surface, which was related to the plausible presence of pores that carved the surface. A quasi-perfect balance between these effects was found for gelatin-coated surfaces, with the consequence that both the contact area and the contact angle remained nearly almost throughout the time span of the investigation. Moreover, the pullulan surface exhibited the most marked hydrophilic features, while pectins showed an intermediate behavior among the biopolymers tested. Having assessed the experimental approach of combined determinations of contact angle, IA and AFM data, a future interesting investigation could be addressed to cast iso-oriented coatings with use of the same biopolymers considered in the present work.

Finally, this part of the PhD research helped to deepen the knowledge about the surface modifications after biopolymers deposition (Farris et al, 2011), an aspect that before has not been fully investigated, especially dealing with food packaging materials. The results obtained can help in engineering new structures, as can be seen in the following part of the PhD research.

### 3.2.4 References

- Bangyekan C, Aht-Ong D, Srikulkit K. 2006, Preparation and properties evaluation of chitosan-coated cassava starch films. *Carbohyd Polym* 63:61–71.
- Białopiotrowicz T, Jańczuk B. 2002, Surface properties of gelatin films. *Langmuir* 18:9462–9468.
- Brodsky B, Ramshaw JAM. 1997, The collagen triple-helix structure. *Matrix Biol* 15:545–554.
- Buliga GS, Brant DA. 1987, Temperature and molecular weight dependence of the unperturbed dimensions of aqueous pullulan. *Int J Biol Macromol* 9:71–76.
- Cunha AG, Fernandes SCM, Freire CSR, Silvestre AJD, Neto CP, Gandini A. 2008, What is the real value of chitosan's surface energy? *Biomacromolecules* 9:610–614.
- Dai CA, Chen YF, Liu MW. 2006, Thermal properties measurements of renatured gelatin using conventional and temperature modulated differential scanning calorimetry. *J Appl Polym Sci* 99:1795–1801.
- Dais P, Vlachou S, Taravel FR. 2001, <sup>13</sup>C nuclear magnetic relaxation study of segmental dynamics of the heteropolysaccharide pullulan in dilute solutions. *Biomacromolecules* 2:1137–1147.
- Farris S, Introzzi L, Biagioni P, Holz T, Schiraldi A, Piergiovanni L. 2011, Wetting of biopolymer coatings: contact angle kinetics and image analysis investigation. *Langmuir*. 27:7563-7574.
- Han JH, Zhang Y, Buffo R. In *Innovations in Food Packaging*; Han JH Ed.; Elsevier Academic Press: San Diego, 2005, p. 46.
- Holly FJ, Refojo MFJ. 1975, Wettability of hydrogels I. Poly(2-hydroxyethyl methacrylate). *J Biomed Mater Res* 9:315–326.
- Jin J, Song M, Hourston, DJ. 2004, Novel chitosan-based films cross-linked by genipin with improved physical properties. *Biomacromolecules* 5:162-168.
- Kampeerapappun P, Aht-Ong D, Pentrakoon D, Srikulkit K. 2007, Preparation of cassava starch/montmorillonite composite film. *Carbohyd Polym* 67:155–163.
- Karbowiak T, Debeaufort F, Champion D, Voilley A. 2006a, Wetting properties at the surface of iota-carrageenan-based edible films. *J Colloid Interf Sci* 294:400–410.
- Karbowiak T, Debeaufort F, Voilley A. 2006b, Importance of surface tension characterization for food, pharmaceutical and packaging products: A review. *Crit Rev Food Sci* 46:391–407.
- Kokoszka S, Debeaufort F, Hambleton A, Lenart A, Voilley A. 2010, Protein and glycerol contents affect physico-chemical properties of soy protein isolate-based edible films. *Innov Food Sci Emerg* 11:503–510.
- Leathers TD. 1993, Substrate regulation and specificity of amylases from *Aureobasidium* strain NRRL Y-12,974. *FEMS Microbiol Lett* 110:217–222.

- Modaressi H, Garnier G. 2002, Mechanism of wetting and absorption of water droplets on sized paper: effects of chemical and physical heterogeneity. *Langmuir* 18:642–649.
- Muszynski L, Walinder MEP, Pirvu C, Garner DJ, Shaler SM. Application of droplet dynamic method for characterization of water penetration into permeable surfaces. In *Contact Angle, Wettability and Adhesion*; Mittal, K. L., Ed.; VSP: Utrecht, 2003, Vol. 3, p. 463.
- Péroval C, Debeaufort F, Despré D, Voilley A. 2002, Edible arabinoxylan-based films. 1. Effects of lipid type on water vapor permeability, film structure, and other physical characteristics. *J Agric Food Chem* 50:3977–3983.
- Podestà A, Indrieri M, Brogioli D, Manning GS, Milani P, Guerra R, Finzi L, Dunlap D. 2005, Positively charged surfaces increase the flexibility of DNA. *Biophys J* 89:2558–2563.
- Rees DA, Wright AW. 1971, Polysaccharide conformation. Part VII. Model building computations for  $\alpha$ -1,4 galacturonan and the kinking function of L-rhamnose residues in pectic substances. *J Chem Soc B* 2:1366–1372.
- Solaro R, Chiellini F, Battisti A. 2010, Targeted delivery of protein drugs by nanocarriers materials. *Materials* 31928–1980.
- Söntjens SHM, Renken RAE, van Gemert GML, Engels TAP, Bosman AW, Janssen HM, Govaert LE, Baaijens FPT. 2008, Thermoplastic elastomers based on strong and well-defined hydrogen-bonding interactions. *Macromolecules* 41:5703–5708.
- Sriamornsak P, Wattanakorn N, Nunthanid J, Puttipipatkachorn S. 2008, Mucoadhesion of pectin as evidence by wettability and chain interpenetration. *Carbohydr Polym* 74:458–467.
- Tang CH, Jiang Y. 2007, Modulation of mechanical and surface hydrophobic properties of food protein films by transglutaminase treatment. *Food Res Int* 40:504–509.
- Van Oss CJ. 2003, Long-range and short-range mechanisms of hydrophobic attraction and hydrophilic repulsion in specific and aspecific interactions. *J Mol Recognit* 16:177–190.
- Van Oss CJ. 1994 *Interfacial forces in aqueous media*. Marcel Dekker: New York, pp 21–22, 89–107.
- Van Oss CJ, Chaudhury MK, Good RJ. 1988, Interfacial Lifshitz-van der Waals and polar interactions in macroscopic systems. *Chem Rev* 88:927–941.
- Vogler EA. 1998, Structure and reactivity of water at biomaterial surfaces. *Adv Colloid Interfac* 74:69–117.
- Walkinshaw MD, Arnott S. 1981, Conformations and interactions of pectins: I. X-ray diffraction analyses of sodium pectate in neutral and acidified forms. *J Mol Biol* 153:1055–1073.
- Yasuda T, Okuno T. 1994, Contact angle of water on polymer surfaces. *Langmuir* 10:2435–2439.

### 3.3 Application of pullulan as antifog coating

In this part of the PhD research one of the biopolymer previously studied was exploited for a particular application in the food packaging field. As a matter of fact, previous results showed undisputably that pullulan has the most hydrophilic features among the polymers taken into consideration, and this characteristic makes it a potential option to the commercially available antifog packaging solutions. The antifog property concerns the capability of the packaging material to avoid the formation of small droplets of water on the internal side of the packaging films.

Fog formation is a consequence of environmental changes in temperature and humidity: a decrease of film surface temperature below the dew point causes the condensation of water vapor present inside the package. The arising ‘foggy’ layer modifies the optical properties of the material, hiding the contents of the package by scattering of the incident light in all directions, due the newly appeared droplets (Grosu et al, 2004). This situation is easily encountered when fresh food and minimally processed (washed, trimmed, sliced) vegetables are refrigerated after packaging operations. However, one of the most important requirements of transparent films is the “see-through” property that offers to consumers an attractive display of the packaged food during its shelf-life, influencing its final merchandising.

Two aspects influence the final transparency of a material:

- the shape of the water droplet;
- the size of the water droplet (Howarter et al, 2008).

The first one relies on the balance between the three interfacial energies (solid-liquid  $\gamma_{SL}$ , liquid-vapor  $\gamma_{LV}$ , and solid-vapor  $\gamma_{SV}$ ) of the three-phases system, as described by Young’s equation (Young, 1805). The higher the contact angle, the higher the incident angle of the light normal to the substrate at the water/air interface, hence the more intense will be the scattering of the visible light.

The second aspect is related to the fact that the smaller the size, the larger the number of droplets and the more pronounced the foggy effect.

Being these two aspects dependent on the physicochemical characteristics of the substrate (Farris et al, 2011) that modifies both the shape and the size of the forming water droplets, a key point can be the modification of the original physicochemical properties of the plastic surface (Cebeci et al, 2006).

Up to date, antifog packaging producers tried to increase the hydrophilic features of hydrophobic surfaces (polyolefins, such as polypropylene (PP) and polyethylene (PE)) including, in the bulk of the materials, additives (e.g., non-ionic surfactants such as sorbitan esters, polyoxyethylene esters, glycerol esters, and more recently, polyglycerol esters) that migrate from the bulk to the surface of the plastic films (Plasman et al, 2005).

Nevertheless, the fast additives migration implies to use the material within a certain period, considering also that these additives can be washed away from the film surface by the condensed vapor, decreasing over time the antifog property. Not less important, the migration of additives poses serious concerns from a safety point of view.

For these reasons, film manufacturers are still struggling with the fog formation problem and a suitable solution has not yet been found. Therefore, the development of high performance, safe, and economical antifog solutions can be considered a still-open issue.

More recently, new alternative approaches have been suggested to achieve the antifog property. For example, Law et al. (2009), investigated the antifog properties of non-UV activated  $\text{TiO}_2$

films, finding that surface roughness is the key parameter dictating the final antifog attribute. Patel et al, 2010, prepared super-hydrophilic surfaces including both polyester films treated with oxygen plasma and indium tin oxide-coated glasses treated by an electrochemical method. Recently antifog coatings, including at least one biopolymer rich in hydrophilic functionalities, have been recently designed (Nuraje et al, 2011). The presence of a hydrophilic surface enhances the spreading of water droplets, enabling the formation of a continuous layer instead of a discrete pattern of fog drops.

For this reason, since pullulan has exhibited the most marked hydrophilic features among the polymers analyzed previously, in this part of the work its antifog performance is discussed in comparison with some commercial antifog packaging films.

The work presented in this part is here reported:

Introzzi L, Fuentes-Alventosa JM, Cozzolino CA, Trabattoni S, Tavazzi S, Bianchi, CL, Schiraldi A, Piergiovanni L, Farris S. 2012, 'Wetting enhancer' pullulan coating for antifog packaging applications. *ACS Appl Mater Interfaces*. 4:3692-3700.

## 3.3.1 Materials and method

### 3.3.1.1 Materials

Pullulan was considered as the only component of the new antifog coating (see paragraph 3.1.1.1.a for details about pullulan). The substrate for coating deposition was a corona-treated low-density polyethylene (LDPE, Figure 26) of  $35 \pm 0.5 \mu\text{m}$  (Ticinoplast, Pogliano Milanese, Italy).

With the aim to provide an improved adhesion of coating on the LDPE film, a primer solution was used (see paragraph 3.1.1.1.c, “adhesion promoter”).

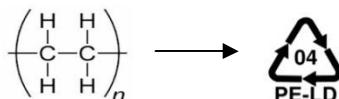


*Figure 26 Molecular structure and plastic identification code of LDPE.*

Two commercially available antifog films were used for comparison purposes:

- PET/ink/tie/LDPE 60  $\mu\text{m}$  thick, coded as AF<sub>a</sub> (Carta Stampa srl, Briosco, Italy)
- LDPE/EVOH/LDPE 70  $\mu\text{m}$  thick, coded as AF<sub>b</sub> (Castagna Univel spa, Guardamiglio, Italy).

According to the information provided by the suppliers, both antifog LDPE layers were loaded ( $\sim 0.5 \text{ wt.}\%$ ) with non-ionic aliphatic OH-functional additives belonging to the polyglycerol esters family.

### 3.3.1.2 Methods

#### 3.3.1.2.a Coating dispersions preparation

See paragraph 3.1.1.2.a (biopolymer coating dispersion preparations, pullulan).

#### 3.3.1.2.b Coated films preparation

See paragraph 3.1.1.2.b for the general procedure. Specifically, after deposition of the adhesion promoter, two subsequent layers of pullulan were applied, achieving a final total thickness of  $\sim 0.5 \mu\text{m}$ .

#### 3.3.1.2.c Contact angle measurements

Contact angle measurements were performed on neat LDPE (corona-untreated side), pullulan antifog coating (AF<sub>pull</sub>), and the two commercial antifog films: AF<sub>a</sub> and AF<sub>b</sub>.

Static and advancing contact angle and surface energy calculation were performed according to paragraph 3.2.1.2.d.

### 3.3.1.2.d Atomic Force Microscopy

See paragraph 3.2.1.2.d.

### 3.3.1.2.e Optical microscopy

An optical microscope (OM) (Micro Nikon Eclipse ME600 Laboratory Imaging; Nikon Instruments, Sesto Fiorentino, Italy) at 10× magnification was used to check water droplet morphology and organization of both untreated LDPE and antifog films (AF<sub>a</sub>, AF<sub>b</sub>, and AF<sub>pull</sub>). Pieces of film (30 × 10 mm<sup>2</sup>) were mounted on a rectangular glass sample holder immediately after storage in the refrigerator and observed without any pre-treatment. Image capture was carried out using NIS-Element software (Nikon Instruments, Sesto Fiorentino, Italy).

### 3.3.1.2.f Antifog test

To perform antifog tests, the real storage condition of many refrigerated fresh foods was simulated. For this purpose, expanded polystyrene (EPS) trays (Sirap Gema, Verolanuova, Italy) previously filled with 50 mL of distilled water were hermetically sealed (top surface area 215×125 mm) with the four different films considered (LDPE pullulan-coated, bare LDPE and the two commercial films) using a vacuum/gas sealing machine (mod. Quick, Tecnovac srl, Grassobbio, Italy) at room temperature.

The trays were then placed in a refrigerator (4.0 ± 0.5°C, 90 ± 2% RH) for 7 days. Water droplet formation was monitored daily by visual inspection. Photographs were taken immediately after drawing the trays out from the cold chamber into the laboratory environment (~20°C) after 7 days of storage.

### 3.3.1.2.g Optical properties

Two types of optical properties were analyzed:

- haze, in accordance with ASTM D 1003-00;
- transparency, in accordance with the ASTM D 1746-88.

Haze is defined as the percentage of transmitted light deviating by more than an angle of 2.5° from the direction of the incident beam: it is responsible for the reduction in the contrast between objects viewed through the specimen (e.g., the coated plastic film). Transparency is measured in terms of specular transmittance: the transmittance value obtained when the transmitted radiant flux includes only the light transmitted in the same direction as that of the incident flux at a 550 nm wavelength. A UV-Vis high-performance spectrophotometer (Lambda 650, PerkinElmer, Waltham, MA, USA) was used, coupling it with a 150 mm integrating sphere (that allows trapping of the diffuse transmitted light) for the haze analyses. Ten replicates were made for each uncoated and coated film sample in both analyses.

### **3.3.1.2.h Statistical analysis**

The statistical significance of differences between samples was determined by one-way analysis of variance (ANOVA), using JMP 5.0.1 software (SAS Campus Drive, Cary, NC). The mean values, where appropriate, were compared by Student's *t*-test with a significance level  $p < 0.05$ .

## 3.2.2 Results and discussion

### 3.3.2.1 Contact angle measurements and Atomic Force Microscopy

Table 10 shows the results arising from the contact angle analyses. The three antifog films exhibited lower static water contact angle values (first column on the left) than the neat LDPE substrate, suggesting that both the commercial antifog films and the pullulan coating effectively increase the wettability of the inherently hydrophobic plastic surface. However, pullulan coating provided the best performance ( $\theta \sim 24^\circ$ ) compared with the AF<sub>b</sub> ( $\theta \sim 39^\circ$ ) and AF<sub>a</sub> ( $\theta \sim 52^\circ$ ) samples. A more in-depth observation also reveals quite a high spreading of the experimental  $\theta$  data around the mean value for the AF<sub>b</sub> sample, presumably owing to the less homogeneous distribution of the antifog additive at the solid/air interface.

**Table 10** Static contact angles ( $\theta$ , °), surface energy components ( $\gamma_s^{LW}$ ,  $\gamma_s^{AB}$ , mJ/m<sup>2</sup>) and parameters of  $\gamma_s^{AB}$  ( $\gamma_s^+$  and  $\gamma_s^-$ , mJ/m<sup>2</sup>) for the films tested in this work.

Solid	Thermodynamic parameter							
	$\theta_{(w)}^*$	$\theta_{(f)}^*$	$\theta_{(d)}^*$	$\gamma_s$	$\gamma_s^{LW}$	$\gamma_s^{AB}$	$\gamma_s^+$	$\gamma_s^-$
LDPE	89.20 ± 1.03	68.96 ± 1.22	60.52 ± 1.67	30.28 ± 1.77	28.28 ± 0.96	1.99 ± 0.11	0.29 ± 0.07	3.42 ± 0.77
AF <sub>a</sub>	52.08 ± 3.17	39.49 ± 3.28	47.49 ± 4.88	46.01 ± 7.01	35.66 ± 2.67	10.36 ± 0.11	1.03 ± 0.67	26.04 ± 4.79
AF <sub>b</sub>	39.22 ± 17.39	68.19 ± 3.27	56.21 ± 9.51	30.41 ± 5.19	30.41 ± 5.42	0.00 ± 0.00	0.00 ± 0.00	80.11 ± 33.0
AF <sub>pull</sub>	24.06** ± 0.92	23.39** ± 1.25	53.77 ± 0.41	53.58 ± 1.31	32.15 ± 0.23	21.43 ± 0.12	2.33 ± 0.18	49.30 ± 1.16

\*  $w$  = water;  $f$  = formamide;  $d$  = diiodomethane; \*\* contact angle values at time = 60 s

Concerning the AFM analysis (Figure 27), different surface morphologies emerged among samples and they would affect the wetting behavior of the substrates. The images clearly show that the presence of the antifog coatings led to an increase in smoothness, with some differences: pullulan layer exhibits the best ‘flattening’ performance compared to the more ‘stain-like’ pattern of the commercial samples. The advancing contact angle data provided a first indication of the different topographies. As can be seen in Figure 28, the  $\theta_{adv}$  versus time profile of the sample AF<sub>b</sub> shows jagged spikes compared to the more regular pattern observed for the neat LDPE substrate and the pullulan coating. Also the commercial antifog film AF<sub>a</sub> disclosed a slightly ‘noisy’ behavior, though with peaks of decidedly smaller size compared with the sample AF<sub>b</sub>.

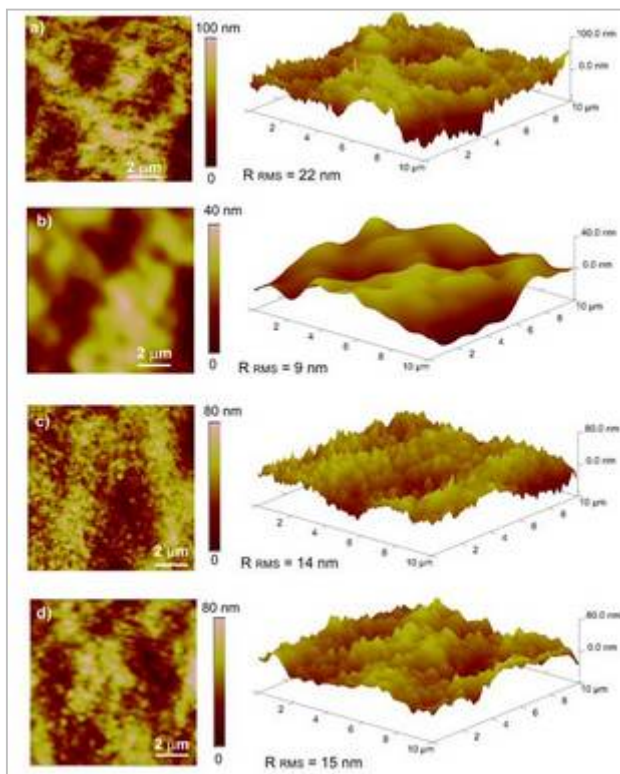


**Figure 27** AFM height and 3D images ( $10 \times 10 \mu\text{m}^2$ ) of the untreated LDPE (a) and of the antifog coatings  $AF_{pull}$  (b),  $AF_a$  (c) and  $AF_b$  (d).

The peculiar behavior observed for the  $AF_b$  sample can be better understood considering the interaction between the ‘advancing’ water droplets and the film surface (Figures 28 and 29): at the beginning ( $t < 2$  s) (Point *a* in Figure 28 and Figure 29a), as more water was dispensed, the volume increase caused a symmetric increase in  $\theta_{adv}$  (i.e., the left and right advancing contact angles increased proportionally) (Point *b* in Figure 2 and Figure 3b). At a certain point, as soon as the water molecules met a more hydrophilic area (i.e., the antifog additive), the wettability increased visibly (i.e., the  $\theta_{adv}$  decreased). However, owing to the patchy surfacing of the antifog additive, the water droplet appeared skewed on one side (Point *c* in Figure 2 and Figure 3c). This asymmetry tended to disappear gradually on further solvent dispensation, to take place again as a new antifog area was encountered.

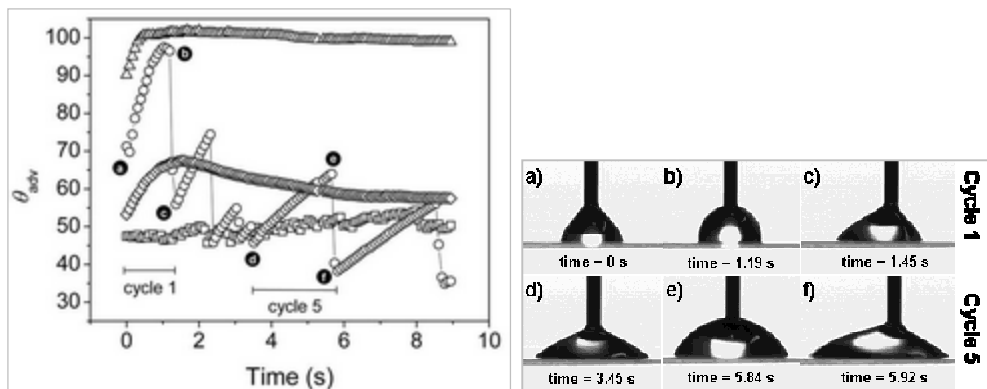


**Figure 28 and 29** Advancing water contact angle evolution for LDPE ( $\triangle$ ), AF<sub>pull</sub> ( $\diamond$ ), AF<sub>a</sub> ( $\square$ ) and AF<sub>b</sub> ( $\circ$ ) over a 10 s time span (on the left); frames captured on the AF<sub>b</sub> antifog film (on the right). Note the skewed shape of the water droplet in frames c) and f).

Several ‘growth-collapse’ cycles of the water droplet were observed on the AF<sub>b</sub> surface during the advancing contact angle experiments, to which corresponded different thermodynamic metastable states, each state producing a given contact angle. The AF<sub>pull</sub> coating exhibited a different profile: following a maximum  $\theta_{adv}$  value (after  $\sim 1.5$  s),  $\theta_{adv}$  decreased monotonically over time. This was demonstrated to be due to the considerable spreading phenomenon of water on the hydrophilic surface of pullulan (Farris et al, 2011). The more homogeneous covering of the pullulan coating on the plastic substrate, as also revealed by the AFM images (Figure 27b), explains why the  $\theta_{adv}$  evolution did not show a ‘step-like’ profile as in the case of the AF<sub>b</sub> sample. This is the key-factor behind the antifog properties of pullulan allowing water to spread easily, thus enabling the formation of a continuous thin layer instead of individual droplets on the plastic film. This, in turn, prevents the scattering of incident light (i.e., the fog-induced optical artifacts).

Relevant considerations also arose from the surface energy calculation of the four different films (Table 10). While both the pullulan coating and the commercial film AF<sub>a</sub> showed higher  $\gamma_s$  compared to the bare, untreated LDPE surface, the AF<sub>b</sub> sample disclosed a  $\gamma_s$  value as low as that of the neat plastic film ( $\sim 30$  mJ/m<sup>2</sup>). This apparently strange behavior of the AF<sub>b</sub> sample can be explained considering the two components (i.e., polar and apolar) of the total surface energy value. More specifically, it can be seen that the antifog treatment (both in the form of coating deposition and additive migration on the surface) led to a marked increase in the electron-donor parameter ( $\gamma^-$ ) of the polar component ( $\gamma^{AB}$ ) for the three antifog materials in comparison with the neat LDPE substrate. On the contrary, the electron-acceptor ( $\gamma^+$ ) parameter increased to a very limited extent for the AF<sub>pull</sub> and AF<sub>a</sub> samples, and was equal to zero for the AF<sub>b</sub> sample. Since equation (5) applies between  $\gamma^-$  and  $\gamma^+$ , the polar component for the AF<sub>b</sub> sample becomes void. This is why, given the total surface energy ( $\gamma_s$ ) expressed by the Equation (6), it has been verified that  $\gamma_s = \gamma^{LW}$  for the AF<sub>b</sub> sample. These results suggest that, for the three antifog samples, the antifog characteristics induced on the LDPE substrate must be attributed exclusively to the electron-donor parameter of the polar component. Pullulan, in particular, behaved as most solid, polar, nonionic hydrophilic surfaces (i.e., as a strong monopolar electron donor with a  $\gamma^-$  value similar to values encountered for synthetic polymers such as poly(ethylene oxide) (PEO) and poly(vinyl alcohol) (PVOH)) (Van Oss, 1994).

As far as the antifog pullulan coating is concerned, the surface energy analysis yielded values of the different components and parameters slightly different from those reported previously

(Farris et al, 2011). Most probably, the reason lies in the different substrates used for the coating deposition (i.e., primed LDPE instead of corona-treated PET). This would have promoted different interactions at the substrate/biopolymer interface, hence a different structuring of pullulan on the plastic surface (Harnett et al, 2007). From these findings, it can be said that considering the components of the surface energy ( $\gamma^{LW}$  and  $\gamma^{AB}$ ) rather than the total surface energy value as a whole ( $\gamma_s$ ) is a more appropriate approach for explaining the thermodynamic equilibrium of water in a realistic way.

### 3.3.2.2 Antifog tests and optical properties

Figure 30 shows the trays samples before and after 7 days of refrigerated storage.

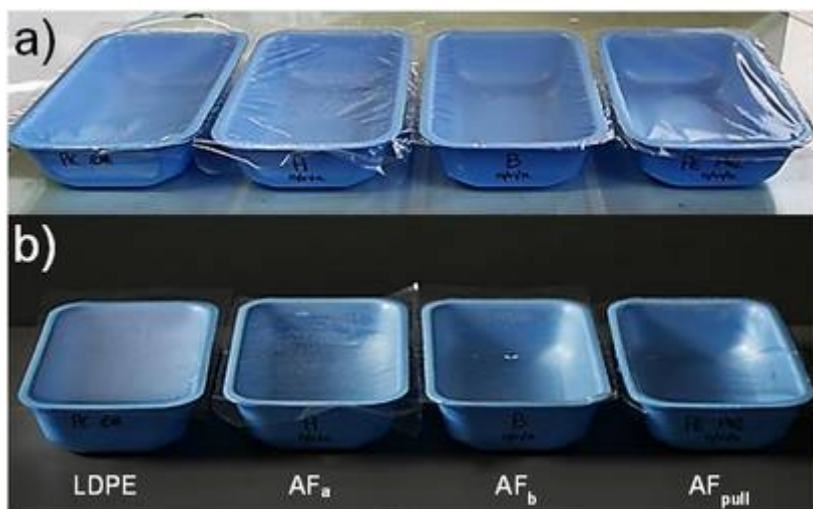


**Figure 30** Trays sealed with untreated LDPE,  $AF_a$ ,  $AF_b$ , and  $AF_{pull}$  before storage (a) and after removal from the refrigerator (7 days at  $-4^\circ\text{C}$ ).

Even if the starting optical properties (haze and transparency) are different (Table 11), the “see-through” quality for all the packages was good enough. It is worth noting that at  $t = 0$  days, the pullulan-coated samples exhibited transparency and haze values slightly larger and lower, respectively, than the neat LDPE: this can be attributable to the smoothing of the original LDPE surface after pullulan coating deposition. The same effect is reported in literature for similar system (Patel et al, 2005; Smith et al, 1996). In particular, for polyolefin thin films ( $< 50 \mu\text{m}$  in thickness), surface scattering has been demonstrated to represent the main component of the measured haze (Ashizawa et al, 1984).

**Table 11** Haze and transparency of untreated LDPE, the two commercial antifog samples ( $AF_a$  and  $AF_b$ ), and the pullulan antifog sample ( $AF_{pull}$ ) before ( $t = 0$ ) and after 7 days ( $t = 7$ ) of storage in the refrigerator at  $-4^\circ\text{C}$ .

Sample	Haze (%)		Transparency (%)	
	t = 0 days	t = 7 days	t = 0 days	t = 7 days
LDPE	$6.06 \pm 0.11^a$	$46.78 \pm 5.07^d$	$82.60 \pm 0.62^A$	$27.56 \pm 2.43^E$
$AF_a$	$10.08 \pm 0.56^b$	$11.69 \pm 1.54^b$	$77.82 \pm 0.46^B$	$63.13 \pm 13.09^{BF}$
$AF_b$	$9.92 \pm 0.13^b$	$12.26 \pm 1.99^b$	$72.85 \pm 0.58^C$	$72.25 \pm 4.28^{CFG}$
$AF_{pull}$	$5.40 \pm 0.23^c$	$6.09 \pm 0.58^e$	$84.44 \pm 1.22^D$	$85.24 \pm 1.05^G$

*Superscripts denote a statistically significant difference within and between groups for each response ( $p < 0.05$ ).*

After 7 days the differences among the trays clearly appear. The LDPE film shows its foggy layer, that cause dramatic changes in haze and transparency values.

The commercial films, additivated with antifog components, reveal that the haze and transparency values are not statistically different before and after storage, however, the visual inspection clearly shows the formation of well-defined droplets, especially for  $AF_a$ . This last phenomenon does not appear with  $AF_{pull}$ , for which the increase in transparency witnesses the probably formation of a very thin continuous layer of water on the surface, that has a positive effect for this property.

### 3.3.2.3 Optical microscopy

The optical microscopy images of the films immediately after removal from the 7 days in the refrigerator (Figure 31) clearly confirm the behavior observed for the trays. In particular, the LDPE film displays distinctly droplets, whose smaller size is an important factor in the increase of the incident light (Howarter et al, 2008). A difference is detectable for the commercial samples, where water forms “islands” that are smaller for the  $AF_a$  sample. However, even if there is an aesthetic modification of the original surface, these “island” are flat enough not to change the starting haze, because for droplets with low contact angle, the negative effect of incident light is negligible (Howarter et al, 2008). The  $AF_{pull}$  sample image, on the other hand, demonstrate that a water spreading has been occurred, confirming the behavior of pullulan as a “wetting enhancer”.

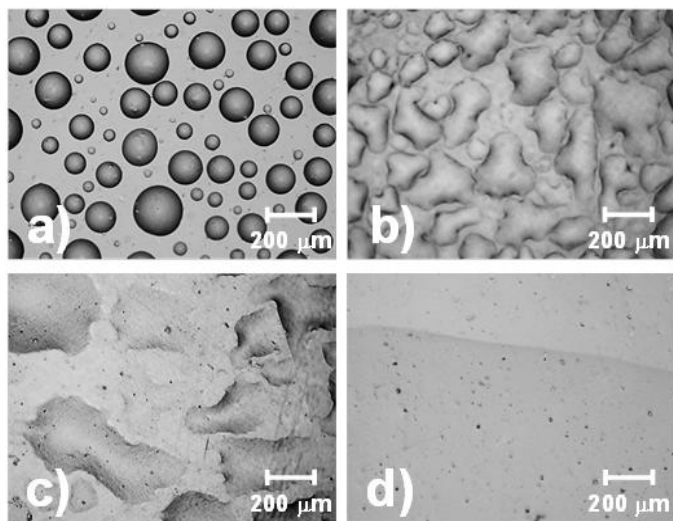


**Figure 31** OM images ( $10\times$ ) of LDPE (a),  $AF_a$  (b),  $AF_b$  (c), and  $AF_{pull}$  (d) immediately after removal from the 7-day storage in the refrigerator at  $4^\circ\text{C}$ .

### 3.2.3 Conclusions

The deposition of a biopolymer with specific hydrophilic features on low-density polyethylene flexible film allowed for the first time to obtain an antifog packaging that can successfully replace those currently available on the market. The obtained results showed that the choice to use a continuous layer of biopolymer on plastic played a pivotal role in determining better overall performances compared with commercial antifog films. These findings clearly represent an advance in the issue of fog formation on food packaging materials (Introzzi et al, 2012). Moreover, it is a confirmation of the possibility for biopolymers to find an application in the packaging market, meeting the increasing request for “green” alternative solutions. Finally, this part of the PhD research clearly showed that the basic research on the surface properties of biopolymers as reported in the previous part (section 3.2), helped to design a bio-based material that is highly competitive if compared with the existing oil-based packaging solutions.

### 3.3.4 References

- Ashizawa H, Spruiell JE, White JL. 1984, An investigation of optical clarity and crystalline orientation in polyethylene tubular film. *Polym Eng Sci* 24:1035–1042.
- Cebeci FC, Wu Z, Zhai L, Cohen RE, Rubner MF. 2006, Nanoporosity-driven superhydrophilicity: a means to create multifunctional antifogging coatings. *Langmuir* 22: 2856–2862.
- Farris S, Introzzi L, Biagioni P, Holz T, Schiraldi A, Piergiovanni L. 2011, Wetting of biopolymer coatings: contact angle kinetics and image analysis investigation. *Langmuir* 27:7563–7574.
- Grosu G, Andrzejewski L, Veilleux G, Ross GG. 2004, Relation between the size of fog droplets and their contact angles with CR39 surfaces. *J Phys D: Appl Phys* 37:3350–3355.
- Harnett EM, Alderman J, Wood T. 2007, The surface energy of various biomaterials coated with adhesion molecules used in cell culture. *Colloids Surf B*. 55:90–97.
- Howarter JA, Youngblood JP. 2008, Self-cleaning and next generation antifog surfaces and coatings. *Macromol Rapid Commun* 29:455–466.
- Introzzi L, Fuentes-Alventosa JM, Cozzolino CA, Trabattoni S, Tavazzi S, Bianchi, CL, Schiraldi A, Piergiovanni L, Farris S. 2012, ‘Wetting enhancer’ pullulan coating for antifog packaging applications. *ACS Appl Mater Interfaces*. 4:3692-3700.
- Law WS, Lam SW, Gan WY, Scott J, Amal R. (2009) Effect of film thickness and agglomerate size on the superwetting and fog-free characteristics of TiO<sub>2</sub> films. *Thin Solid Films* 517:5425–5430.
- Nuraje N, Asmatulu R, Cohen RE, Rubner MF. 2011, Durable antifog films from layer-by-layer molecularly blended hydrophilic polysaccharides. *Langmuir* 27:782–791.
- Patel P, Choi CK, Meng DD. 2010, Superhydrophilic surfaces for antifogging and antifouling microfluidic devices. *Journal of the Association for Laboratory Automation (JALA)*. 15:114–119.
- Patel R, Ratta V, Saavendra P, Li J. 2005, Surface haze and surface morphology of blown film compositions. *J Plast Film Sheet* 21:217–231.
- Plasman V, Caulier T, Boulos N. 2005, Polyglycerol esters demonstrate superior antifogging properties for films. *Plastics, Additives & Compounding*. 7:30–33.
- Smith PF, Chun I, Liu G, Dimitrievich D, Rasburn J, Vancso GJ. 1996, Studies of optical haze and surface morphology of blown polyethylene films using atomic force microscopy. *Polym Eng Sci* 36:2129–2134.
- Van Oss CJ. In *Interfacial Forces in Aqueous Media*. Marcel Dekker: New York, 1994; pp 21–22, 89–107.
- Young T. An essay on the cohesion of fluids. In *Philosophical Transactions of the Royal Society of London* 1805; Vol. 95, pp 65–87.

## 4. PHASE 2

# TWO-COMPONENTS COATINGS

---

As previously stated, one of the main characteristics of biopolymers is their high sensitivity to water. On one hand, this characteristic can be profitably exploited for particular applications (e.g., antifog coatings, see paragraph 3.3). On the other hand, moisture sensitivity may represent a drawback that hinders some applications. In particular biopolymer coatings applied on plastics cannot find widespread use as high oxygen barrier when this performance is required even at high relative humidity values, namely in most realistic situations of food packaging.

Therefore, in this part of the research, one of the biopolymers previously tested (pullulan) has been chosen due to its promising performances and combined with another coating component, an inorganic one. As for pullulan is concerned, its physical and chemical characteristics made it the selected biopolymer for an oxygen barrier property improvement at high relative humidity.

The specific aim was to design a new tridimensional structure in which the organic component (pullulan) confers flexibility to the final system, while the inorganic one provides resistance to humidity.

To properly combine the two components, two different nanotechnology approaches have been adopted:

- ✓ bottom-up approach
- ✓ top-down approach

The first one indicates the chemical controlled assembling of molecules or molecular aggregates, used as building blocks, to produce nanostructures (from some chemical precursors to a nanostructure); the second approach, on the other hand, foresees the progressive reduction in size of macrostructure up to nanoparticles (from “macro” to “nano”) with physical methods.

The final goal was to obtain a bio-based coating with the highest oxygen barrier performances at high relative humidity (~70% RH).

## 4.1 Bio-nanostructured coatings

In this part of the research the bottom-up approach taken from nanotechnology was exploited. In particular, the bottom-up approach has been widely used to create a new class of transparent organic–inorganic nanocomposite materials prepared by the sol–gel methodology, through the incorporation of oligomeric or polymeric molecules into a solution formed by a precursor of the inorganic phase (Minelli et al, 2010).

The hybrid materials obtained with this route are sometimes referred as “ormocers” (organically modified ceramics), or “ormosils” (organically modified silicates) (Lee et al, 1999) and they have a nanocomposite structure.

The hybrids have combined characteristics of organic and inorganic substances, and the final material properties can be tuned between those of the polymeric component and the inorganic glass. Usually, the organic phase guarantees tenacity, flexibility, and adhesion to the polymeric substrate, and the inorganic one gives toughness and thermal, chemical, and flame resistance, as well as improved gas barrier properties. These materials have, in perspective, interesting applications in the field of packaging (Minelli et al, 2008).

They can be produced under mild conditions by using monomers able to form an inorganic glass-like network (typically containing siloxane and silanol groups) highly interconnected with an organic phase. The chemical reactions involved in this process are the hydrolysis and the simultaneous condensation in solution (sol) of an inorganic metal-alkoxide precursor, till a three-dimensional network (gel) is formed. The presence in solution of proper organic compounds leads to the formation of nanocomposite hybrid materials, in which organic and inorganic components are organized in strictly interconnected phases. The domain dimensions, smaller than the visible-light wavelengths, give rise to the high transparency of these materials (differently from traditional composite materials) (Toselli et al, 2007).

From the standpoint of interactions at the interface between organic and inorganic compounds, there is a distinction between two classes of hybrids:

- class I includes hybrids in which the interaction between organic and inorganic constituents is weak and is due to secondary forces (van der Waals, hydrogen bonds and electrostatic forces);
- class II concerns hybrids in which the interaction between organic and inorganic constituents is strong and is due to covalent bonds (Ștefănescu et al, 2007).

In the literature, with the aim to provide to the final films a high oxygen barrier property, different types of organic–inorganic hybrid coatings have been developed. In these hybrid coating materials, polymer oil-based resins, such as poly(vinyl alcohol), poly(vinyl acetate), poly(vinylidene chloride), and poly(ethylene-co-vinyl alcohol) were applied as the organic components (Bang et al, 2012).

On the other hand, in this part of the PhD work, a biopolymer was chosen, pullulan, as the counterpart of a metal alkoxide precursor (tetraethoxysilane, TEOS). Through a bottom-up approach, based on the sol-gel route, the molecular self-assembly process brought to the formation of a nanostructure with improved final properties. The hypothesis was that pullulan can mimic oil-derived polymers in its interaction with TEOS to form high oxygen barrier hybrid coating.

The work presented in this part is here reported:

Farris S, Introzzi L, Fuentes-Alventosa JM, Santo N, Rocca R, Piergiorganni L. 2012, Self-assembled pullulan-silica oxygen barrier hybrid coatings for food packaging applications. *J Agric Food Chem.* 60:782-790.

## 4.1.1 Materials and methods

### 4.1.1.1 Materials

Pullulan was considered as the organic component (see paragraph 3.1.1.1.a for further details about pullulan).

High purity tetraethoxylane (TEOS, Sigma-Aldrich, Milan, Italy) was used as the metal alkoxide precursor of the inorganic phase; 1 M hydrochloric acid (Sigma-Aldrich, Milan Italy) was used as the catalyst of the sol-gel reaction. Ethanol (Sigma-Aldrich, Milan, Italy) and Milli-Q water (18.3 M $\Omega$ ) were used as solvents.

PET film was used as the substrate for coating deposition (see paragraph 3.1.1.1.b for film specifications).

### 4.1.1.1 Methods

#### 4.1.1.2.a Coating dispersions preparation

With the aim to understand the influence of organic/inorganic ratio [O/I, defined as the pullulan /Si(OH)<sub>4</sub> weight ratio for a complete hydrolysis process] on the final oxygen barrier properties of the hybrid coatings, six different solutions were prepared by varying the O/I ratio of the coating from 100/0 to 50/100, as reported in Table 12.

See paragraph 3.1.1.2.b for the preparation of pullulan solution. The final biopolymer concentration in solution is reported in Table 1, according to the different formulations. The pullulan solution was then mixed with the inorganic part after the chemical reaction (i.e. hydrolysis) occurred (Figure 32), according the typical scheme of a sol-gel route. The reaction involves the hydrolysis of the metal alkoxide, usually using a catalyst (e.g., HCl), that brings to the formation of silanol species Si(OH)<sub>n</sub>. Then, a condensation reaction takes place, following two routes (water and alcohol condensation) to yield in both cases SiO<sub>2</sub> covalent bonds (water or alcohol are the byproducts). If the reaction goes on without constraints, the formation of Si-O-Si linkages is typically about 80-85% of the theoretical value (Geppi et al, 2007). In the presence of pullulan, in addition to the condensation reaction, Si(OH)<sub>n</sub> groups can interact via hydrogen bonds with the pendant hydroxyl groups of the biopolymer, to form a hybrid network, as reported in Figure 32. Whether these two routes (the condensation reaction and hydrogen-bond formation) proceed simultaneously or not depends strictly on many factors, such as the concentration of reagents and the pH of the medium.

TEOS was prepared as an acidic hydroalcoholic solution (30 wt % ethanol, pH = 2.0 ± 0.8) by using 1 M HCl as a catalyst. The molar ratio H<sub>2</sub>O:TEOS was fixed at 4:1. After approximately 1 hour, in which hydrolysis reaction took place, the inorganic and the organic phases were mixed together for 1 hour, allowing the formation of the hybrid network.

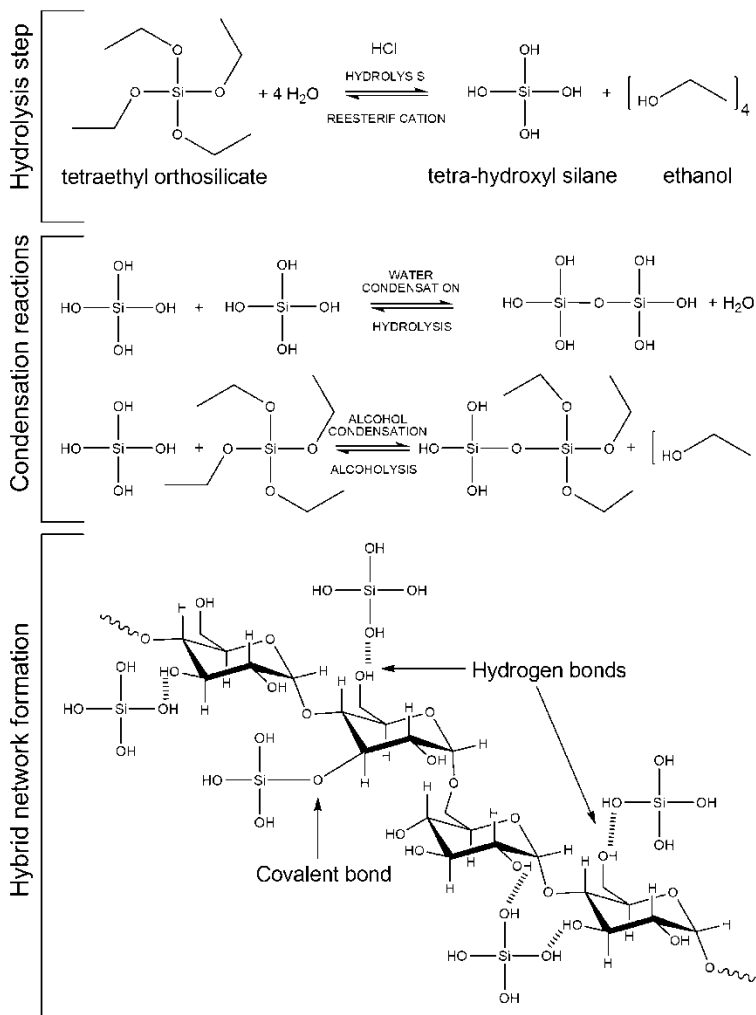


Figure 32 Schematic representation of the reaction expected in the sol-gel hybrid network formation.

Table 12. Coatings' formulations and thickness.

Exp. n°	Coded Name	Pullulan (wt %)	Si(OH) <sub>4</sub> (wt %)	(O/I*) ratio	Coating thickness (µm)**
1	H <sub>0</sub>	10	0	/	1.27 ± 0.12 <sup>a</sup>
2	H <sub>3</sub>	7.5	2.5	3	1.37 ± 0.18 <sup>ab</sup>
3	H <sub>2</sub>	6.66	3.33	2	1.31 ± 0.07 <sup>ab</sup>
4	H <sub>1</sub>	5	5	1	1.26 ± 0.14 <sup>ab</sup>
5	H <sub>0.75</sub>	4.3	5.7	0.75	1.19 ± 0.08 <sup>ab</sup>
6	H <sub>0.5</sub>	3.33	6.66	0.5	1.15 ± 0.09 <sup>b</sup>

\* "I" refers to the silanol form, Si(OH)<sub>4</sub>, calculated by the initial TEOS content and assuming the completion of the hydrolysis reaction.

\*\*Different superscripts denote statistically significant differences within groups (p < 0.05).

#### **4.1.1.2.b Coated films preparation**

The different coatings formulations were deposited on PET film, according to the procedure reported in paragraph 3.1.1.2.b.

#### **4.1.1.2.c Thickness determination**

See paragraph 3.1.1.2.c.

#### **4.1.1.2.d Fourier Transform Infrared - Attenuated Total Reflectance (FTIR-ATR)**

The structural characteristics and chemical bonding of the coatings at different O/I ratios were investigated by a PerkinElmer FT-IR Spectrum 100 Series spectrometer (PerkinElmer, Waltham, MA, USA) equipped with a universal attenuated total reflectance (UATR) accessory featuring a single-reflection sampling plate with a 1.8 mm round germanium surface. To ensure satisfactory physical contact between the samples and the crystal surface, a high-pressure clamping device was used. Spectra were recorded at room temperature within the range of 650–4000  $\text{cm}^{-1}$  at 4  $\text{cm}^{-1}$  resolution. Spectrum 6.0 software was used for data acquisition and analysis.

#### **4.1.1.2.e Microscopy analyses**

Transmission electron microscopy (TEM) images were captured to visualize the individual phases (i.e., the inorganic  $\text{SiO}_2$  and the organic pullulan phase) as well as the hybrid network growth. For this purpose, 5  $\mu\text{L}$  of the hybrid dispersions were deposited onto a Formvar-coated Cu grid (400-mesh). After adsorption, the grid was stained with a droplet (5  $\mu\text{L}$ ) of 1% uranyl acetate and dried with filter paper. Observations were made using a LEO 912 AB energy-filtering transmission electron microscope (EFTEM) (Carl Zeiss, Oberkochen, Germany) operating at 80 kV. Digital images were recorded with a ProScan 1K Slow-Scan CCD camera (Proscan, Scheuring, Germany).

The global organization of coated surfaces and the possible presence of fractures on the coated layers were visualized using an optical microscope (OM) (Micro Nikon Eclipse ME600 Laboratory Imaging; Nikon Instruments, Sesto Fiorentino, Italy) at 10 $\times$  magnification. Pieces of coated films (30  $\times$  10 mm) after storage in the desiccator were fixed on a rectangular steel sample holder and observed without any pre-treatment. Image capture and refining were carried out using NIS-Element software (Nikon Instruments, Sesto Fiorentino, Italy).

#### **4.1.1.2.f Oxygen barrier properties**

See paragraph 3.1.1.2.e.

#### **4.1.1.2.g Statistical analysis**

See paragraph 3.3.1.2.h.

## 4.1.2 Results and discussion

### 4.1.2.1 Coating thickness

Coating thicknesses are reported in Table 12. Despite the same initial solid content of 10 wt%, formulations with a higher inorganic content had a tendentially reduced thickness. It can be explained considering a dilution effect arising from ethanol byproduct formation.

### 4.1.2.2 FTIR-ATR analyses

FTIR-ATR analyses are summarized in Figure 33. Spectra of pure pullulan and reacted TEOS (i.e. after hydrolysis and condensation reactions) are displayed in panels a and b, respectively, with evidence of some characteristics peaks (Limpo et al, 1933; Shingel, 2002). Panel c and d show the two most significant spectral regions where changed occurred in the hybrid coatings at different O/I ratios.

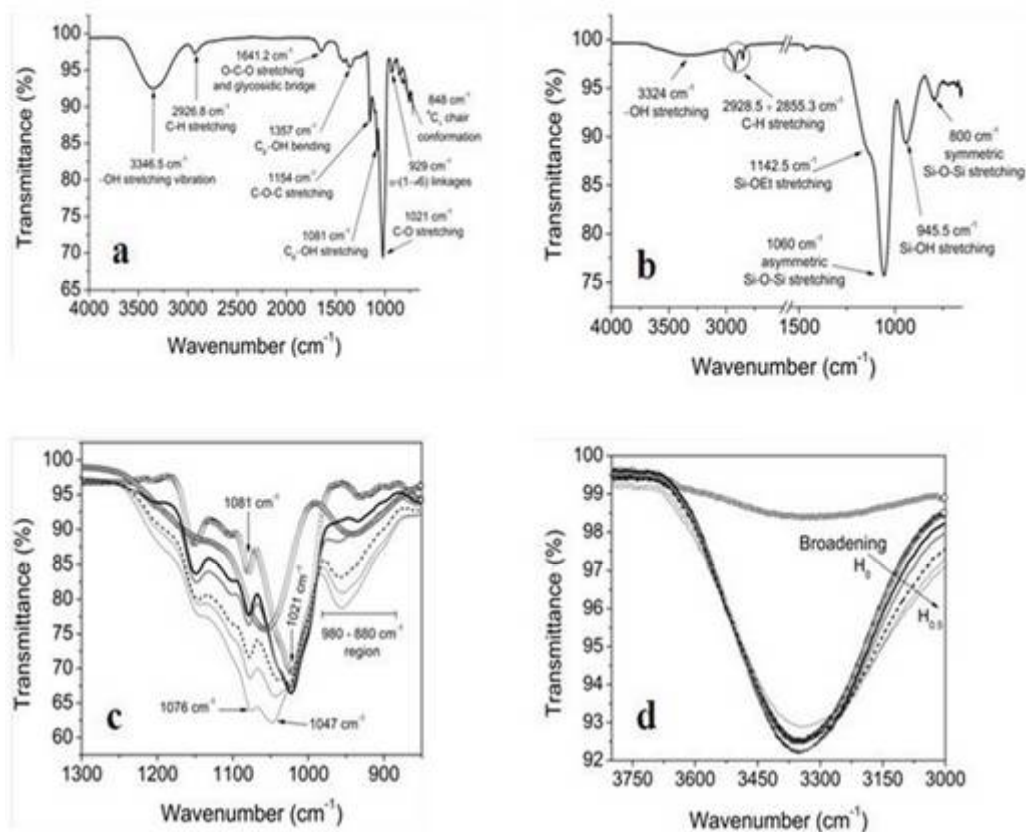


**Figure 33** FTIR-ATR spectra of pullulan (a), reacted TEOS (b) and pullulan (□), reacted TEOS (○), and hybrid coatings  $H_{0.5}$  (—),  $H_{0.75}$  (⋯⋯⋯),  $H_1$  (- - -),  $H_2$  (—),  $H_3$  (—) within 1300  $cm^{-1}$  – 850  $cm^{-1}$  (c) and 3800  $cm^{-1}$  – 3000  $cm^{-1}$  (d) spectral ranges.

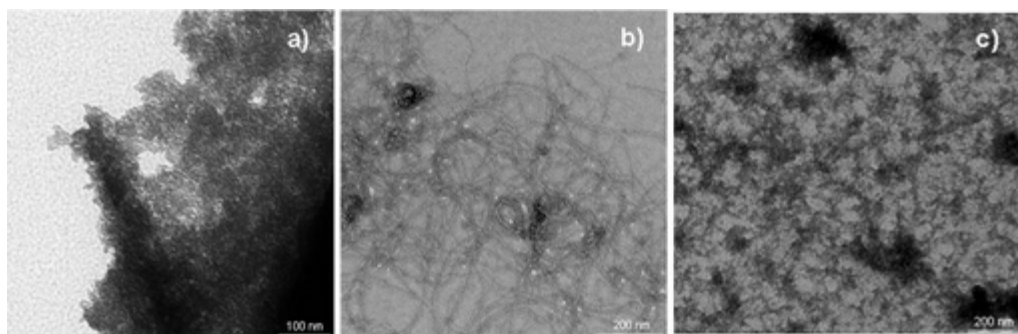
In Figure 33c and 33d are visible three important events related to the increase in the inorganic content formulation:

- 1) in the region  $980\text{--}880\text{ cm}^{-1}$  the band including two overlapping peaks (Si–OH of TEOS and  $\alpha$ -(1-6) linkages of pullulan) gradually shifted towards higher wavenumbers;
- 2) the same happened for the peak of pure pullulan at  $1081\text{ cm}^{-1}$ , that shifted up to  $1076\text{ cm}^{-1}$ ;
- 3) at around  $3300\text{ cm}^{-1}$ , the band, associated to hydroxyl group stretching became broader compared to that of pure pullulan and slightly shifted towards higher wavenumbers.

These phenomena are associated with possible formation of hydrogen bonding between the silanol of TEOS and the hydroxyl groups of pullulan (Uragami et al, 2002; Lee et al, 1999; Tong et al, 2008). Finally, there is a peak at around  $1047\text{ cm}^{-1}$  that could be related to the initial sharp peak at  $1021\text{ cm}^{-1}$  of pullulan. This peak could be tentatively explained with the formation of covalent bonds between TEOS and pullulan: however, even if the formation of covalent bonds from TEOS and hydroxyl groups of an organic phase (PVOH) has been claimed (Minelli et al, 2010; Uragami et al, 2002), it is a premature hypothesis that needs further experimental confirmations.

#### 4.1.2.3 Transmission electron microscopy analyses

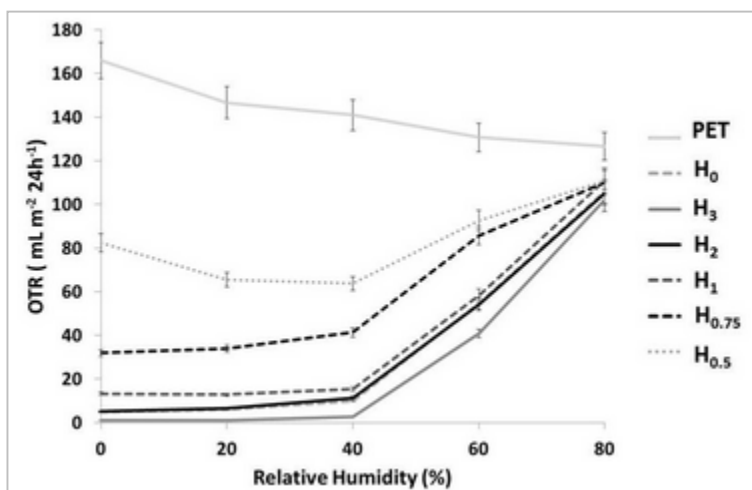
Figure 34 displays representative TEM images of pure silica, pullulan and hybrid coating  $H_1$ . TEM image 34a displays the  $\text{SiO}_2$  network after hydrolysis and condensation of the metal alkoxide precursor (i.e., TEOS): the inorganic network was formed by silica particles approximately 30–50 nm in diameter: they form a compact organization that reflect the typical high rigidity of pure silica coating. Conversely, in the TEM figure 34b pullulan appeared with a more disordered organization and entanglements, linked to the flexibility of the high molecular weight chains, with an estimated diameter of approximately 5–7 nm. The association of the two phases (i.e., organic and inorganic) led to a new scenario (Figure 34c): the larger-size silica clusters appear to be twisted by pullulan chains. The final silica–pullulan structure can thus be conceived as a self-assembled three-dimensional hybrid network, where the organic and inorganic phases interact spontaneously through intermolecular hydrogen bonding, as also shown by FTIR-ATR.



**Figure 34** TEM images of (a) reacted TEOS, (b) pullulan, and (c) hybrid coating  $H_1$ . All images are from 0.5 wt % hybrid dispersions 1 h after preparation.

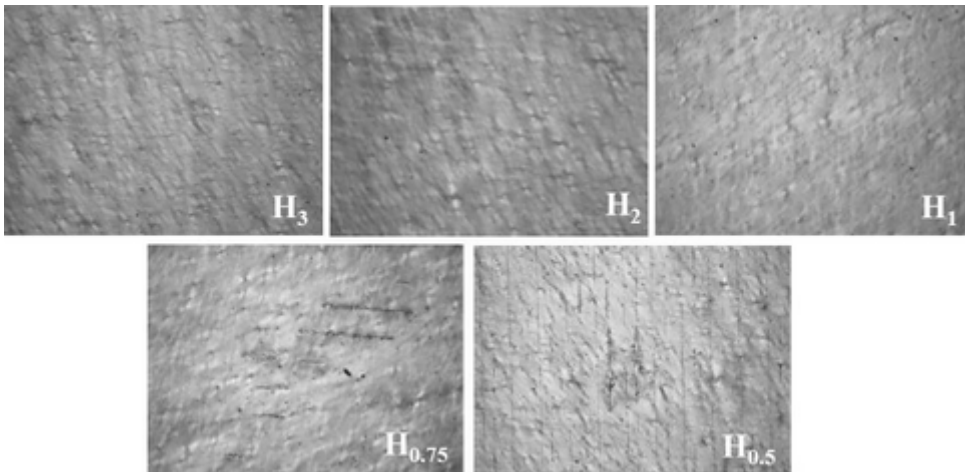
#### 4.1.2.4 Oxygen barrier properties and optical microscopy analyses

Figure 35 shows the oxygen barrier results for each film analyzed. It can be seen that all hybrid coatings provided an OTR reduction compared to the neat substrate (PET), at least up to 60% relative humidity, but the best performance is shown by formulation H<sub>3</sub>. However, the general trend indicates that increasing the inorganic concentration had a detrimental effect on the barrier properties of the final structure. This is in contrast to what was expected, as it is well established that decreasing the O/I ratio should improve the barrier properties.



**Figure 35** OTR evolution for PET, pullulan, and the five hybrid coatings over the 0%–80% relative humidity gradient range at 23°C.

The cause can be linked to some physical changes, induced by the decrease in the O/I ratio, on the overall organization of the final coatings: increasing the inorganic component yielded a concomitant increase in the inherent rigidity of the silica network, which prevailed on the innate flexibility of pullulan, thereby causing ruptures and cracks that dramatically affected the film's permeability. To confirm this hypothesis, optical microscopy images helped understanding the final structures: increasing TEOS content, bright veins started to appear and they became clear surface failures, evident in sample H<sub>0.5</sub>.



**Figure 36** Optical microscope images of coating surfaces at 10× magnification.

The failures appeared as parallel cracks of  $\sim 10 \mu\text{m}$  and separated by  $\sim 100 \mu\text{m}$  one from the other, suggesting that they probably formed along the tracks of the wires of the rod used to lay the coating dispersion on PET substrate. The main reason probably lies in the shrinking of the matrix during the solvent evaporation step, as also reported by many authors (Lee et al, 1999; Fabbri et al, 2006; Kim, 2008). This ruptures affected the oxygen transmission rate for two reasons. First of all they acted as gaps in the matrix and secondly they amplifies water vapor penetration in the coating network, accelerating pullulan swelling, which in turn affect the final oxygen permeability.

### 4.1.3 Conclusions

This part of the PhD research has demonstrated that the bottom-up approach can be profitably used to generate bio-hybrid coatings. The combination of pullulan with TEOS has generated oxygen barrier layers formed by a hybrid network stabilized by intermolecular hydrogen bonds between the SiOH groups of hydrolyzed TEOS and the pendant hydroxyl groups of pullulan. The formulations tested led to a reduction of the OTR values (ranging from ~99% to ~27%) compared to the neat PET substrate, however they lost their barrier capacity at 80% RH. The best performance was reached by the hybrid coating with the lowest amount of silica (H<sub>3</sub>), fully comparable to those reported in literature for similar organic/inorganic hybrid coatings, at least up to 60% relative humidity (Minelli et al, 2008). This behavior is attributable to the protective effect of the inorganic phase toward the surrounding humidity, together with absence of cracks and pinholes that easily formed in formulations with higher silica content. The biopolymer used emerged as a valid alternative, in association with silica, to the commonly used organic polymers derived from petrol for the development of oxygen barriers coatings for food packaging applications (Farris et al, 2012).

The main hurdle to the application is represented by pullulan cost. Based on the latest quotation of each component, the unit cost of PET film (12 µm) coated with the H<sub>3</sub> formulation is estimated at around 3.7 €/kg, which is higher than the sale price of the today's oil-derived alternatives (e.g., the price of PET 12 µm coated with PVOH 1.0 µm is ~2.6 €/kg).

## 4.1.4 References

- Bang G, Kim SW. 2012, Biodegradable poly(lactic acid)-based hybrid coating materials for food packaging films with gas barrier properties. *Journal of Industrial and Engineering Chemistry*. 18:1063–1068.
- Fabbri P, Singh B, Leterrier Y, Manson JAE, Messori M, Pilati F. 2006, Cohesive and adhesive properties of polycaprolactone/silica hybrid coatings on poly (methyl methacrylate) substrates. *Surf Coat Tech* 200:6706–6712.
- Farris S, Introzzi L, Fuentes-Alventosa JM, Santo N, Rocca R, Piergiovanni L. 2012, Self-assembled pullulan-silica oxygen barrier hybrid coatings for food packaging applications. *J Agric Food Chem*. 60:782-790.
- Geppi M, Mollica G, Borsacchi S, Marini M, Toselli M, Pilati F. 2007, Solid state NMR characterization of PE-PEG/silica hybrid materials prepared by microwave-assisted sol-gel process. *J Mater Res* 22:3516–25.
- Kim SW. 2008, Preparation and barrier property of poly (vinyl alcohol)/SiO<sub>2</sub> hybrid coating films. *Korean J Chem Eng* 25:1195–1200.
- Lee SY, Lee JD, Yang SM. 1999, Preparation of silica-based hybrid materials coated on polypropylene film. *J Mater Sci* 34:1233–1241.
- Limpo J, Rubio J, Oteo JL. 1993, Estudio por FT-IR de la hidrolisis del tetraetilortosilicato. *Bol Soc Esp Ceram V* 1:31–35.
- Minelli M, De Angelis MG, Doghieri F, Marini M, Toselli M, Pilati F. 2008, Oxygen permeability of novel organic–inorganic coatings: I. Effects of organic–inorganic ratio and molecular weight of the organic component. *Eur Polym J*. 44:2581–2588.
- Minelli M, De Angelis MG, Doghieri F, Rocchetti M, Montenero A. 2010, Barrier properties of organic-inorganic hybrid coatings based on polyvinyl alcohol with improved water resistance. *Polym Eng Sci* 50:144–153.
- Shingel KI. 2002, Determination of structural peculiarities of dextran, pullulan and  $\gamma$ -irradiated pullulan by Fourier-transform IR spectroscopy. *Carbohyd Res* 337:1445–1451.
- Ștefănescu M, Stoia M, Ștefănescu O, Popa A, Simon M, Ionescu C. 2007, The interaction between TEOS and some polyols. Thermal analysis and FTIR. *J Therm Anal Calorim*. 88:19–26.
- Tong Q, Xiao Q, Lim LT. 2008, Preparation and properties of pullulan–alginate–carboxymethylcellulose blend films. *Food Res Int* 41:1007–1014.
- Toselli M, Marini M, Fabbri P, Messori M, Pilati F 2007, Sol-gel derived hybrid coatings for the improvement of scratch resistance of polyethylene. *J Sol-Gel Sci Technol*. 43:73–83.
- Uragami T, Okazaki K, Matsugi H, Miyata T. 2002, Structure and permeation characteristics of an aqueous ethanol solution of organic-inorganic hybrid membranes composed of poly(vinyl alcohol) and tetraethoxysilane. *Macromolecules* 35:9156–9163.

## 4.2 Bio-nanocomposite coatings

In this part of the work, the nanotechnology approach called top-down was exploited to produce (bio)nanocomposite materials in the form of coatings. In particular, a natural montmorillonite, Cloisite® Na<sup>+</sup> was chosen as the inorganic component together with a biopolymer, for the design of the final bio-nanocomposite coating to be applied on PET film, to improve its oxygen barrier properties. The biopolymer chosen was pullulan, which resulted to be a valid candidate for replacing synthetic polymers in oxygen barrier applications, as discussed in the previous parts of the PhD research. As for the nano-sized particles, recent advantages in nanotechnology showed their effectiveness in depressing the permeation of oxygen molecules across the material thickness (Pojanavaraphan et al, 2010; Liu et al, 2011; Svagan et al, 2012). However, the key point to exploit the potential of nanoparticles relies on their complete exfoliation in the polymer matrix, in such a way that they are able to expose their high surface area to the polymer (Figure 37).

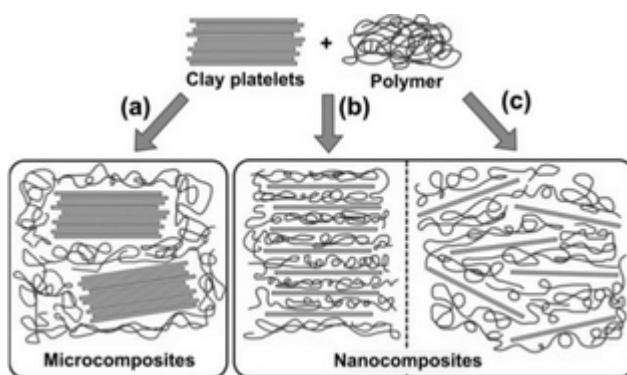


**Figure 37** Tactoid (a), intercalated (b) and exfoliated (c) polymer–clay nanocomposite morphologies. Source: Duncan et al, 2011.

Taking into account the above considerations, nano-sized inorganic components adequately dispersed in a polymer matrix can affect its permeability in two specific ways (Duncan, 2011):

- the oxygen diffusion is reduced due to the presence of a more tortuous path (Figure 38);
- the interface phenomena at the polymer/filler interface make the polymer matrix partially immobilized, thus reducing the so-called ‘segmental mobility’ of polymer chains.

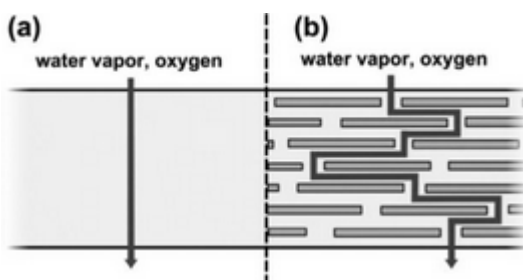


**Figure 38** Illustration of the “tortuous pathway” created by incorporation of exfoliated clay nanoplatelets into a polymer matrix film. Source: Duncan et al, 2011.

For a proper dispersion of the platelets, several physical processes can be used. Among others, ultrasonication is capturing an increasing attention due to its advantages over other methods. Ultrasonication works through ultrasound waves that are able to deagglomerate and progressively downsize the original particle. These effects are achieved thanks to the cavitation phenomenon, which refers to the formation, growth, and implosive collapse of bubbles in a liquid (Hielscher, 2005). After bubbles collapse, a number of major local events prompt the deagglomeration of micro-sized particles dispersed in the medium: heating (~5000 K), high pressure (~1000 atm), huge heating-cooling rates ( $> 10^9 \text{ K s}^{-1}$ ), and abrupt liquid jet streams (~400 km h<sup>-1</sup>) (Suslick, 1998). All of these phenomena overcome the attraction forces (electrostatic, van der Waals) holding together the platelets stacked on top of one another to form the aforementioned tactoids.

To date, many examples of bionanocomposites can be retrieved in the literature, envisaging the incorporation of the inorganic phase into the bulky polymer (Darder et al, 2003; Zhou et al, 2009; Sehaqui et al, 2011; Abalde-Cela et al, 2011; Cabedo et al, 2006; Yu et al, 2007; Zheng et al, 2009; Zhou et al, 2009; Ahmadi et al, 2011). On the other hand, dealing with bionanocomposites coatings, only two papers have been found in our research: one made of chitosan and nanoclays laid on PLA (Svagan et al, 2012), and on LDPE film (Vartiainen et al, 2010).

Hereinafter the performances (in terms of barrier and optical properties) of a pullulan based nanocomposite are reported, and they were investigated in light of the ultrasound treatment process. The oxygen permeation characteristics were also compared with predictions by various theories available in the literature.

The work presented in this part is here reported:

Introzzi L, Blomfeldt TOJ, Trabattoni S, Tavazzi S, Santo N, Schiraldi A, Piergiovanni L, Farris S. 2012, Ultrasound-assisted pullulan/montmorillonite bionanocomposite coating with high oxygen barrier properties. *Langmuir*. 28:11206-11214.

## 4.2.1 Materials and methods

### 4.2.1.1 Materials

Pullulan was considered as the organic component (see paragraph 3.1.1.1.a for more details about pullulan).

The inorganic component was a natural montmorillonite, Cloisite® Na<sup>+</sup> (Southern Clay Products Inc., Rockwood Additives, Gonzales, TX).

PET film was used as the substrate for coating deposition (see paragraph 3.1.1.1.b for film specifications).

### 4.2.1.2 Methods

#### 4.2.1.2.a Coating dispersions preparation

A fixed amount of pullulan (4 wt % wet basis) was dissolved in water at 25° C for 1 h under gentle stirring (500 rpm). At the same time, clay powder, in a quantity ranging from 0.2 and 3.0 wt %, was dispersed in water under vigorous stirring (1000 rpm) for 15 minutes. The resulting dispersion was ultrasonicated by means of an UP400S (power<sub>max</sub> = 400 W; frequency = 24 kHz) ultrasonic device (Hielscher, Teltow, Germany) equipped with a cylindrical titanium sonotrode (mod. H14, tip Ø 14 mm, amplitude<sub>max</sub> = 125 µm; surface intensity = 105 W cm<sup>-2</sup>) under the following conditions: 0.5 cycles and 50% amplitude. The duration of the ultrasonic treatment varied in accordance with the experimental design (see Table 13, fourth column). The organic pullulan solution and the inorganic dispersion were then mixed together under gentle stirring (500 rpm) for additional 90 minutes. After mixing, the concentrations of the two components corresponded to an inorganic/organic (I/O) ratio ranging from 0.05 to 0.75 (see Table 13, third column).

**Table 13** Worksheet of the CCF factorial design.

Exp. N°	Run order	Variable levels		Responses	
		X <sub>1</sub> (x <sub>1</sub> ) <sup>a</sup>	X <sub>2</sub> (x <sub>2</sub> ) <sup>b</sup>	Y <sub>1</sub> <sup>c</sup>	Y <sub>2</sub> <sup>d</sup>
1	11	0.05 (-1)	15 (-1)	887.44	1.89
2	8	0.75 (+1)	15 (-1)	196.10	4.25
3	9	0.05 (-1)	45 (+1)	913.61	1.80
4	4	0.75 (+1)	45 (+1)	249.94	4.16
5	10	0.05 (-1)	30 (0)	950.66	1.87
6	3	0.75 (+1)	30 (0)	181.688	4.48
7	6	0.4 (0)	15 (-1)	236.99	3.15
8	7	0.4 (0)	45 (+1)	239.42	2.80
9	5	0.4 (0)	30 (0)	297.60	3.12
10	2	0.4 (0)	30 (0)	307.27	2.72
11	1	0.4 (0)	30 (0)	309.82	2.88

<sup>a</sup> Inorganic/organic ratio (I/O). <sup>b</sup> Ultrasonication time (min). <sup>c</sup> Oxygen permeability coefficient (P'O<sub>2</sub>, mL µm m<sup>-2</sup> 24h<sup>-1</sup> atm<sup>-1</sup>). <sup>d</sup> Haze (%). Coded values are reported between brackets.

### 4.2.1.2.b Coated films preparation

The deposition of the coating on PET films is the same as reported in paragraph 3.1.1.2.b. Differences in solids between formulations were reset by means of two sequential depositions and using steel horizontal rods with different engraved patterns, which yielded final coatings of comparable nominal thickness of 1  $\mu\text{m}$  after water evaporation. Scanning electron microscopy (SEM) analysis confirmed the final coating thicknesses (Figure 39).

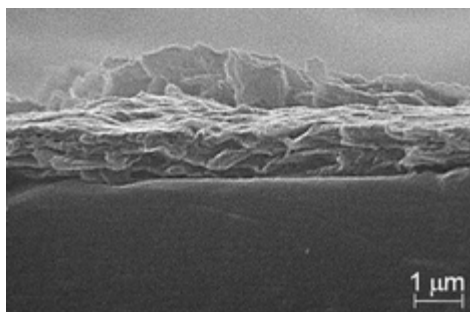


**Figure 39** FE-SEM cross-sectional image of the bionanocomposite coating on the PET substrate at  $20k\times$  magnification. Note the thickness of the coating being  $\sim 1.0\ \mu\text{m}$ .

### 4.2.1.2.c Oxygen permeability ( $P'O_2$ ) measurements

The oxygen barrier properties of both uncoated and coated PET films were assessed on a 50  $\text{cm}^2$  surface sample using a MultiPerm permeability analyzer (ExtraSolution® Srl, Capannori, Italy), equipped with an electrochemical sensor, according to the standard method ASTM F2622-08 and with a carrier flow ( $\text{N}_2$ ) of 10  $\text{mL min}^{-1}$ . With the goal of quantifying the influence of the external relative humidity conditions on the films barrier properties, measurements were performed at 23°C and at 70% of relative humidity. The results, each one from three replicates, were expressed as the Oxygen Transmission Rate (OTR,  $\text{mL m}^{-2} 24\ \text{h}^{-1}$  at one atmosphere pressure difference).

Final  $P'O_2$  coefficients were calculated according to the following equation:

$$P'O_2 = PO_2 \times t = \frac{O_2TR}{\Delta p} \times t \quad (17)$$

Where:

- $P'O_2$  is the oxygen permeability coefficient ( $\text{mL } \mu\text{m m}^{-2} 24\text{h}^{-1} \text{atm}^{-1}$ );
- $PO_2$  is the permeance (defined as the ratio of the  $O_2TR$  to the difference between the partial pressure of the gas on the two sides of the film,  $\Delta p$ );
- $t$  is the total thickness of the material (substrate plus coating).

#### 4.2.1.2.d Haze

See paragraph 3.3.1.2.g.

#### 4.2.1.2.e Experimental design

A chemometric approach based on the Design of Experiment (DoE) technique was used to map the simultaneous evolution of the two dependent variables ( $Y_1$  = oxygen permeability coefficient, P'O<sub>2</sub>;  $Y_2$  = haze). Haze was considered too because the inclusion of an inorganic phase can jeopardize the aspect of the final materials. The independent variables considered were two ( $X_1$  = inorganic/organic ratio (I/O);  $X_2$  = ultrasonication time) within the experimental range defined by a minimum (coded as -1) and a maximum (coded as +1) (see Table 13). The design selected was a central composite face (CCF) one supported by a polynomial equation that allows the development of a semiempirical model of the general formula:

$$Y = b_0 + b_1X_1 + b_2X_2 + b_{12}X_1X_2 + b_{11}X_1^2 + b_{22}X_2^2 + \varepsilon \quad (18)$$

Where:

- $Y$  represents the two responses (P'O<sub>2</sub> and haze);
- $X_1$  and  $X_2$  are the codified values of the two factors (inorganic/organic ratio and ultrasonication time);
- $b_0$  is the response value when all factors are set at the medium level (center point);
- $b_1$  and  $b_2$  are linear regression coefficients;
- $b_{12}$  is the interaction regression coefficient;
- $b_{11}$  and  $b_{22}$  are quadratic regression coefficients;
- $\varepsilon$  is the residual response variation not explained by the model.

This approach allowed pinpointing the best factors combination according to the optimization criteria set up for each response. The MODDE software package (MODDE 2006, version 8.0; UMETRICS AB, Umea, Sweden) was used throughout the investigation for the evaluation of raw data and regression analysis.

#### 4.2.1.2.f Particle size analysis

The size distribution in water dispersion of the Na<sup>+</sup>-MMT clays before and after ultrasonic treatment was assessed using an IKO-Sizer CC-1 nanoparticle analyzer (IKO Science, Tallin, Estonia). This instrument, a photon counter mounted on an avalanche photodiode (APD), measures the particle size based on the photon correlation spectroscopy (PCS) technique. More specifically, the instrument determines the velocity distribution of particle movement by measuring the dynamic fluctuations of the intensity of light (635 nm) scattered at 90°.

The prepared clay dispersions were diluted to a droplet concentration of approximately 0.006 wt % before analysis. The Photocor-FC correlator software was used for the data analysis. The particle size measurements are reported as the average and standard deviation of measurements made on two freshly prepared samples, with three readings made per sample.

#### 4.2.1.2.g Electron microscopy analysis

Transmission electron microscopy (TEM) images were captured to visualize the extent of deagglomeration and dispersion of the Na<sup>+</sup>-MMT clays in both distilled water and pullulan matrix. To this purpose, 5  $\mu$ L of a 3.0 wt % water dispersion were deposited onto a Formvar-coated Cu grid (400 mesh). Observations were made after 24 hours (i.e., the time required to allow solvent evaporation) using an LEO 912 AB energy-filtering transmission electron microscope (EFTEM) (Carl Zeiss, Oberkochen, Germany) operating at 80 kV. Digital images were recorded with a ProScan 1K Slow-Scan CCD camera (Proscan, Scheuring, Germany).

Field-emission scanning electron microscopy (FE-SEM) micrographs were obtained to acquire more detailed information on the morphology and global organization of both pure pullulan and clay-loaded pullulan coatings as well as to determine the thickness of the final nanocomposite coatings. Both cross-sections and surfaces of the samples were examined using a Hitachi S-4800 FE-SEM (Schaumburg, IL, USA). Surface test specimens were mounted with carbon tape on stubs. Cross-sectioned samples were cut into thin pieces with a scalpel and mounted on a Hitachi thin specimen split mount holder, M4 (prod. No 15335-4). Before insertion into the microscope, the samples were sputter-coated with gold to a thickness of approximately 10 nm (to avoid charging the samples) using an Agar High Resolution Sputter Coater (model 208RH) equipped with a gold target/Agar thickness monitor controller.

#### 4.2.1.2.h Atomic force microscopy

The surface morphology of pure pullulan coatings and pullulan nanocomposite coatings was analyzed using an atomic force microscope (AFM) Nanoscope V MultiMode (Veeco) in tapping mode. Measurements were carried out in air using a silicon tip (resonance frequency 287-346 kHz, spring constant 20–80 N/m). The images were recorded with a resolution of 512  $\times$  512 pixels and corrected using a second-order polynomial background filter. The root mean square roughness  $S$  was also evaluated for each sample as the standard deviation of the topography over the 10  $\times$  10  $\mu$ m<sup>2</sup> scanning area ( $M \times N$  pixels):

$$S = \sqrt{\frac{1}{MN} \sum_{i=1}^M \sum_{j=1}^N |z(x_i, y_j) - \bar{z}|^2} \quad (19)$$

where  $\bar{z}$  is the mean value of the topography  $z(x,y)$ .

## 4.2.2 Results and discussion

### 4.2.2.1 Effect of clay concentration and ultrasound treatment time on oxygen barrier and haze properties

Based on the experimental data, equation (18) has been used to model the dependence of haze and  $P'O_2$  on I/O ratio and sonication time (see Table 13). The regression coefficient values, graphically displayed in Figure 40, are reported in Table 14 together with the correspondent level of significance. The final models adequately described the responses, as indicated by the ANOVA table reported in Table 15 and, in particular, by the coefficient  $R_2$  (fitting capability) and  $K_2$  (prediction capability) which are very close to unity.

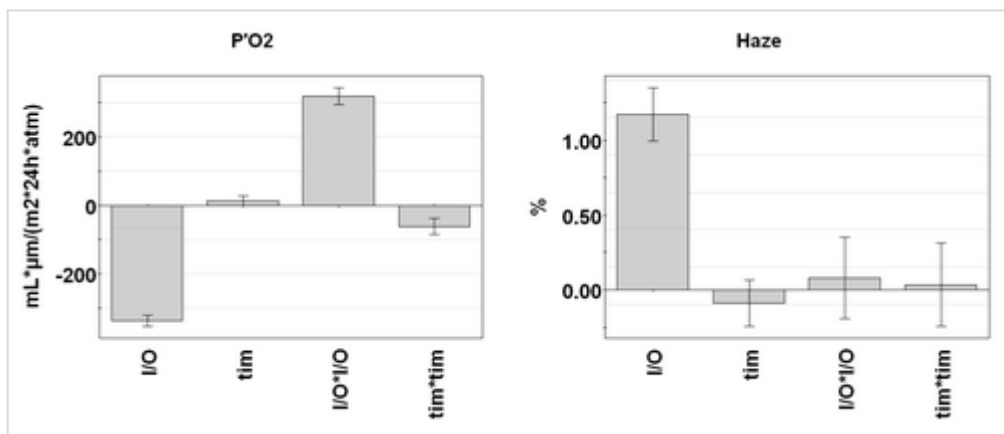


Figure 40 Coefficient plots for  $P'O_2$  and haze responses.

Table 14 Regression coefficients and level of significance for the fitted model.

Factor	$P'O_2$			Haze		
	effect (mL µm m <sup>-2</sup> 24h <sup>-1</sup> atm <sup>-1</sup> )	standard error	p-value	effect (%)	standard error	p-value
$b_0$	302.529	7.0199	0.0000♦	2.92	0.0783	0.0000♦
$b_1$	-336.9810	6.2048	0.0000♦	1.1700	0.0692	0.0000♦
$b_2$	13.7389	5.3615	0.0505	-0.0883	0.0598	0.1998
$b_1b_1$	318.249	9.3690	0.0000♦	-0.0800	0.1045	0.4786
$b_2b_2$	-60.7758	9.6124	0.0015♦	0.0350	0.1072	0.7574

♣Factors:  $b_0$  = constant;  $b_1$  = (I/O);  $b_2$  = sonication time;  $b_1b_1$  = (I/O)\*(I/O);  $b_2b_2$  = sonication time\*sonication time. ♦Significant factors ( $p < 0.05$  or 95% confidence interval).

**Table 15** Analysis of variance for  $P'O_2$  response and haze

Source of variation	$Y_1$ (permeability coefficient)					$Y_2$ (haze)				
	DF <sup>a</sup>	SS <sup>b</sup>	MS <sup>c</sup>	F <sup>d</sup>	p <sup>e</sup>	DF <sup>a</sup>	SS <sup>b</sup>	MS <sup>c</sup>	F <sup>d</sup>	p <sup>e</sup>
Constant	1	12460.1	12460.1			1	82.024	82.024		
Total corrected	9	5406.0	600.6			9	6.8418	0.7602		
Regression	4	5400.9	1350.2	1323.0	0.000	4	6.7345	1.6836	78.43	0.000
Residual	5	5.1028	1.0205			5	0.1073	0.0214		
Lack of fit (Model error)	3	4.6109	1.537	6.2498	0.141	3	0.0262	0.0087	0.2160	0.879
Pure error (Replicate error)	2	0.4918	0.2459			2	0.0810	0.0405		
		$R^2 = 0.999$ $K^2 = 0.994$					$R^2 = 0.984$ $K^2 = 0.955$			

<sup>a</sup>Degrees of freedom. <sup>b</sup>Sum of squares. <sup>c</sup>Mean square. <sup>d</sup>F ratio, the model significance (regression/residual). <sup>e</sup>p-value.

First, the dependence of haze and  $P'O_2$  on the clay concentration (I/O ratio) is discussed. Figure 41a shows that haze increased with an increase in I/O, due to the higher extent of visible light diffused by the inorganic particles. Concerning the permeability coefficient, in Figure 41b, and for a better comprehension in Figure 42, is evident that  $P'O_2$  decreased when I/O increased to approximately 0.55. Above this value, an additional increase in inorganic content did not bring any improvement. Even, the highest I/O value (0.75) seems to have a detrimental effect on the barrier property of the coated films. As already reported (Bordes et al, 2009; Wilson et al, 2011) when the clay content was increased beyond a certain limit, the reaggregation of the platelets to again form tactoids may occur, leading to a micro-composite instead of a nanocomposite structure. It is known that this may reduce the oxygen-barrier performance.

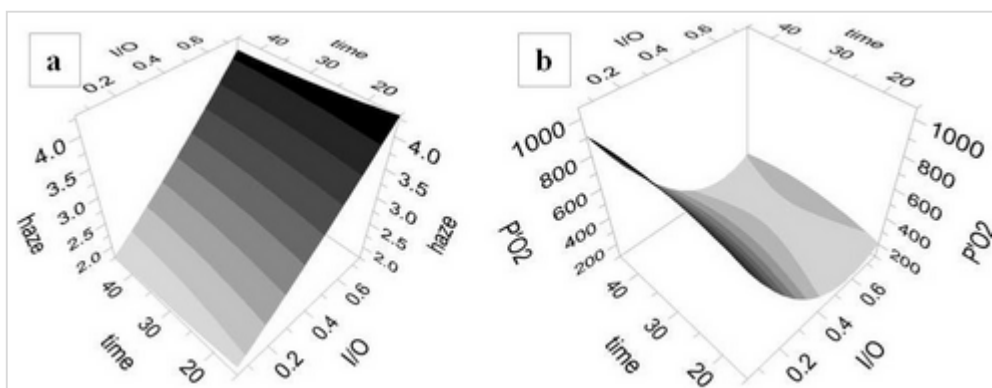


**Figure 41** Response surface plots showing the influence of I/O and sonication time (min) on haze (a) and on  $P'O_2$  (b).

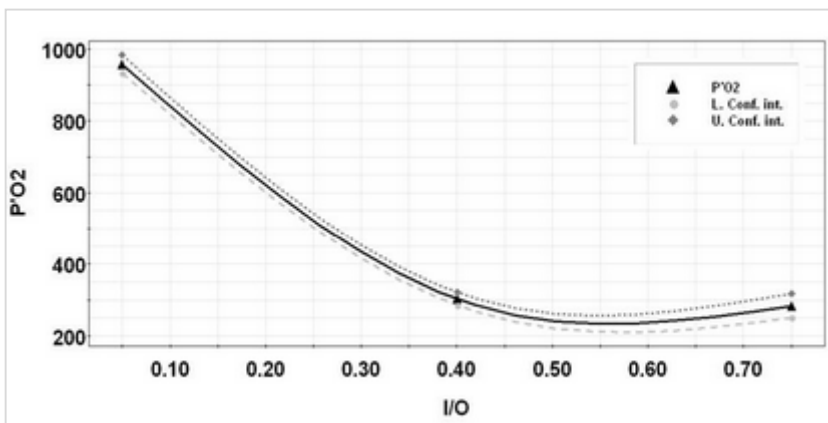


Figure 42 Response prediction plot showing the influence of I/O on P'O<sub>2</sub>.

Concerning the effect of the sonication time, haze is not significantly affected by prolonged treatment (Figure 41a and static values in Table 14), whereas some considerations can be made for the permeability coefficient response (Figure 41b). The observed P'O<sub>2</sub> variation (see also Figure 43) indicates that time can be optimized: a treatment that exceed the 15 minutes, that means a higher energy input to the system, may promote reagglomeration of platelets; then, after a certain point their fragmentation is probably promoted. In other words, for a fixed amount of clays the most effective sonication time was found to be 15 minutes, while longer ultrasound treatment increases the P'O<sub>2</sub> value (due to reaggregation) which decreases again at the highest sonication time (45 min), presumably owing to the fragmentation of both platelets and tactoids.

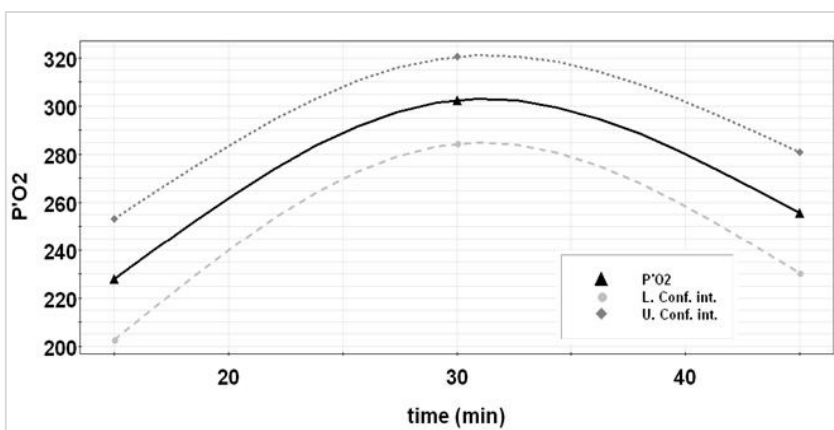


Figure 43 Response prediction plot showing the influence of sonication time (min) on P'O<sub>2</sub>.

Therefore, not only the clay concentration (I/O) but also reaggregation and fragmentation dramatically affect the final barrier properties of the composite coatings. Reaggregation causes voids and discontinuities within the main polymer matrix (pullulan in this case), which eventually yields free volume increases (Wilson et al, 2011); fragmentation leads to a remarkable reduction in the aspect ratio of the inorganic filler. The invariance of haze as a

function of the sonication time allows selecting the proper time to improve the oxygen-barrier performances without substantially affecting the optical properties.

Moreover, the above findings have an important practical implication as they can lead to a significant reduction in energy consumption in terms of energy output per unit volume, which can be calculated according to the following formula:

$$E = \frac{I \cdot S}{V} \times t \quad (20)$$

Where:

- E = unit energy output (Ws mL<sup>-1</sup>);
- I = surface intensity (W cm<sup>-2</sup>);
- S = sonotrode surface area (cm<sup>2</sup>);
- t = time of exposure to the ultrasonic treatment (s);
- V = sample volume (mL).

According to the experimental setup adopted in this work, an energy unit output of 725 Ws mL<sup>-1</sup> was calculated for the 15-minute treatment while an extended ultrasonication time of 45 minutes yielded a unit energy consumption of 2060 Ws mL<sup>-1</sup>. This would allow the saving of quite a high amount of energy throughout the whole process, which will eventually be reflected in the final throughput costs.

#### 4.2.2.2 Modeling the $P'O_2$ data

The semi-empirical model expressed by equation (18) made it possible to extrapolate the  $P'O_2$  values of the bionanocomposite-coated PET films for any clay loading within the experimental I/O range of 0.05–0.75. In turn, this allowed the computation of the contribution of the nanocomposite coatings to the total (i.e., substrate plus coating)  $P'O_2$  values, in accordance with the well-known series resistance formula intended for multilayer systems (Lee et al, 2008):

$$\frac{l_{tot}}{P_{tot}} = \frac{l_{PET}}{P_{PET}} + \frac{l_{coating}}{P_{coating}} \quad (21)$$

where:

- $P$  = oxygen permeability coefficient ( $P'O_2$ , mL  $\mu\text{m m}^{-2} 24\text{h}^{-1} \text{atm}^{-1}$ ) of the layer;
- $l$  = the layer's thickness ( $\mu\text{m}$ ).

With knowledge of  $l_{tot}$ ,  $l_{PET}$ ,  $l_{coating}$ ,  $P_{tot}$ , and  $P_{PET}$ , the  $P'O_2$  coefficient ( $P_{coating}$ ) for the nanocomposite coatings can be calculated from equation 21. The results are summarized in Table 16. Finally, these values were fitted with both Nielsen's and Cussler's permeation theoretical models, which describe the permeation phenomenon across a two-phase film - for impermeable square platelets dispersed in a continuous polymer matrix (Takahashi et al, 2006):

$$P_0/P \cdot (1 - \phi) = 1 + (\alpha\phi)/2 \quad (22)$$

$$P_0/P \cdot (1 - \phi) = 1 + (\alpha\phi)^2/4 \quad (23a)$$

$$P_0/P \cdot (1-\phi) = 1 + (\alpha\phi/3)^2 \quad (23b)$$

where:

- $P_0$  = permeability parameter of the pure biopolymer coating
- $P$  = permeability parameter of the bionanocomposite coatings
- $\alpha$  = aspect ratio of the platelets (the width divided by the thickness)
- $\Phi$  = volume fraction of the platelets dispersed in the biopolymer matrix

**Table 16.** Volume fraction of the filler, oxygen permeability coefficient ( $P'O_2$ ) of the coated PET and of the bionanocomposite coatings.

Filler volume fraction <sup>a</sup>	$P'O_2$ (total) <sup>b</sup> (mL $\mu\text{m m}^{-2} 24\text{h}^{-1} \text{atm}^{-1}$ )	$P'O_2$ (coating) <sup>c</sup> (mL $\mu\text{m m}^{-2} 24\text{h}^{-1} \text{atm}^{-1}$ )
0.017	883.24	142.32
0.046	659.76	83.25
0.073	476.06	50.98
0.098	332.15	31.79
0.123	228.01	20.27
0.145	163.66	13.93
0.167	139.08	11.65
0.188	154.29	13.06
0.207	209.28	18.37

<sup>a</sup>Calculated for a given filler density  $\rho_{\text{clays}} = 2.86 \text{ g cm}^{-3}$ . <sup>b</sup>Data extrapolated from the software, according to the model developed with reference to equation (18) in the text. <sup>c</sup>According to equation (21) in the text and considering  $P'O_2 \text{ PET}$  (70% RH and 23°C)  $\sim 1560 \text{ mL } \mu\text{m m}^{-2} 24 \text{ h}^{-1} \text{atm}^{-1}$ .

The above models are different because Nielsen (eq. 22) assumes that the filler is evenly dispersed within the matrix and the permeation rate of the gas across the polymer matrix is influenced only by the tortuosity of the path; Cussler's models, by contrast, also consider the orientation of the inorganic platelets, which can be either oriented (equation 23a) or randomly dispersed (eq. 23b). Figure 44 displays the experimental  $P'O_2$  data for the pullulan nanocomposite coatings at different filler volume ratios ( $\Phi$ ), along with the  $P'O_2$  data predicted by Nielsen's and Cussler's models for different aspect ratios ( $\alpha$ ) between 10 and 100.

For both models, the overall trend of the predicted values is in line with the experimental data generated by the software. Nevertheless, for volume ratios above 0.18, the experimental data deviated from the calculated curve most likely due to the reagglomeration of the platelets, which causes depletion in the barrier performance following an increase in the free volume of the polymer matrix (Lee et al, 2008). Interestingly, up to  $\Phi = 0.073$  the best prediction obtained by Nielsen's model was for an estimated  $\alpha = 100$ , which is actually in line with the expected aspect ratio of approximately 100–150 for montmorillonite clays (Sinha et al, 2003; Utracki et al, 2007). However, above  $\Phi = 0.073$  the best fitting was obtained for  $\alpha = 50$ . This finding suggests that the clay distribution in the polymer matrix as exfoliated platelets is preserved up to an I/O  $\sim 0.225$  (i.e., clay concentration  $\sim 0.9$  wt %, wet basis). After this value, increasing the amount of clay leads to a decrease of  $\alpha$ , presumably due to the platelets partially stacking on top of one another, according to the proposed "self-similar clay aggregation mechanism" (Alexandre et al, 2000). In addition, it is worth noting that the Cussler's model, envisaging a random distribution of the platelets (eq. 23a), provided a better fitting compared with the model

(eq. 23b), accounting for a more oriented distribution. This result indicates that the platelets apparently assumed a random rather than an oriented distribution.

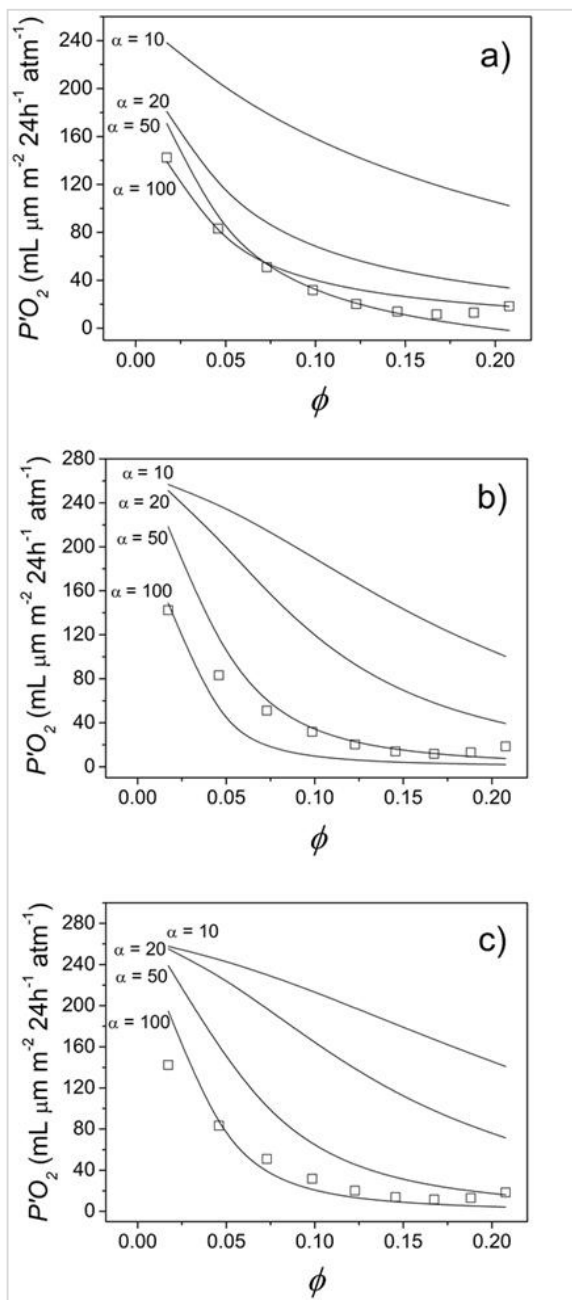


**Figure 44** Oxygen permeability of the bionanocomposite coatings. Experimental “software-generated” values ( $\square$ ) and values predicted by Nielsen’s (a) and Cussler’s (b and c) models (equation 22 and equations 23a and 23b in the text, respectively) for different aspect ratios ( $\alpha$ ).

### 4.2.2.3 Characterization of the best pullulan/clay nanocomposite coating

Arising from the considerations above, through a software-assisted procedure, it was possible to pinpoint the best factor combination able to achieve the lowest  $P'O_2$  value while keeping haze within the 3% threshold:

- I/O = 0.3925;
- sonication time = 15 minutes.

Accordingly, the “software-generated” predicted values for the selected response were:

- $P'O_2 = 239.72 \text{ mL } \mu\text{m m}^{-2} 24\text{h}^{-1} \text{ atm}^{-1}$  (23°C and 70% RH);
- haze = 2.99%.

The experimental  $P'O_2$  of the PET/pullulan nanocomposite coating according to the optimized formulation was indeed equal to  $258.05 \pm 13.78 \text{ mL } \mu\text{m m}^{-2} 24\text{h}^{-1} \text{ atm}^{-1}$  at 70% RH, in agreement with the predicted value and well below the  $P'O_2$  value of the neat PET film under the same conditions ( $\sim 1560 \text{ mL } \mu\text{m m}^{-2} 24 \text{ h}^{-1} \text{ atm}^{-1}$ ). This result unequivocally demonstrates that the bionanocomposite coating is effective in decreasing the oxygen permeability of the plastic substrate even at high RH. The same “optimized” bionanocomposite coating provided an impressive  $P'O_2$  value of  $1.43 \pm 0.39 \text{ mL } \mu\text{m m}^{-2} 24\text{h}^{-1} \text{ atm}^{-1}$  ( $\equiv O_2TR = 0.11 \text{ mL m}^{-2} 24\text{h}^{-1}$ ) under dry conditions. These values are decidedly better than those of oxygen barrier polymers such as polyvinyl alcohol (PVOH) and ethylene vinyl alcohol (EVOH), which gradually lose much of their barrier properties starting from RH > 50% (Zhang et al, 2001). More noticeably, the final PET/bionanocomposite coating structure presented here exhibits an overall performance fully comparable with one of the most widely used oxygen barrier film, the PET/polyvinylidene chloride (PVDC) coating, which has an  $O_2TR \sim 7.5 \text{ mL m}^{-2} 24 \text{ h}^{-1}$  at 23°C under dry conditions (PET thickness = 12  $\mu\text{m}$ ; coating thickness = 1.4  $\mu\text{m}$ ) (web source: toray.fr).

To find a first confirmation of the disaggregation of the  $\text{Na}^+$ -MMT tactoids and the consequent formation of nano-platelets, particle size analyses were conducted on platelets solutions (of the optimized formulation) before and after ultrasound treatment.

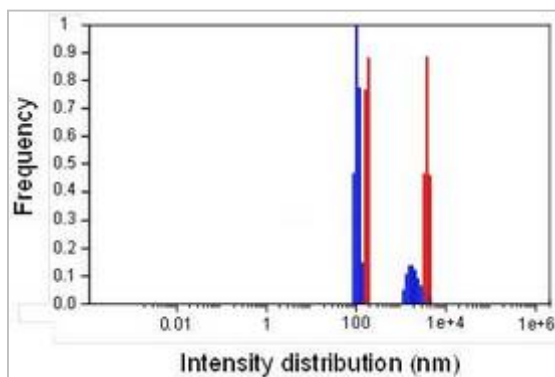


**Figure 45** Particle size distribution of the  $\text{Na}^+$ -MMT before (—) and after (—) sonication according to the optimized formulation (see text).

As shown in Figure 45, the particle size distribution of the non-treated clays (red line) included two main groups around two mean values:

- ~ 52.4% with a mean size of  $3965.0 \pm 462.6$  nm;
- ~ 47.6% with a mean size of  $178.90 \pm 15.52$  nm.

After ultrasonic treatment (blue line), a shift toward lower size is clearly observed with a concomitant increase in the percentage of the particles with the smallest size:

- ~ 70% with a mean size of  $108.2 \pm 18.9$  nm;
- ~ 23.6% with a mean size of  $2151.0 \pm 894.8$  nm.

These values indicate that the optimized coating shows the best performance as an oxygen barrier thanks to its nanostructure (~70% with a mean size of  $108.2 \pm 18.9$  nm), which is able to maintain an acceptable haze value.

The information arising from the particle size analysis is in agreement with TEM observations. Figure 46 indicates that exfoliation was achieved after 15 minutes of ultrasound treatments with an apparently randomly dispersion of the platelets, that might explain the excellent oxygen barrier properties of the composite coating even at high relative humidity, despite the moderate filler loading. These observations are in agreement with the discussion made in paragraphs 4.2.2.1 and 4.2.2.2 on the findings that resulted from the Design of Experiment and from the modeling of permeability data, in particular with equation 23b.

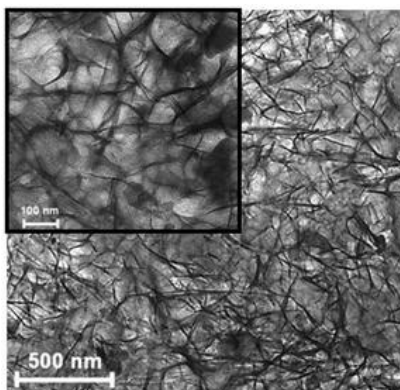


**Figure 46** TEM micrographs at two different magnifications of a 3.0 wt %  $\text{Na}^+$ -MMT water dispersion after ultrasonic treatment according to the optimized procedure (15 min, 0.5 cycles, and 50% amplitude).

The FE-SEM surface micrographs (Figure 47) further confirmed the apparently random organization of the clays. Cross-sectional images, besides confirming the average thickness of the bionanocomposite coatings centered at  $\sim 1$   $\mu\text{m}$  (Figure 39), more clearly disclosed a pattern with the platelets oriented along the two dimensions, with a high clay concentration cropping out to the surface (Figures 47b and 47d). In addition, more detailed inspection revealed that ensuing from the ultrasonic treatment, the exfoliated clays interacted with the biopolymer matrix insomuch as every single platelet was “wrapped” by pullulan (Figure 47c). These interactions, presumably mediated by hydrogen bonds between  $-\text{OH}$  groups of both pullulan and  $\text{Na}^+$ -MMT (Chivrac et al, 2009) had two main consequences:

- I. the organic/inorganic interface increased dramatically, altering many properties of the polymer matrix, such as the molecular mobility. In turn, this would affect the final oxygen barrier performance of the resulting nanocomposite coating under humid conditions as the relaxation behavior of the strongly hydrophilic biopolymer matrix would have been greatly restricted (Alexandre et al, 2000).
- II. Intercalation of biopolymer chains between pullulan and silicate layers prevented reagglomeration of the clay sheets, pullulan acting as a spacer. This is in agreement with the previously discussed modeling results of the permeability data. Nevertheless,

SEM images (Figure 47c) also showed that the well-dispersed and exfoliated clays arranged in a compact structure consisting of two, three, or more platelets stacked on top of one another as if they were forced into a confined space (the coating thickness) upon the drying of the coating.

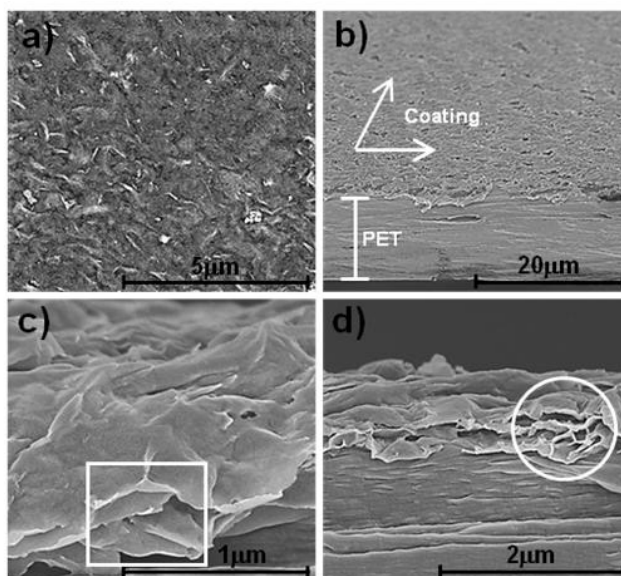


**Figure 47** FE-SEM micrographs of the optimized pullulan nanocomposite coating: surface image of the coating at  $5k\times$  magnification with apparently randomly distributed platelets (a); cross-sectional overview at  $2k\times$  magnification of the coating on top of the PET substrate, with the direction of the orientation indicated by the arrows (b); exfoliated platelets “wrapped” by pullulan at  $50k\times$  magnification, with four stacked layers within the frame (c); cell-like morphology at  $25k\times$  magnification, highlighted by the circle (d).

The  $1\ \mu\text{m}$  thick coating has been characterized so far in terms of composition, oxygen barrier, haze properties, and architecture. In terms of architecture, the addition of the inorganic filler dramatically changed the surface morphology of the pullulan coatings. Interestingly, in the absence of the montmorillonite platelets, condensed matter structures referred to as spherulites (Figure 48) were randomly detected on the pullulan coatings’ surface. The perfectly spherical particles can be viewed as high-order semi-crystalline self-assemblies already observed in many other natural polymers, such as cellulose (Kobayashi et al, 2000), chitin (Murray et al, 1998), chitosan (Murray et al, 1997), and amylase (Ring et al, 1987). In the present study, we hypothesize that the thermodynamic incompatibility between pullulan and PET triggers a phase separation that leads to the aggregation of pullulan, which undergoes a partial crystallization with radial growth around a starting nucleus. To the best of our knowledge, this is the first time that the simultaneous presence of these two spherulitic formations in pullulan has been described.

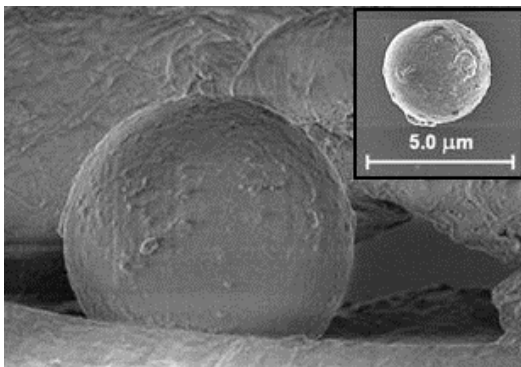


**Figure 48** SEM micrographs of spherulitic formations on the pure pullulan coating surfaces: perfectly spherical self-associations at  $15k\times$  magnification. The top view is shown in the inset.

Another morphological change owing to the filler addition is the increase in the roughness of the coating's surface. As highlighted by the AFM analysis on  $(10 \times 10) \mu\text{m}^2$  areas, the pure pullulan coatings showed highly smooth topographies, with an average roughness of  $\sim 1.2$  nm (Figure 49a). The addition of the clays led to a more jagged and wrinkled topography, characterized by a spiky morphology due to the unordered distribution of the platelets within the pullulan matrix. This finally yielded an increased roughness, which, for the optimized formulation, was  $\sim 14.7$  nm (Figure 49b).

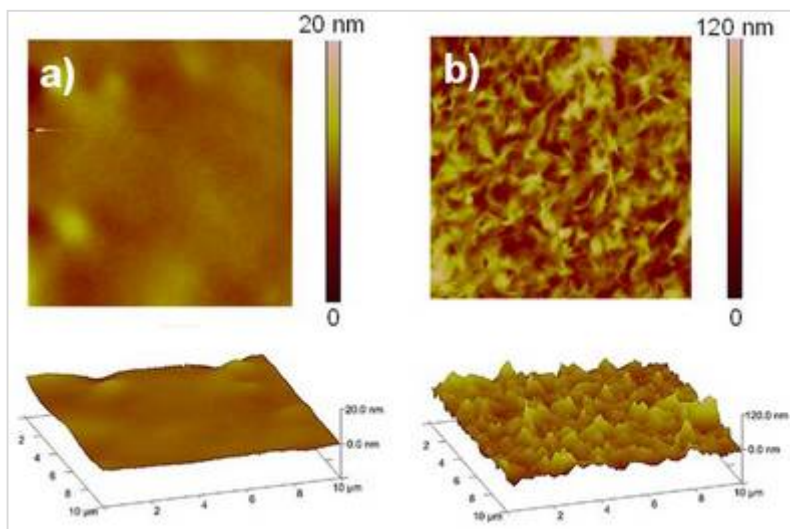


**Figure 49** AFM height (upper) and 3D (lower) images ( $10 \times 10 \mu\text{m}^2$ ) of pure pullulan coatings (a) and pullulan nanocomposite coatings according to the optimized formulation (b).

### 4.2.3 Conclusions

This part of the PhD research demonstrated that the top-down approach can be profitably used to generate bionanocomposite coatings: layers based on pullulan and Na<sup>+</sup>-MMT were successfully obtained for the first time. The ultrasound-assisted procedure for the exfoliation of the inorganic tactoids resulted in an effective and efficient tool for the final performance of the PET/bionanocomposite material to be achieved as it allowed full exfoliation of the platelets during the preparation of the coating water dispersions. This was reflected in the final oxygen barrier properties of the bionanocomposite coatings, due to both the “tortuosity path” and “organic/inorganic interface” effects. In addition, the final morphology of the coatings might have contributed to the excellent barrier performance even at high RH conditions. Although the addition of the clays led to an increase in haze, this did not compromise the ultimate optical properties of the final structure. The findings arising from this work reflect convincingly the fact that pullulan nanocomposite coatings are a promising alternative to the currently available synthetic oxygen barrier polymer coatings (Introzzi et al, 2012)

## 4.2.4 References

[http://www.toray.fr/pdf\\_upload/tfe-lumirror-22.00\\_194.pdf](http://www.toray.fr/pdf_upload/tfe-lumirror-22.00_194.pdf) (accessed 30/10/12).

- Abalde-Cela S, Augu   B, Fischlechner M, Huck WTS, Alvarez-Puebla RA, Liz-Marz  n LM, Abell C. 2011, Microdroplet fabrication of silver-agarose nanocomposite beads for SERS optical accumulation. *Soft Matter* 7:1321–1325.
- Ahmadi E, Sareminezhad S, Azizi MH. 2011, The effect of ultrasound treatment on some properties of methylcellulose films. *Food Hydrocolloids* 25:1399–1401.
- Alexandre M, Dubois P. 2000, Polymer-layered silicate nanocomposites: preparation, properties and uses of a new class of materials. *Mater Sci Eng.* 28:1–63.
- Bordes P, Pollet E, Av  rous L. 2009, Nano-biocomposites: biodegradable polyester/nanoclay systems. *Prog Polym Sci* 34:125–155.
- Cabedo L, Feijoo JL, Villanueva MP, Lagaron JM, Gimenez E. 2006, Optimization of biodegradable nanocomposites based on a PLA/PCL blends for food packaging applications. *Macromol Symp* 233:191–197.
- Chivrac F, Pollet E, Av  rous L. 2009, Progress in nano-biocomposites based on polysaccharides and nanoclays. *Mater Sci Eng R.* 67:1–17.
- Darder, M.; Colilla, M.; Ruiz-Hitzky, E. Biopolymer-clay nanocomposites based on chitosan intercalated in montmorillonite. *Chem Mater.* 2003, 15, 3774–3780.
- Duncan TV. 2011, Applications of nanotechnology in food packaging and food safety: barrier materials, antimicrobials and sensors. *J Colloid Interface Sci* 363:1–24.
- Hielscher T. Ultrasonic production of nano-size dispersions and emulsions. *Proceedings of European Nanosystems Conference ENS '05, Paris, 2005.*
- Introzzi L, Blomfeldt TOJ, Trabattoni S, Tavazzi S, Santo N, Schiraldi A, Piergiovanni L, Farris S. 2012, Ultrasound-assisted pullulan/montmorillonite bionanocomposite coating with high oxygen barrier properties. *Langmuir.* 28:11206-11214.
- Kobayashi S, Hobson LJ, Sakamoto J, Kimura S, Sugiyama J, Imai T, Itoh T. 2000, Formation and structure of artificial cellulose spherulites via enzymatic polymerization. *Biomacromolecules* 2000, 1:168–173.
- Lee DS, Yam KL, Piergiovanni L. *Food Packaging Science and Technology*; CRC Press: Boca Raton, Florida, 2008. p. 88.
- Liu A, Walther A, Ikkala O, Belova L, Berglund LA. 2011, Clay nanopaper with tough cellulose nanofiber matrix for fire retardancy and gas barrier functions. *Biomacromolecules* 12:633–641.
- Murray SB, Neville AC. 1997, The role of the electrostatic coat in the formation of cholesteric liquid crystal spherulites from  $\alpha$ -chitin. *Int J Biol Macromol.* 20:123–130.
- Murray SB, Neville AC. 1998, The role of pH, temperature and nucleation in the formation of cholesteric liquid crystal spherulites from chitin and chitosan. *Int J Biol Macromol.* 22:137–144.

- Pojanavaraphan T., Magaraphan R, Chiou BS, Schiraldi DA. 2010, Development of biodegradable foamlite materials based on casein and sodium montmorillonite clay. *Biomacromolecules* 11:2640–2646.
- Ring SG, Miles MJ, Morris VJ, Turner R, Colonna P. 1987, Spherulitic crystallization of short chain amylase. *Int J Biol Macromol.* 9:158–160.
- Sehaqui H, Zhou Q, Berglund LA. 2011, Nanostructured biocomposites of high toughness—A wood cellulose nanofiber network in ductile hydroxyethylcellulose matrix. *Soft Matter* 7:7342–7350.
- Sinha Ray S, Okamoto M. 2003, Polymer/layered silicate nanocomposites: a review from preparation to processing. *Prog Polym Sci.* 28:1539–1541.
- Suslick KS. *Kirk-Othmer Encyclopedia of Chemical Technology*, 4th Ed., J. Wiley & Sons: New York, 1998.
- Svagan AJ, Åkesson A, Cárdenas M, Bulut S, Knudsen JC, Risbo J, Plackett D. 2012 Transparent films based on PLA and montmorillonite with tunable oxygen barrier properties. *Biomacromolecules* 13:397–405.
- Takahashi S, Goldberg HA, Feeney CA, Karim DP, Farrell M, O’Leary K, Paul DR. 2006, Gas barrier properties of butyl rubber/vermiculite nanocomposite coatings. *Polymer* 47:3083–3093.
- Utracki LA, Sepehr M, Boccaleri E. 2007, Synthetic, layered nanoparticles for polymeric nanocomposites (PNCs). *Polym Adv Technol.* 18:1–37.
- Vartiainen J, Tuominen M, Nättinen K. 2010, Bio-hybrid nanocomposite coatings from sonicated chitosan and nanoclay. *J Appl Polym Sci* 2010, 116:3638–3647.
- Wilson R, Plivelic TS, Aprem AS, Ranganathaiah C, Kumar SA, Thomas S. 2011, Preparation and characterization of EVA/clay nanocomposites with improved barrier performance. *J Appl Polym Sci.* 123:3806–3818.
- Yu J, Cui G, Wei M, Huang J. 2007, Facile exfoliation of rectorite nanoplatelets in soy protein matrix and reinforced bionanocomposites thereof *J Appl Polym Sci* 104:3367–3377.
- Zhang Z, Britt IJ, Tung MA. 2001, Permeation of oxygen and water vapor through EVOH films as influenced by relative humidity. *J Appl Polym Sci.* 82:1866–1872.
- Zheng H, Ai F, Chang PR, Huang J, Dufresne A. 2009, Structure and properties of starch nanocrystal-reinforced soy protein plastics. *Polym Composite* 30:474–480.
- Zhou Q, Malm E, Nilsson H, Larsson PT, Iversen T, Berglund LA, Bulone V. 2009, Nanostructured biocomposites based on bacterial cellulosic nanofibers compartmentalized by a soft hydroxyethylcellulose matrix coating. *Soft Matter* 5:4124–4130.
- Zhou JJ, Wang SY, Gunasekaran S. 2009, Preparation and characterization of whey protein film incorporated with TiO<sub>2</sub> nanoparticles. *J Food Sci.* 74:N50–N56.

# 5. PHASE 3

## THREE-COMPONENTS COATINGS

---

### - PERSPECTIVES-

The third part of the PhD project is conceived as a link between the two parts discussed in section 2 of the research. The idea is to develop a coating made of three components:

1. a biopolymer, pullulan;
2. an inorganic component, TEOS;
3. an inorganic filler, Na<sup>+</sup>-MMT.

To properly combine them, both the nano-approaches previously used (the top-down and the bottom-up approaches) are simultaneously exploited to finally obtain a bionanocomposite hybrid coatings.

Figure 50 schematically displays the three component coating development:

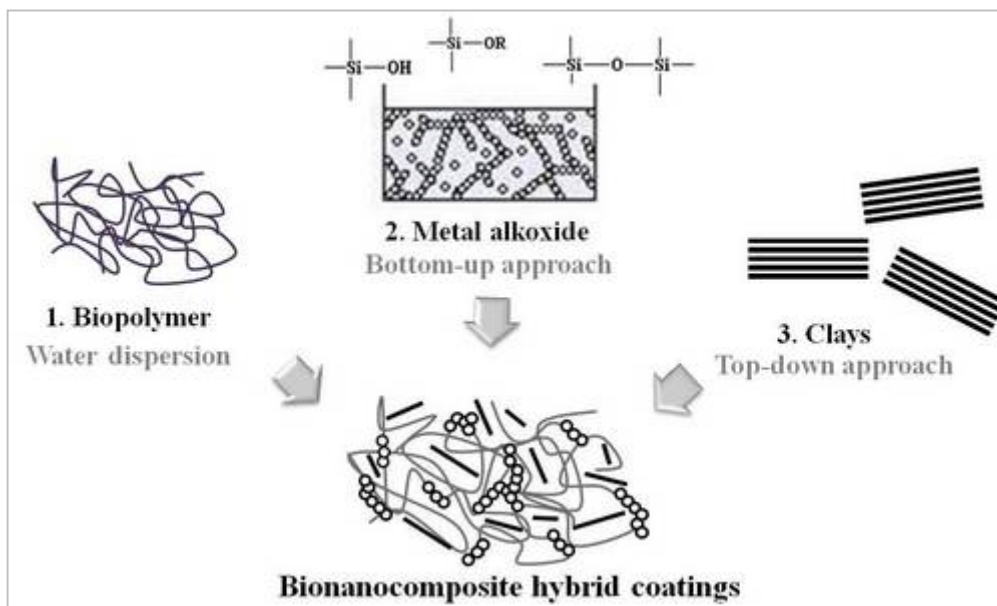


**Figure 50** Schematic representation of the project about the development of the three-component coating using both the bottom-up and the top-down approaches.

The goal is, as in the previous part, to develop a material that can take advantage of the best properties of each component and any potential synergistic effect, which would finally allow enhancing the overall performance of the final material as well as obtaining new, unforeseen properties (Sadjadi et al, 2011). The idea to combine together both the bottom-up and the top-down approach for the design of a material has emerged only recently (Ijichi et al, 2011; Chang et al, 2011); however in the literature, to the best of our knowledge there is not application for food packaging/coating technology. At the same time, approaches from nanotechnology have enabled a number of key innovations in nanoscience such as photonic and phononic crystals, micro/nano frames, nanoporous filters (Chang et al, 2011), and so its full exploitation represents an appealing strategy to innovate also the food packaging field.

The multi-disciplinary approach for the development of new materials is growing day-to-day. This involves matching different areas of expertise and various aspects of chemistry (organic, polymers, physical, materials chemistry, biochemistry, etc), where soft matter and ingenious processing are synergistically coupled (Nicole et al, 2010). These cross-cutting approaches, used to develop hybrid multifunctional architectures, yield what is called “Integrative Chemistry” (Nicole et al, 2010). These organic-inorganic or bio-inorganic structures make possible innovative industrial applications, due to the properties of these materials that are influenced by the strong synergy created by an extensive hybrid interface and not only from the sum of the individual contributions of the material components (Sanchez et al, 2010).

For the present research, the integration of the top-down approach, the bottom-up one and the use of a biopolymer could be a new success inside of this “Integrative Chemistry”.

The final goal, which is actually the first, main goal of the overall PhD project, is to obtain a very thin, high-performance three dimensional layer, with special interest towards the oxygen barrier properties in a broad range of relative humidity. The layer will be intended for a plastic or a bio-based flexible substrate.

The procedure, indicated in Figure 50, foresees the independent preparation of the components (as reported in the Materials and Methods of the Phase 2) and their final mixing. The feasibility of the different steps has been already checked, and different analyses are expected to be performed. Some of them are in progress and can be underlined: Oxygen Transmission Rate analysis, optical characterization, microscopy investigations, X-ray diffraction.

## 5.1 References

- Chang CH, L. Tian L, Hesse WR, Gao H, Choi HJ, Kim JG, Siddiqui M, Barbastathis G. 2011, From two-dimensional colloidal self-assembly to three-dimensional nanolithography. *Nano Lett.* 11:2533–2537.
- Ijichi K, Fukuoka A, Shimojima A, Sugiyama M, Okubo T. 2011, A combined top-down and bottom-up approach to fabricate silica films with bimodal porosity. *Materials Letters.* 65: 828–831.
- Nicole L, Rozes L, Sanchez C. 2010, Integrative approaches to hybrid multifunctional materials: from multidisciplinary research to applied technologies. *Adv. Mater.* 22:3208–3214.
- Sadjadi MS, Farhadyar N, Zare K. Preparation and Characterization of Inorganic-Organic Nanocomposite Coatings, *Advances in Nanocomposites - Synthesis, Characterization and Industrial Applications*, Dr. Boreddy Reddy (Ed.), 2011, pp 3-22. InTech, available from: <http://www.intechopen.com/books/advances-in-nanocomposites-synthesis-characterization-and-industrial-applications/preparation-and-characterization-of-inorganic-organic-nanocomposite-coatings> (accessed 03/12/12).
- Sanchez C, Rozes L, Ribot F, Laberty-Robert C, Grosso D, Sassoye C, Boissiere C, Nicole L. 2010, ‘‘Chimie douce’’: a land of opportunities for the designed construction of functional inorganic and hybrid organic-inorganic nanomaterials. *C. R. Chimie.* 13:3-39.

## 6. GLOSSARY

(most used acronym - alphabetical order)

---

<b>CA</b>	Contact Angle
<b>DA</b>	Degree of Amidation
<b>DE</b>	Degree of Esterification
<b>FE-SEM</b>	Field-Emission Scanning Electron Microscopy
<b>FTIR-ATR</b>	Fourier Transform Infrared - Attenuated Total Reflectance
<b>IA</b>	Image Analysis
<b>LDPE</b>	Low Density Polyethylene
<b>MMT</b>	Montmorillonite
<b>OTR</b>	Oxygen Transmission Rate
<b><math>P'O_2</math></b>	Permeability coefficient
<b>PE</b>	Polyethylene
<b>PET</b>	Polyethylene terephthalate
<b>PLA</b>	Polylactic acid
<b>PP</b>	Polypropylene
<b>PVOH</b>	Polyvinyl alcohol
<b>RH</b>	Relative Humidity
<b>SEM</b>	Scanning Electron Microscopy
<b>TEM</b>	Transmission Electron Microscopy
<b>TEOS</b>	Tetraethyl orthosilicate

## *Acknowledgements*

---

First of all, I would like to thank my tutor, Prof. Schiraldi, and co-tutor, Prof. Piergiovanni. I am very grateful to Prof. Schiraldi for his scientific approach, expert guidance and pleasant work attitude. It has been a true pleasure to collaborate with you. My vivid gratitude goes to Prof. Piergiovanni, who guided me over my academic education, convincing me not to stop my studies years ago. Thanks for all the valuable opportunities you have offered me.

Dr. Stefano Farris is particularly thanked for his supervision during my studies. We were able to work for fruitful scientific productions, always enjoying the work.

I wish to express my gratitude also to Metalvuoto SpA, in particular to Gianni Ronchi, Roberto Rocca and Imerio Zucchi. You allowed me to learn a lot about industrial aspects.

I am grateful to all former and present people working in the packaging (and cereal) laboratory of DeFENS, for making it a friendly place to work. With some of you I spent more than the three PhD years: you are my dear good friends, thanks for everything!

Special thanks to my old friends and “life” outside the university.

My family is warmly thanked too. You always loved and supported me, and this has been valuable.

Finally, I would like to mention the oncoming future: whatever lies ahead... the best is yet to come.

***Conference's abstract***

**MATBIM 2010**  
**1<sup>st</sup> International meeting on Material/Bioproduct Interaction 3-5**  
**March 2010, AgroParis Tech, Paris**

**DEVELOPMENT AND CHARACTERIZATION OF A GELATIN-BASED  
COATING WITH UNIQUE SEALING PROPERTIES**

Stefano Farris, Carlo A. Cozzolino, Laura Introzzi, Luciano Piergiovanni

Department of Food Science and Microbiology – Packaging laboratory  
University of Milan Via Celoria, 2 - 20133 Milan, Italy  
Fax: +39 0250316672; E-mail: stefano.farris@unimi.it

### Introduction

The packaging sector is a major field of application of coatings, either to improve bulk properties of their substrates like barrier, optical, mechanical, thermal, anticorrosion, sealing,<sup>1</sup> or to add new features such as the antimicrobial activity.<sup>2</sup> Only recently it has been expressed an increasing interest towards new formulations originating from natural and renewable resources,<sup>3</sup> not only due to the increase in the price of crude oil but also because of other established advantages mostly related to their versatile nature and chemical structure. In addition, biobased coatings have been indicated as a promising way to face the waste disposal issue.<sup>4</sup> Of late, gelatin-based coatings have been formulated in the attempt of exploiting its ancient feature, i.e. the adhesive property. In the attempt to provide further information on the development of bio-based functional coatings, this work aimed at: 1) quantifying the effect of the components used in the coating formulation as well as of the pH of the starting solution on the seal strength of coated polypropylene strips; 2) pinpointing the best sealing performance by a proper combination of the most influencing factors formulation. To this purpose, we decided to adopt a modeling approach, which has been shown as a powerful tool for designing and engineering polymers with adhesive properties.<sup>5</sup> The main key-features of the optimized coating are also discussed, with special emphasis on the mode of failure of the seal.

### Materials and Methods

**Coating preparation.** Type A, 133 Bloom, pigskin gelatin powder (Weishardt International, Grauliet Cedex, France), acetic acid esters from monoglycerides (Grindstedt® Acetem 70-00 P, Danisco A/S, Langebrogade, Denmark), glycerol (Giomavaro, Brugherio, Italy) and milli-Q water (18.3 M $\Omega$ ) were used for the starting hydrogel solutions preparation, in amount defined by each run of the experimental design. The bio-coated plastic films were prepared according to the procedure protected by international patent WO 2008/075396 A1.<sup>6</sup>

**Experimental design.** A central composite face-centred (CCF) design imbedding a full factorial 2<sup>4</sup> design was used in this work, in order to obtain a semi-empirical quadratic model for the prediction of the selected response - strain energy (Y), judged as the best measure for quantifying the seal strength of a bio-based coating.<sup>7</sup> The experimental design was planned by combining mixture and process variables: pH of the starting hydrogel solution (X<sub>1</sub>) as a process factor; gelatin (X<sub>2</sub>), glycerol (X<sub>3</sub>) and lipid (X<sub>4</sub>) as mixture factors; the solvent, as a controlled filler. Each of the independent variables was assessed at three levels (-1, 0 and +1), resulting in 30 experiments. The semi-empirical modeling adopted made it possible to detect the best factors combination enabling the highest seal strength (i.e., the response was maximized).

**Characterization techniques.** The coated plastic films were analyzed concerning their thickness (Dialmatic DDI030M, Bowers Metrology, Bradford, UK), seal strength (dynamometer mod. Z005, Zwick Roell, Ulm, Germany), thermal behavior (DSC Mettler Toledo, Columbus, OH), transparency (spectrophotometer Lambda 650, PerkinElmer, Waltham, USA) and structure (Phenom™ SEM, FEI Co., Inc., Hillsboro, OR / Particle Size measurement Zetasizer NanoZS, Malvern Instruments, Worcestershire, United Kingdom).

### Results and Discussion

The selected response (strain energy) was significantly influenced by four factors: the amount of plasticizer (X<sub>3</sub>), the pH of the starting hydrogel solution (X<sub>1</sub>), the interaction 'plasticizer-hydrophobic

component' ( $X_3X_4$ ) and, even though to a minor extent, the interaction 'pH-gelatin' ( $X_1X_2$ ). The hydrophobic component had a positive effect only up to a certain level (1 wt.-%, weight percent), beyond which it affected the seal strength attribute, as shown in Figure 1.

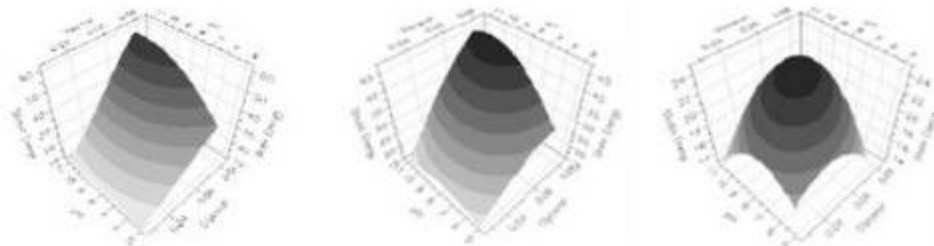


Figure 1. Response surface plot for pH and glycerol vs. strain energy (N x mm) varying the lipid component from -1 to +1 coded level. Gelatin set at +1 coded levels.

The optimized seal formulation (pH = 11; gelatin = 10.15 wt.-%; plasticizer = 7.5 wt.-%; lipid = 1 wt.-%; H<sub>2</sub>O = 81.35 wt.-%) led to an optimum seal strength value of approximately 60 N x mm, to which corresponded a maximum force required to break the joints of 2.25 N. The heat-seal (temperature 90°C; dwell time: 1 s; pressure: 4 bar) failed in both peeling and tearing mode failure, as confirmed by microscopy, spectrophotometric and particle size analyses. It is confirmed by Figure 2 showing the SEM images collected after rupture of the seal. Three different zones were clearly visualized: 1) the substrate (OPP); 2) the coating initially lied on the upper OPP strip, de-bound from the substrate after rupture; 3) the coating initially lied on the lower OPP strip, still bound to the substrate. It is likely that two different modes took place during joints separation: region 3 suggests that the heat-seal failed in peeling mode failure, whereas regions 1 and 2 may be explained in terms of tearing mode failure, which is typical of strength of the seal higher than the strength at the substrate/coating interface.

### Conclusions

Based upon these present results, biomacromolecules such as gelatin, acetylated monoglycerides and a proper plasticizer (e.g., glycerol) show the potential as a sealable coating for many packaging applications. Further, our findings suggest that a new class of coatings may be accurately designed to originate tailored seals, i.e. ranging from weak peelable to hermetic.

### References

- Schrieber, R.; Gareis, H. *Gelatine Handbook: Theory and Industrial Practice*, 1st edition, Wiley-VCH, Weinheim, 2007, p. 1.
- Chalier, P.; Ben Arfa, A.; Preziosi-Belloy, L.; Gontard, N. *J Appl Polym Sci* 2007, 106, 611.
- Liu, L. S.; Finkenstadt, V. L.; Liu, C.-K.; Jin, T.; Fishman, M. L.; Hicks, K. B. *J Appl Polym Sci* 2007, 106, 801.
- Farris, S.; Schaich, K. M.; Liu, L.; Piergiovanni, L.; Yam, K. *Trends Food Sci Tech* 2009, 20, 316.
- Jovanovic, R.; McKenna, T. F.; Dube', M. A. *Macromol Mater Eng* 2004, 289, 467.
- WO 075396 A1 (2008), Mirante srl, S. Farris, L. Piergiovanni, G. Ronchi, R. Rocca.
- Farris, S.; Cozzolino, C.A.; Introzzi, L.; Piergiovanni, L. *Packag Technol Sci* 2009, 22, 359.

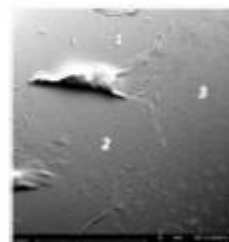


Figure 2. SEM images of sealed interface after rupture in topographical mode

## **SLIM 2010, 4<sup>th</sup> Shelf Life International Meeting Zaragoza, 23-25 June 2010**

---

**SLIM** (Shelf Life International Meeting)

23<sup>rd</sup> – 25<sup>th</sup> June 2010

### **PN08 — EFFECTS OF DIFFERENT SEALING CONDITIONS ON THE SEAL STRENGTH OF POLYPROPYLENE FILMS COATED WITH A BIO-BASED THIN LAYER**

**S. Farris, C.A. Cozzolino, L. Introzzi, L. Pierviviani**

diSTAM, Department of Food Science and Microbiology, Università di Milano, Via Celoria 2 - 20133 Milano, Italy

Hermeticity is a necessary prerequisite of sealed packages in order to guarantee the safety requirements of any packaged food item as well as to assure an adequate shelf-life. For this reason, sealability is deemed as one of the most important parameters to take into consideration when dealing with shelf-life optimization tasks. The results of an investigation carried out on oriented polypropylene films coated with a gelatin-based thin layer are here presented. The main goal of this research was to investigate the influence of the most important sealing process variables on the heat-seal strength by means of a chemometric approach, namely through the Design of Experiment (DoE) technique. To this purpose, three quantitative controllable factors (bar temperature,  $X_1$ ; dwell time,  $X_2$ ; and pressure,  $X_3$ ) and two dependent variables ( $Y_1$  and  $Y_2$ ) as a measure of the seal strength (maximum force, N and strain energy, N mm) were combined in a  $2^3$  full factorial design, with 33 total runs. Surprisingly, the factor affecting both responses the most was the bar pressure rather than the sealing temperature. The negative effect on seal strength due to an increase in bar pressure (from 2.5 bars to 4.5 bars) could be explained in terms of "squeezing" effect exerted by the pressure. We hypothesize, that increasing the bar pressure, the intimate contact between the two coated sides of the plastic film is exaggerated in so much as the bio-coating comes out from the sealing contact area. This effect is of course emphasized by the bars temperature setting, since the melting process of the biosealant is faster at higher temperatures for a given pressure value. The final result is the weakening of the seal due to a drastic reduction in the thickness of the touching coated surfaces. Contrary to the bar pressure, the sealing temperature had a positive effect. Dwell time did not have any significant influence as a main factor, while influencing negatively the seal strength as an interaction term (i.e. time x pressure), together with the further interaction temperature x pressure. The mathematical models obtained for the two responses provided different results in terms of fitting capability ( $R^2$ ) and prediction ability ( $Q^2$ ). In particular, for the maximum force response,  $R^2$  and  $Q^2$  were equal to 0.571 and 0.405 respectively, whereas the model supporting the strain energy response gave  $R^2=0.932$  and  $Q^2=0.937$ , highlighting that for quantifying the seal strength, the energy necessary to break a seal is a better measure than the maximum force. The highest seal strength values obtained during this work were of 0.6615 N and 19.6 N mm for maximum force and strain energy, respectively.

**Keywords:** bio-coating, design of experiment (DoE), gelatin, heat-seal strength, shelf-life

**SLIM 2010, 4<sup>th</sup> Shelf Life International Meeting  
Zaragoza, 23-25 June 2010**

SLIM (Shelf Life International Meeting)

23<sup>rd</sup> – 25<sup>th</sup> June 2010

**PT23 — MOISTURE EFFECTS ON WATER VAPOR PERMEABILITY  
MEASUREMENTS OF POLYLACTIDE FILMS**

F. Li, L. Introzzi, S. Farris, L. Piergiovanni

Università degli studi di Milano, Dipartimento di Scienze e Tecnologie Alimentari e Microbiologiche - Packlab, Via  
Celoria 2, 20133 Milano – Italia

The water-polymer interactions can affect significantly both the permeability and the mechanical properties of PLA polymers. Even if low amounts of moisture absorbed can be crucial for the general performance of the packaging material, only few investigations have been carried out so far on this topic. The aim of this work was to evaluate the moisture effects on the water vapor transmission rate (WVTR) for a widely used thermo-sealable PLA film. Its moisture sorption was measured at 38 °C, in the range between 11 and 86% of relative humidity and, in the same RH range and at the same temperature, its WVTR was measured using two different methods.

The moisture sorption of the PLA film at 38 °C was quite limited at the lowest RH values (11 – 52%), but increases quickly, reaching the values reported by other Authors (about 6000 ppm), above that range. The amount of water absorbed by PLA film tested, thus, seems strongly affected by the relative humidity of the surrounding environment and the moisture increase is not linearly proportional to the RH values. On the contrary, the values of WVTR obtained both with a gravimetric method and with a isostatic equipment, appear linearly related to the driving force. Therefore, it must be concluded that the different amounts of water absorbed by the PLA film tested at the various relative humidity (demonstrated by the isotherm experiment) do not affect the proportionality of the water transmission to the  $\Delta RH$ , at least in the RH range considered and at the temperature of 38°C.

**10° CISETA**  
**Fieramilano (Rho, Milano), 10-11 maggio 2011**

Autori: Laura Introzzi, Ilaria Giuliano, Stefano Farris, Luciano Piergiovanni

**Università degli Studi di Milano, via Celoria 2, 20133 Milano**

**DiSTAM, Dipartimento di Scienze e Tecnologie Alimentari e  
Microbiologiche**

***MODIFICAZIONE DELLE PROPRIETA' BARRIERA DI UN FILM DI  
ACIDO POLILATTICO (PLA) ATTRAVERSO L'USO DI (BIO)COATINGS***

L'utilizzo di coatings applicati su substrati plastici rappresenta, all'interno del settore dell'imballaggio alimentare, un'efficace strada per il miglioramento di specifiche performances. Dato l'interesse del mercato globale verso soluzioni di packaging sempre più "green", il presente lavoro prende in considerazione la possibilità di utilizzare biomacromolecole per la realizzazione di coatings su films di acido polilattico (PLA), per modificarne la proprietà di barriera all'ossigeno, nell'ottica di renderlo concorrenziale rispetto ai comuni films plastici attualmente in commercio. A tale scopo, sono stati utilizzati cinque differenti biopolimeri sotto forma di coatings: chitosano, gelatina, due pectine e pullulano. I risultati ottenuti hanno evidenziato come la deposizione di biocoatings aventi spessore medio di  $1.15 \pm 0.1 \mu\text{m}$  ha consentito l'ottenimento di valori di OTR (Oxygen Transmission Rate) inferiori a  $1 \text{ mL m}^{-2} \text{ day}^{-1}$  in condizioni anidre ( $23^\circ\text{C}$ ). Tale valore, tuttavia, è risultato essere fortemente influenzato dall'umidità relativa. In particolare; per valori superiori al 40% la permeabilità aumenta, mantenendosi comunque al di sotto di quella del PLA tal quale. Dal confronto di questi valori con quelli ottenuti da films di PLA laccati con i tradizionali coatings di origine sintetica è possibile affermare come le biomacromolecole testate possono essere efficacemente utilizzate per talune applicazioni nel settore dell'imballaggio alimentare.

**MATBIM 2012**  
**2<sup>nd</sup> International meeting on Material/Bioproduct Interaction**  
**22-25 April 2012, Dijon, France**

**INVESTIGATION OF THE WETTING PHENOMENA INVOLVED AT THE  
 WATER/BIOPOLYMER COATINGS INTERFACE**

**Laura Introzzi<sup>1</sup>, Paolo Biagioni<sup>2</sup>, Torsten Holz<sup>3</sup>, Luciano Piergiovanni<sup>1</sup>, Alberto Schiraldi<sup>1</sup>, Stefano Farris<sup>1</sup>**

<sup>1</sup> DiSTAM, Department of Food Science and Microbiology, University of Milan, Via Celoria 2 - 20133, Milan, Italy (E-mail: stefano.farris@unimi.it; laura.introzzi@unimi.it; luciano.piergiovanni@unimi.it; alberto.schiraldi@unimi.it)

<sup>2</sup> CNISM-Department of Physics, Politecnico di Milano, Piazza L. da Vinci 32 - 20133, Milan, Italy (E-mail: paolo.biagioni@polimi.it)

<sup>3</sup> DataPhysics Instruments GmbH, Raiffeisenstrasse 34 - 70794, Filderstadt, Germany (E-mail: info@dataphysics.de)

### Introduction

Recent years have witnessed a rapid and increasing interest towards new packaging materials totally or partially obtained from renewable resources. Within this context, biopolymer coatings have raised enormous attention due to the potential of enhancing the performance of the substrate beneath, such as barrier, optical, thermal and mechanical properties, sealability, ink printability, etc (1). To date, the modification of the surface properties of packaging materials after biocoating deposition has not been fully investigated (2). In particular, few papers in literature deal with the behaviors of bio-coated surfaces with respect to water, especially concerning the physicochemical phenomena involved at the solid/liquid interface (3). The comprehension of the final coated-films behavior can possibly lead to new and enhanced material designs for many different applications.

In this research (4) some biomacromolecules have been selected as coating materials on polyethylene terephthalate (PET) films and the surface changes induced by the coating application were investigated by the contact angle technique. Dealing with biopolymers and their inherent hydrophilic character, water contact angle equilibrium is unattainable. Thus, the following aspects were considered: the variation of contact angle in a temporal window of 60 seconds and the mechanisms at the liquid/solid interface (i.e., absorption, spreading and swelling). To this purpose, a simple decay function was first fit to the experimental data and a combined contact angle (CA)/image analysis (IA) approach was used in a second step in order to elucidate the phenomena at the interface. For a better comprehension, a surface topography investigation (AFM) was also conducted.

### Materials and Methods

Five different biopolymers were used: a high methoxyl pectin (DE 72), an amidated pectin (DE 27, DA 20), pig skin gelatin type A, 133 Bloom, shellfish chitosan (with a degree of deacetylation of 85%) and pullulan. Poly(ethylene terephthalate) (PET, 12.0 ± 0.5 µm thick) was used as the plastic substrate for coating deposition. The coating dispersions were prepared on the basis of the biopolymer properties. The PET was coated using an automatic coating applicator (ref 1137, Sheen Instrument, Kingston, UK). Contact angle measurements were performed using the apparatus OCA 15Plus (DataPhysics instruments GmbH, Filderstadt, Germany) equipped with a video measuring system. SCA 20 software was used for data acquisition. The sessile drop method was used and the following shape parameters collected, starting from the deposition of the drop up to 60 seconds: contact angle evolution ( $\theta$ , °), droplet volume ( $V$ , µL), droplet surface area ( $A$ , mm<sup>2</sup>), droplet height ( $h$ , mm), and droplet base diameter ( $2r$ , mm). To describe the phenomenology of the water droplet kinetics, a semiempirical approach was used where a decay function was fitted to the data with no intended physical meaning (Tablecurve 4.0, Jandel Scientific, San Rafael, CA). To understand the phenomena at the interface, the water droplet has been assumed as being a segment of a sphere so that different equations were assessed taking into account geometric and trigonometric parameters.

### Results and Discussion

The analyses were carried out on coatings of 1.18 ± 0.13 µm. The five biopolymer coatings considered have shown different water drops evolutions (figure 1), and a three parameters decay function (very similar to the well-known Avrami model) has been used to model the water droplet kinetics. New findings were then obtained using a geometric-trigonometric approach, based on an image analysis of the water droplet. The simultaneous detection of contact angle ( $\theta$ ) and of some shape parameters (see Materials and Methods), allowed assessing the spherical geometry condition, which

in turn made possible to split the overall contact angle evolution in two main phenomena (figure 2): absorption (volume changes), and/or spreading (widening of the basal area of the droplet).

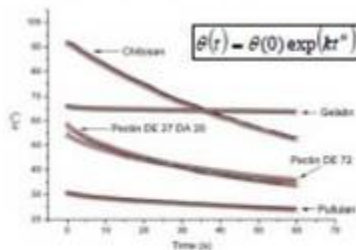
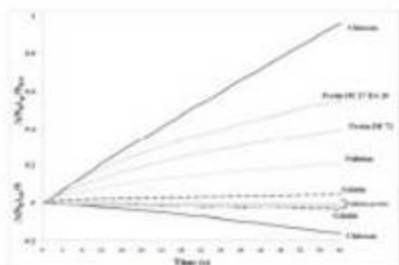


Figure 1 Water contact angle evolution during 60 seconds of analysis. Solid lines were obtained by fitting experimental data to the equation reported.



$$(\Delta S_s)_{spreading} = 3V_s \left[ \frac{1}{h} \left( \frac{1 + \cos \theta}{2 + \cos \theta} \right) - \frac{1}{h_0} \left( \frac{1 + \cos \theta_0}{2 + \cos \theta_0} \right) \right] \quad (1)$$

$$(\Delta S_s)_{absorption} = 3 \left[ \frac{(V - V_0)}{h} \times \left( \frac{1 + \cos \theta}{2 + \cos \theta} \right) \right] \quad (2)$$

Figure 2 Changes in the basal area of the water droplets due to spreading and absorption effects, determined by the equations (1) and (2).

The AFM images allow understanding whether the different topographical surface patterns of the bio-coatings could explain the different contact angle behaviors (figure 3).

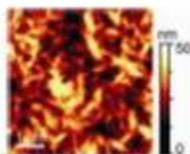


Figure 3 AFM height image (5 × 5 μm<sup>2</sup>) of chitosan surface denoting the web-like formation of molecular clusters, which allowed a larger and faster absorption than the other coatings.

### Conclusions

Coatings prepared with five different biopolymers exhibit different wetting properties. The assessment of a geometric-trigonometric approach firstly allowed understanding the spherical geometry of the water droplet placed on a coating surface; in addition, the adopted approach disclosed the possibility to quantify and to split the phenomena occurring at the liquid/solid interface. Next investigation will be addressed to confirm the influence of the molecular chains orientation on the wettability of biopolymer coatings.

### References

- (1) Farris S., Introzzi L. & Piergiovanni L. Evaluation of a bio-coating as a solution to improve barrier, friction and optical properties of plastic films. *Packag. Technol. Sci.* 2009, 22, 69–83.
- (2) Karbowski T.; Debeaufort F. & Voilley A. Importance of surface tension characterization for food, pharmaceutical and packaging products: a review. *Crit. Rev. Food Sci.* 2006, 46, 391–407.
- (3) Kokoszka S., Debeaufort F., Hambleton A., Lenart A. & Voilley A. Protein and glycerol contents affect physico-chemical properties of soy protein isolate-based edible films. *Innovat Food Sci Emerg Tech.*, 2010, 11, 503-510.
- (4) Farris S., Introzzi L., Biagioni P., Holz T., Schiraldi A. & Piergiovanni L. Wetting of biopolymer coatings: contact angle kinetics and image analysis investigation. *Langmuir* 2011, 27, 7563–7574.

**SLIM 2012, 5<sup>th</sup> Shelf Life International Meeting  
Changwon, South Korea, May 30- June 1, 2012**

New Technologies for Shelf Life Extension: New materials

SLIM (Shelf Life International Meeting)

30<sup>th</sup> May–1<sup>st</sup> June 2012

PN57

**DEVELOPMENT OF OXYGEN BARRIER PULLULAN/CLAY  
NANOCOMPOSITE COATINGS FOR FOOD PACKAGING  
APPLICATIONS**

*Laura Introzzi<sup>a</sup>, Thomas O. J. Blomfeldt<sup>b</sup>, Luciano Piergiovanni<sup>a</sup>, Stefano Farris<sup>a</sup>*

<sup>a</sup>DiSTAM, Department of Food Science and Microbiology, University of Milan, Italy;

<sup>b</sup>Department of Fiber and Polymer Technology, Royal Institute of Technology, Sweden

E-mail: stefano.farris@unimi.it

In the last years nanotechnology has been exploited to improve several properties of food packaging materials. In particular, the use of inorganic clays has been proved to be effective in the design of oxygen barrier films, generating the so-called nanocomposites. In this research we describe the development of a new bionanocomposite coating made of pullulan and Na<sup>+</sup>-montmorillonite by means of the ultrasound technology (Hielscher Ultrasonic device UP400S, sonotrode H14). Coating water dispersions were laid on a polyethylene terephthalate film (PET, 12.5 ± 0.5 μm) by means of an automatic applicator. Oxygen Transmission Rate (OTR) (23°C, 70% relative humidity) and haze analyses were performed. The use of the Design of Experiment (DoE) technique allowed to understand the effects of the factors on the selected responses. Interestingly, the amount of clays had a positive effect on the OTR up to a certain value, beyond of which the overall performance decreased, probably due to the formation of aggregates at higher loading. The ultrasound process time had a similar effect, because an excessive treatment appeared deleterious for the exfoliation process. The model obtained from the DoE approach also allowed to pinpoint the best factors combination (sonication time: 15 min; clay concentration: 1.57 wt.%) that yielded the minimum oxygen transmission rate of about 18.44 ml m<sup>-2</sup> 24h<sup>-1</sup> by keeping the haze within the 3% threshold generally accepted for commercial applications. Additional analyses were carried out to better understand the final coating system: particle size analysis, to check the effectiveness of the clays dispersion operated by the ultrasound technique; Field Emission Scanning Electron Microscopy (FE-SEM), to figure out the final morphology of the composite system; atomic force microscopy (AFM), to gather more information on the topography changes induced by the clays loading. Findings arising from this work can be seen as a step forward for the generation of a new category of oxygen barrier coatings for food packaging applications.

**Keywords:** Bionanocomposite, montmorillonite, oxygen transmission rate, packaging, ultrasound technology)

## **Frontiers in Water Biophysics 2012**

### **23-26 September 2012 Perugia, Italy**

Frontiers in Water Biophysics 2012 - Perugia, Italy

poster

#### **A NOVEL ANTI-FOG PULLULAN COATING FOR FOOD PACKAGING APPLICATIONS**

*S. Farris, L. Introzzi, L. Piergiovanni and A. Schiraldi*

DeFENSE Department of Food, Environmental and Nutritional Sciences, University of Milan – via Celoria 2, 20133 Milan, Italy. [stefano.farris@unimi.it](mailto:stefano.farris@unimi.it)

Current food packaging materials are conceived as a multifunctional tool enabling containment, protection and preservation of foods. One of the additional properties required is the anti-fog property, which concerns the capability of the packaging material to avoid the forming small droplets of water on the internal side of the packaging film. Fog has a detrimental effect on the transparency of the material, mainly due to the shape of the droplets [1], which is reflected by the balance between the three interfacial energies (solid-liquid  $\gamma_{SL}$ , liquid-vapor  $\gamma_{LV}$ , and solid-vapor  $\gamma_{SV}$ ) of the three-phase system, as described by Young's equation [2]. The higher the contact angle, the higher the incident angle of the light normal to the substrate at the water/air interface, hence the more intense will be the scattering of the visible light. Not only the shape, but also the size of the droplets is another important factor to consider with regards to the anti-fog property of a material [1]: the smaller the size, the larger the number of droplets and the more pronounce the foggy effect. As both the shape and the size of the water droplets depend on the physicochemical characteristics of the substrate [3], modifying the original physicochemical properties of the plastic surface can be the key to controlling water droplet formation [4].

The approach of applying a bio-based coating is here described, and a new anti-fog coating made of pullulan is proposed [5]. The anti-fog properties are discussed in terms of wettability, surface chemistry / morphology, and by quantitative assessment of the optical properties (haze and transparency) before and after fog formation. The work also presents the results of anti-fog tests simulating the typical storage conditions of fresh foods. In these tests, the anti-fog efficiency of the pullulan coating was compared with that of two commercial anti-fog films, whereas an untreated low-density polyethylene (LDPE) film was used as a reference. The obtained results revealed that the pullulan coating behaved as a 'wetting enhancer', mainly due to the low water contact angle ( $\sim 24^\circ$ ), which in turn can be ascribed to the inherent hydrophilic nature of this polysaccharide, as also suggested by the X-ray photoelectron spectroscopy experiments. Unlike the case of untreated LDPE and commercial anti-fog samples, no discrete water formations (i.e., droplets or stains) were observed on the anti-fog pullulan coating on refrigeration during testing. Rather, an invisible, continuous and thin layer of water occurred on the biopolymer surface, which was the reason for the unaltered haze and increased transparency, with the layer of water possibly behaving as an anti-reflection layer. As confirmed by atomic force microscopy analysis, the even deposition of the coating on the plastic substrate compared to the patchy surfacing of the anti-fog additives in the commercial films is another important factor dictating the best performance of the anti-fog pullulan coating.

#### **References**

1. J. A. Howarter and J. P. Youngblood. *Macromol. Rapid Commun.* 29, 455–466 (2008).
2. T. Young, *Philosophical Transactions of the Royal Society of London* 1805, Vol. 95, pp 65–87.
3. S. Farris, L. Introzzi, P. Biagioni, T. Holz, A. Schiraldi and L. Piergiovanni. *Langmuir* 27, 7563–7574 (2011).
4. F. C. Cebeci, Z. Wu, L. Zhai, R. E. Cohen and M. F. Rubner. *Langmuir* 22, 2856–2862 (2006).
5. L. Introzzi, J. M. Fuentes-Alventosa, C. A. Cozzolino, S. Trabattori, S. Tavazzi, C. L. Bianchi, A. Schiraldi, L. Piergiovanni and S. Farris. *ACS Appl. Mater. Interfaces* (accepted). DOI:10.1021/am300784n

## **Frontiers in Water Biophysics 2012**

### **23-26 September 2012 Perugia, Italy**

Frontiers in Water Biophysics 2012 - Perugia, Italy

poster

#### **WETTING OF BIOPOLYMER COATINGS: CONTACT ANGLE KINETICS AND IMAGE ANALYSIS INVESTIGATION**

*S. Farris, L. Introzzi, L. Piergiovanni and A. Schiraldi*

DeFENSE Department of Food, Environmental and Nutritional Sciences, University of Milan – via Celoria 2, 20133 Milan, Italy. [stefano.farris@unimi.it](mailto:stefano.farris@unimi.it)

The use of coatings made of biopolymers on packaging materials, especially plastics, has significantly increased over the past few years [1,2]. However, the modification of the surface properties of packaging materials after biocoating deposition has not been fully investigated so far [3]. In particular, few papers in literature deal with the behavior of bio-coated surfaces with respect to water, especially concerning the physicochemical phenomena involved at the solid/liquid interface [4].

In this work [5], the surface wetting of five biopolymers, used as coating materials for a plastic film, was monitored over a span of 8 min by means of the optical contact angle technique. Because most of the total variation was observed to occur during the first 60 s, we decided to focus on this curtailed temporal window. Initial contact angle values ( $\theta_0$ ) ranged from 91° for chitosan to 30° for pullulan. However, the water drop profile began to change immediately following drop deposition for all biocoatings, confirming that the concept of water contact angle equilibrium is not applicable to most biopolymers. First, a three-parameter decay equation [ $\theta(t) = \theta(0) \exp(kt^n)$ ] was fit to the experimental contact angle data to describe the kinetics of the contact angle change for each biocoating. Interestingly, the  $k$  constant correlated well with the contact angle evolution rate and the  $n$  exponent seemed to be somehow linked to the physicochemical phenomena underlying the overall kinetics process. Second, to achieve a reliable description of droplet evolution, the contact angle (CA) analysis was coupled with image analysis (IA) through a combined geometric/trigonometric approach. Absorption and spreading were the key factors governing the overall mechanism of surface wetting during the 60 s analysis, although the individual quantification of both phenomena demonstrated that spreading provided the largest contribution for all biopolymers, with the only exception of gelatin, which showed two quasi-equivalent and counterbalancing effects. The possible correlation between these two phenomena and the topography of the biopolymer surfaces are then discussed on the basis of atomic force microscopy analyses.

#### **References**

1. J. W. Rhim, J. H. Lee and S. I. Hong. Food Sci. Technol.-Leb. 39, 806–813 (2006).
2. S. Farris, L. Introzzi and L. Piergiovanni. Packag. Technol. Sci. 22, 69–83 (2009).
3. T. Karbowiak; F. Debeaufort and A. Voilley. Crit. Rev. Food Sci. 46, 391–407 (2006).
4. S. Kokoszka, F. Debeaufort, A. Hambleton, A. Lenart and A. Voilley. Innovat. Food Sci. Emerg. Tech. 11, 503–510 (2010).
5. S. Farris, L. Introzzi, P. Biagioni, T. Holz, A. Schiraldi and L. Piergiovanni. Langmuir 27, 7563–7574 (2011).

***Honors and awards***

**SLIM 2010, 4<sup>th</sup> Shelf Life International Meeting  
Zaragoza, 23-25 June 2010**



4<sup>TH</sup> SHELF LIFE  
INTERNATIONAL MEETING  
23-25 JUNE 2010

**SLIM 20**  
4<sup>TH</sup> SHELF LIFE INTERNATIONAL MEETING

**SESSION: NEW TECHNOLOGIES  
FOR SHELF LIFE EXTENSION**

**SLIM POSTER AWARD**

CERTIFICATE OF MERIT  
AWARDED TO

EFFECTS OF DIFFERENT SEALING CONDITIONS ON THE SEAL STRENGTH OF PP FILMS  
COATED WITH A BIOBASED THIN LAYER - S. Farris, C.A. Corzuelmo, L. Introzzi,  
L. Piergiovanni

FOR THE ORIGINAL CONTRIBUTION AND QUALITY  
OF THE RESEARCH ACTIVITY  
IN FOOD PACKAGING AND SHELF-LIFE

COMMITTEE OF REFEREES

GSICA

UNIVERSIDAD DE SARAGOZA

**MATBIM 2012**  
**2<sup>nd</sup> International meeting on Material/Bioproduct Interaction**  
**22-25 April 2012, Dijon, France**



The image shows a certificate for the Best Poster Award. At the top left are the logos for UB (University of Burgundy) and IUT Dijon. To the right is the text: "University of Burgundy, Institute of Technology of Dijon-Auxerre, 7 Blvd Docteur Petitjean - BP17867, 210078 DIJON Cedex". The main text reads: "Best Poster AWARD", "Introzzi Laura", "from DISTAM University of Milan - Italy.", "was awarded by the scientific committee of the 2<sup>nd</sup> International Meeting on Packaging Material-BioProduct Interaction (MATBIM 2012 - France, 22-25<sup>th</sup> April 2012)", "based on the topic originality, the science and communication qualities". Below this is a signature and a circular stamp from the "UNIVERSITE DE BOURGOGNE, Département Génie Biologique, UFR de Dijon". At the bottom left is the MATBIM 2012 logo, and at the bottom right is the text "Dijon 22-25 April 2012".

UB IUT Dijon

University of Burgundy  
Institute of Technology of Dijon-Auxerre  
7 Blvd Docteur Petitjean - BP17867  
210078 DIJON Cedex

**Best Poster AWARD**

*Introzzi Laura*  
from DISTAM University of Milan - Italy.

was awarded by the scientific committee of the  
**2<sup>nd</sup> International Meeting on  
Packaging Material-BioProduct Interaction**  
(MATBIM 2012 - France, 22-25<sup>th</sup> April 2012)

based on the topic originality, the science and communication qualities

For the organising committee

  
Prof. F. Debeaufort

UNIVERSITE DE BOURGOGNE  
Département  
Génie Biologique  
UFR de Dijon

 **MATBIM 2012**  
2<sup>nd</sup> International meeting on Material/BioProduct Interaction

Dijon 22-25 April 2012

***Patents and publications***

(12) INTERNATIONAL APPLICATION PUBLISHED UNDER THE PATENT COOPERATION TREATY (PCT)

(19) World Intellectual Property Organization  
International Bureau



(43) International Publication Date  
12 August 2010 (12.08.2010)

(10) International Publication Number  
**WO 2010/089787 A1**

- (51) International Patent Classification:  
C09D 105/00 (2006.01) C09D 189/00 (2006.01)
- (21) International Application Number:  
PCT/IT2010/000016
- (22) International Filing Date:  
25 January 2010 (25.01.2010)
- (25) Filing Language: English
- (26) Publication Language: English
- (30) Priority Data:  
MI2009A 000126 3 February 2009 (03.02.2009) IT
- (71) Applicant (for all designated States except US): **MIRANTE S.R.L.** [IT/IT]; Via Camillo Benso di Cavour 50B, I-23900 Lecco (LC) (IT).
- (72) Inventors; and
- (75) Inventors/Applicants (for US only): **FARRIS, Stefano** [IT/IT]; Via Parpignano 29, I-07041 Alghero (SS) (IT). **PIERGIOVANNI, Luciano** [IT/IT]; Via Dell'Ortano 3/54, I-20090 Rodano (MI) (IT). **RONCHI, Giovanni** [IT/IT]; Via Roma 38, I-20044 Bernateggio (MI) (IT). **ROCCA, Roberto** [IT/IT]; Via Matteotti 54, I-20040 Roncello (MI) (IT). **INTROZZI, Laura** [IT/IT]; Via Ronzoni 25, I-22072 Cerenate (CO) (IT).
- (74) Agent: **INCOLLINGO, Italo**; Piazzale Lavater 3, I-20129 MILANO (MI) (IT).

- (81) Designated States (unless otherwise indicated, for every kind of national protection available): AE, AG, AL, AM, AO, AT, AU, AZ, BA, BB, BG, BH, BR, BW, BY, BZ, CA, CH, CL, CN, CO, CR, CU, CZ, DE, DK, DM, DO, DZ, EC, EE, EG, ES, FI, GB, GD, GE, GH, GM, GT, HN, HR, HU, ID, IL, IN, IS, JP, KE, KG, KM, KN, KP, KR, KZ, LA, LC, LK, LR, LS, LT, LU, LY, MA, MD, ME, MG, MK, MN, MW, MX, MY, MZ, NA, NG, NI, NO, NZ, OM, PE, PG, PH, PL, PT, RO, RS, RU, SC, SD, SE, SG, SK, SL, SM, ST, SV, SY, TH, TJ, TM, TN, TR, TT, TZ, UA, UG, US, UZ, VC, VN, ZA, ZM, ZW.
- (84) Designated States (unless otherwise indicated, for every kind of regional protection available): ARIPO (BW, GH, GM, KE, LS, MW, MZ, NA, SD, SL, SZ, TZ, UG, ZM, ZW), Eurasian (AM, AZ, BY, KG, KZ, MD, RU, TJ, TM), European (AT, BE, BG, CH, CY, CZ, DE, DK, EE, ES, FI, FR, GB, GR, HR, HU, IE, IS, IT, LT, LU, LV, MC, MK, MT, NL, NO, PL, PT, RO, SE, SI, SK, SM, TR), OAPI (BF, BJ, CF, CG, CI, CM, GA, GN, GQ, GW, ML, MR, NE, SN, TD, TG).

**Declarations under Rule 4.17:**

- as to the applicant's entitlement to claim the priority of the earlier application (Rule 4.17(iii))
- of inventorship (Rule 4.17(iv))

**Published:**

- with international search report (Art. 21(3))



**WO 2010/089787 A1**

(54) Title: COATINGS FROM NATURAL MACROMOLECULES, WITH GAS BARRIER PROPERTIES TAILORED IN SITU, AND RELATED PREPARATION METHOD

(57) Abstract: The invention concerns lake compositions based on natural macromolecules (gelatin, chitosan, pectine etc.) with possible additions of vinyl polymers, metal-alkoxides etc., characterized by a barrier effect modulated in situ, in particular as a function of the relative humidity in the exterior ambient.

# Development and Characterization of a Gelatin-Based Coating with Unique Sealing Properties

Stefano Farris, Carlo A. Cozzolino, Laura Introzzi, Luciano Piergiovanni

Department of Food Science and Microbiology, Packaging Laboratory, University of Milan, Milan 20133, Italy

Received 31 October 2009; accepted 19 April 2010

DOI 10.1002/app.32708

Published online 1 July 2010 in Wiley InterScience (www.interscience.wiley.com).

**ABSTRACT:** The experimental results on the development of thin ( $\sim 1.5 \mu\text{m}$ ) gelatin-based coatings and the investigation on their sealing attribute when applied onto oriented polypropylene (OPP) are reported. The sealing performance, expressed as the strain energy required to separate the sealed joints, was studied as a function of three different influencing factors. pH of the hydrogel solution was varied between 5 and 11. The highest seal strength values were obtained for pH values beyond the isoelectric point (IEP) of the gelatin molecule. The effect of the plasticizer (glycerol) was studied by changing its concentration from 2.5 wt % to 7.5 wt % to the total weight of the hydrogel solution. Glycerol concentration = 7.5 wt % was found to be the best for achieving adequate strain energy values. The influence of a hydrophobic component on the capability of the coating to act as a sealant has also

been assessed. The hydrophobic component had a positive effect only up to a certain level (1 wt %, weight percent), whereas beyond this value, it affected the seal strength attribute. According to the best setting conditions, seal strength values for the OPP biocoated films of  $\sim 61 \text{ N} \times \text{mm}$  were attained, with a corresponding maximum force required to break the joints of 2.4 N. These results are discussed by taking into consideration the modality of seals opening. Interestingly, the heat-seal (temperature: 90°C; dwell time: 1 s; pressure: 4 bar) failed in both peeling and tearing mode failure, as confirmed by microscopy, spectrophotometric, and particle size analyzes. © 2010 Wiley Periodicals, Inc. *J Appl Polym Sci* 118: 2969–2975, 2010

**Key words:** DSC; failure; heat-seal strength; poly(propylene); SEM

---

Correspondence to: S. Farris (stefano.farris@unimi.it).

*Journal of Applied Polymer Science*, Vol. 118, 2969–2975 (2010)  
© 2010 Wiley Periodicals, Inc.

## Wetting of Biopolymer Coatings: Contact Angle Kinetics and Image Analysis Investigation

Stefano Farris,<sup>\*,†</sup> Laura Introzzi,<sup>‡</sup> Paolo Biagioni,<sup>‡</sup> Torsten Holz,<sup>§</sup> Alberto Schiraldi,<sup>‡</sup> and Luciano Piergiovanni<sup>‡</sup>

<sup>†</sup>DISTAM, Department of Food Science and Microbiology, University of Milan, Via Celoria 2 – 20133, Milan, Italy

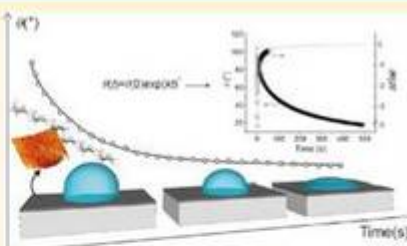
<sup>‡</sup>CNISM-Department of Physics, Politecnico di Milano, Piazza L. da Vinci 32 – 20133, Milan, Italy

<sup>§</sup>DataPhysics Instruments GmbH, Raiffeisenstrasse 34 – 70794, Filderstadt, Germany

**S** Supporting Information

**ABSTRACT:** The surface wetting of five biopolymers, used as coating materials for a plastic film, was monitored over a span of 8 min by means of the optical contact angle technique. Because most of the total variation was observed to occur during the first 60 s, we decided to focus on this curtailed temporal window. Initial contact angle values ( $\theta_0$ ) ranged from  $\sim 91^\circ$  for chitosan to  $\sim 30^\circ$  for pullulan. However, the water drop profile began to change immediately following drop deposition for all biocoatings, confirming that the concept of water contact angle equilibrium is not applicable to most biopolymers. First, a three-parameter decay equation [ $\theta(t) = \theta(0) \exp(kt^n)$ ] was fit to the experimental contact angle data to describe the kinetics of the contact angle change for each biocoating. Interestingly, the  $k$  constant correlated well with the contact angle evolution rate and the  $n$  exponent seemed to be somehow linked to the physicochemical phenomena underlying the overall kinetics process.

Second, to achieve a reliable description of droplet evolution, the contact angle (CA) analysis was coupled with image analysis (IA) through a combined geometric/trigonometric approach. Absorption and spreading were the key factors governing the overall mechanism of surface wetting during the 60 s analysis, although the individual quantification of both phenomena demonstrated that spreading provided the largest contribution for all biopolymers, with the only exception of gelatin, which showed two quasi-equivalent and counterbalancing effects. The possible correlation between these two phenomena and the topography of the biopolymer surfaces are then discussed on the basis of atomic force microscopy analyses.



## “Wetting Enhancer” Pullulan Coating for Antifog Packaging Applications

Laura Introzzi,<sup>†</sup> José María Fuentes-Alventosa,<sup>†,‡</sup> Carlo A. Cozzolino,<sup>†,§</sup> Silvia Trabattoni,<sup>‡</sup> Silvia Tavazzi,<sup>‡</sup> Claudia L. Bianchi,<sup>#</sup> Alberto Schiraldi,<sup>‡</sup> Luciano Piergiovanni,<sup>‡</sup> and Stefano Farris<sup>\*,†</sup>

<sup>†</sup>DeFENS, Department of Food, Environmental and Nutritional Sciences, Packaging Division, University of Milan, Via Celonia 2, I – 20133 Milan, Italy

<sup>‡</sup>Centro de Investigación y Formación Agraria “Alameda del Obispo”, Instituto de Investigación y Formación Agraria y Pesquera (IFAPA), Avenida Menéndez Pidal s/n. 14004 Córdoba, Spain

<sup>§</sup>STAA, Department of Agriculture, University of Sassari, Viale Italia 39/A, I – 07100 Sassari, Italy

<sup>‡</sup>Department of Materials Science, University of Milano Bicocca, Via Cozzi 53, I – 20125 Milano, Italy

<sup>#</sup>Department of Chemistry, University of Milan, Via Golgi 19, I – 20133 Milano, Italy

### Supporting Information

**ABSTRACT:** A new antifog coating made of pullulan is described in this work. The antifog properties are discussed in terms of wettability, surface chemistry/morphology, and by quantitative assessment of the optical properties (haze and transparency) before and after fog formation. The work also presents the results of antifog tests simulating the typical storage conditions of fresh foods. In these tests, the antifog efficiency of the pullulan coating was compared with that of two commercial antifog films, whereas an untreated low-density polyethylene (LDPE) film was used as a reference. The obtained results revealed that the pullulan coating behaved as a “wetting enhancer”, mainly due to the low water contact angle ( $\sim 24^\circ$ ), which in turn can be ascribed to the inherent hydrophilic nature of this polysaccharide, as also suggested by the X-ray photoelectron spectroscopy experiments. Unlike the case of untreated LDPE and commercial antifog samples, no discrete water formations (i.e., droplets or stains) were observed on the antifog pullulan coating on refrigeration during testing. Rather, an invisible, continuous and thin layer of water occurred on the biopolymer surface, which was the reason for the unaltered haze and increased transparency, with the layer of water possibly behaving as an antireflection layer. As confirmed by atomic force microscopy analysis, the even deposition of the coating on the plastic substrate compared to the patchy surfacing of the antifog additives in the commercial films is another important factor dictating the best performance of the antifog pullulan coating.

**KEYWORDS:** antifog, coating, packaging, pullulan, surface, wetting



## Self-Assembled Pullulan–Silica Oxygen Barrier Hybrid Coatings for Food Packaging Applications

Stefano Farris,<sup>\*,†</sup> Laura Introzzi,<sup>†</sup> José Maria Fuentes-Alventosa,<sup>†,‡</sup> Nadia Santo,<sup>§</sup> Roberto Rocca,<sup>||</sup> and Luciano Piergiovanni<sup>†</sup>

<sup>†</sup>DISTAM, Department of Food Science and Microbiology, Packaging Division, University of Milan, Via Celoria 2, 20133 Milan, Italy

<sup>‡</sup>Centro de Investigación y Formación Agraria "Alameda del Obispo", Instituto de Investigación y Formación Agraria y Pesquera (IFAPA), Avda. Menéndez Pidal s/n, 14004 Córdoba, Spain

<sup>§</sup>Interdepartmental Center of Advanced Microscopy, CIMA, University of Milan, Via Celoria 26, 20133 Milan, Italy

<sup>||</sup>Metahvoto Spa, Via L. da Vinci 3, 20040 Milan, Italy

### Supporting Information

**ABSTRACT:** The scope of this study encompassed the evaluation of pullulan as a suitable biopolymer for the development of oxygen barrier coatings to be applied on poly(ethylene terephthalate) (PET), especially for food packaging applications. To enhance the oxygen barrier properties of the organic phase (pullulan) even at high relative humidity values, an inorganic phase (silica), obtained through *in situ* polymerization, was also utilized to obtain hybrid coatings via the sol–gel technique. Transmission electron microscopy (TEM) images and Fourier transform infrared (FT-IR) spectra showed that mixing the two phases yielded a three-dimensional hybrid network formed by self-assembly and mediated by the occurrence of new hydrogen-bond interactions at the intermolecular level, although the formation of new covalent bonds could not be excluded. The deposition of the hybrid coatings decreased the oxygen transmission rate (OTR) of the plastic substrate by up to 2 orders of magnitude under dry conditions. The best performance throughout the scanned humidity range (0%–80% relative humidity) was obtained for the formulation with the lowest amount of silica (that is, an organic/inorganic ratio equal to 3).

**KEYWORDS:** *Fourier transform infrared (FT-IR) spectroscopy, oxygen transmission rate (OTR), packaging, pullulan, transmission electron microscopy (TEM)*

## Ultrasound-Assisted Pullulan/Montmorillonite Bionanocomposite Coating with High Oxygen Barrier Properties

Laura Introzzi,<sup>†</sup> Thomas O. J. Blomfeldt,<sup>‡</sup> Silvia Trabattoni,<sup>§</sup> Silvia Tavazzi,<sup>§</sup> Nadia Santo,<sup>||</sup> Alberto Schiraldi,<sup>†</sup> Luciano Piergiovanni,<sup>†</sup> and Stefano Farris<sup>\*,†</sup>

<sup>†</sup>Department of Food, Environmental and Nutritional Sciences—Packaging Division, University of Milan, Via Celoria 2, 20133 Milan, Italy

<sup>‡</sup>Department of Fiber and Polymer Technology, Royal Institute of Technology, SE-10044, Stockholm, Sweden

<sup>§</sup>Department of Materials Science, University of Milano Bicocca, Via Cozzi 53, I-20125 Milan, Italy

<sup>||</sup>Interdepartmental Center of Advanced Microscopy, University of Milan, Via Celoria 26, 20133 Milan, Italy

### Supporting Information

**ABSTRACT:** In this paper, the preparation and characterization of oxygen barrier pullulan sodium montmorillonite (Na<sup>+</sup>-MMT) nanocomposite coatings are presented for the first time. Full exfoliation of platelets during preparation of the coating water dispersions was mediated by ultrasonic treatment, which turned out to be a pivotal factor in the oxygen barrier performance of the final material even at high relative humidity (RH) conditions [oxygen permeability coefficients  $\sim 1.43 \pm 0.39$  and  $258.05 \pm 13.78 \text{ mL} \cdot \mu\text{m}^{-1} \cdot (24 \text{ h})^{-1} \cdot \text{atm}^{-1}$  at 23 °C and 0% RH and 70% RH, respectively]. At the micro- and nanoscale, the reasons are discussed. The final morphology of the coatings revealed that clay lamellae were stacked on top of one another, probably due to the forced confinement of the platelets within the coating thickness after solvent evaporation. This was also confirmed by modeling the experimental oxygen permeability data with the well-known Nielsen and Cussler permeation theoretical models, which suggested a reasonable aspect ratio ( $\alpha$ ) of  $\sim 100$ . Electron microscopic analyses also disclosed a peculiar cell-like arrangement of the platelets. The stacking of the clay lamellae and the cell-like arrangement create the excellent oxygen barrier properties. Finally, we demonstrated that the slight haze increase in the bionanocomposite coating materials arising from the addition of the clays depends on the clay concentration but not so much on the sonication time, due to the balance of opposite effects after sonication (an increase in the number of scattering centers but a reduction in their size).



## SUBMITTED ARTICLES

- Bettuelli M, Trabattoni S, Fagnola M, Tavazzi S, Introzzi L, Farris S. Surface properties and wear performances of siloxane-hydrogel contact lenses. Submitted to Journal of Biomedical Materials Research: Part B – Applied Biomaterials.

